IntechOpen

Refrigeration

Edited by Orhan Ekren

REFRIGERATION

Edited by **Orhan Ekren**

Refrigeration
http://dx.doi.org/10.5772/65998
Edited by Orhan Ekren

Contributors

Muhammad Sultan, Takahiko Miyazaki, Gunnar Suchaneck, Oleg Pakhomov, Gerald Gerlach, Asma Etoumi, Santiago Benito, Fernando Calderón, Ángel Benito, Eva Navascués, Radu Rosca, Ioan Tenu, Petru Carlescu, Orhan Ekren

Notice

First published in Croatia, 2017 by INTECH d.o.o.
eBook (PDF) Published by IN TECH d.o.o.
Place and year of publication of eBook (PDF): Rijeka, 2019.
IntechOpen is the global imprint of IN TECH d.o.o.
Printed in Croatia

Legal deposit, Croatia: National and University Library in Zagreb

Additional hard and PDF copies can be obtained from orders@intechopen.com

Refrigeration
Edited by Orhan Ekren

p. cm.

Print ISBN 978-953-51-3497-8

Online ISBN 978-953-51-3498-5

eBook (PDF) ISBN 978-953-51-4693-3

Meet the editor

Dr. Orhan Ekren is an associate professor at Ege University. He received his MSc degree from the Department of Energy Engineering and PhD degree from the Department of Mechanical Engineering (Thermodynamics). He studied as a postdoc researcher in the Southern Illinois University, USA. His main research interests are energy efficiency, energy saving, capacity modulation on refrigeration and HVAC&R systems, renewable heating and cooling, magnetic cooling, integration of renewable energy systems into buildings, optimum sizing of hybrid renewable energy sources (wind/solar, etc.), and also sustainability in energy and buildings. Dr. Ekren has authored and coauthored many international journal papers, international conference papers, and also books and book chapters. He is currently involved in several research projects funded by national research council (TUBITAK) and EC-FP7 project (EcoShopping).

Contents

Preface

In the beginning, the sole purpose of utilization of the refrigeration was to conserve food (BC 1100). But today in our daily life, refrigeration is one of the necessary areas for the aim of not only food conservation but also comfort, industrial production, electronic equipments' performance, safe and proper operation of telecommunication stations and computer rooms, space studies, etc.

Recently, there are many strategies under evaluation regarding the efficient and novel heating-cooling methods. The main reason for that is heating-cooling uses the largest portion of overall energy in domestic and industrial usage (this rate is 45% of the final energy consumption in the EU). Therefore, the importance and wide application range of the refrigeration require new techniques and researches. In this respect, this book covers but is not limited to energy efficiency, cycle analysis, alternative techniques, modeling, industrial application, and capacity modulation point of view.

It is categorized into six chapters, namely:

Chapter 1. A Simple Approach to Calculate/Minimize the Refrigeration Power Requirements

Chapter 2. Electrocaloric Cooling

Chapter 3. Food Chilling Methods and CFD Analysis of a Refrigeration Cabinet as a Case Study

Chapter 4. Refrigeration in Winemaking Industry

Chapter 5. Energy-Efficient Air-Conditioning Systems for Nonhuman Applications

Chapter 6. Refrigeration System Capacity Modulation Methods

I believe that the readers not only engineering but also other science majors will find useful and practical information in the book *Refrigeration*. I would like to thank the authors for their contributions to this book.

Assoc. Prof. Dr. Orhan Ekren
Solar Energy Institute, Ege University
Turkey

Chapter 1

A Simple Approach to Calculate/Minimize the Refrigeration Power Requirements

Asma Etoumi

Additional information is available at the end of the chapter

http://dx.doi.org/10.5772/intechopen.69130

Abstract

The vapor compression refrigeration cycle is the most common method used for removing heat from a lower temperature level to a higher temperature level using a mechanical work. At lower temperatures (typically lower than −40°C), complex refrigeration schemes, such as cascaded refrigeration cycles, may be needed, increasing the complexity of the models used to predict the power requirements. This chapter introduces a new linear refrigeration model to predict the shaft power demand of the refrigeration cycle given the cooling demand, the condensing, and evaporation temperatures. The refrigeration model is based on regression of rigorous simulation results. This chapter also proposes a new systematic optimization method for minimizing the work consumed in refrigeration system. The methodology employs nonlinear model to find the optimum refrigeration temperature levels and their cooling duties. To solve the nonlinear problem, generalized reduced gradient algorithm is used. A case study is presented to demonstrate the advantage using of the proposed methodology. Results show that the difference in power prediction between rigorous simulation and the new refrigeration model is about 10%. The work consumed in refrigeration cycle can be reduced to 9% compared to the base case when the operating conditions are optimized.

Keywords: The coefficient of performance, multi-stage cycle, cascade cycle, an ethylene cold-end process

1. Introduction

Refrigeration systems are commonly used to provide cooling to sub-ambient processes. The most common refrigeration system in use today is the vapor compression refrigeration cycle [1]. Heat is extracted from a lower temperature heat source and pumped to a higher temperature by means of the work of the compressor. This higher temperature might be to an

external cooling utility (e.g., cooling water), a heat sink within the process or to another refrigeration system [2]. The power demand of the cycle depends strongly on the temperature at which cooling is required, the temperature at which the refrigerant is condensed, as well as the type of refrigerant being used [3].

Generally, a simple refrigeration cycle (i.e., a single-stage compression cycle) cannot be used to provide cooling at very low temperature due to industrial limitation of refrigerant [4] and a complex cycle (e.g., a multi-stage cycle) or cascaded is used as an alternative. Complex refrigeration system that utilizes a multi-stage compressor presents lower energy consumption when compared to the simple cycle [2]. Although complex cycle reduces power consumption, the design and optimization of this cycle are challenging because there are a large number of design alternatives and, consequently, their design fundamental interaction.

Branan [5] presented graphs that help prediction of power requirements for simple and multi-level refrigeration cycles at various temperature ranges using propane, propylene, ethane, or ethylene as the refrigerant. In preliminary design stage and in optimization where evaluation of a large number of cycles may be required, shortcut methods may be preferred because they allow faster evaluation without needing detailed specification of refrigeration design parameters (e.g., refrigerant mass flow rate, cooling duty, and the partition temperature in cascaded cycle). A shortcut method to predict the coefficient of performance (COP) of simple vapor compression cycles for pure refrigerants under the assumption of isentropic compression was proposed by Shelton and Grossman [6]. The shortcut model predicted the COP by using system temperatures and thermodynamic data of refrigerant (i.e., specific heat capacity and molar latent heat of vaporization). This chapter proposes a new refrigeration model to predict the net power demand for various design options (refrigerants and configuration) of the refrigeration cycle. The new proposed model predicts the actual coefficient of performance as function of the ideal performance (i.e., the Carnot cycle). This chapter also addresses refrigeration integration with sub-ambient process streams and provides a systematic methodology required for operational optimization of refrigeration cycles. Inputs to the optimization model include process stream data and initial estimate of operating conditions. The outputs of optimization are evaporation temperatures and cooling duties of each level and shaft work of each stage. The proposed optimization is less complicated than recently published work of Montanez-Morantes et al. [7]. Also, it is very useful for students who do not have strong mathematical background.

This chapter is organized in the following way: first, an introduction that outlines the basic configurations on which the model is based and that illustrates how the complex cycles can be decomposed into an associated simple cycles is presented. Then, the approach that is used to develop new refrigeration models is presented. After that, two examples are introduced to illustrate the effectiveness of the new refrigeration model for predicting the power demand in multi-level refrigeration cycles. Section 3 introduces a systematic methodology for the optimization of operating conditions in multi-level refrigeration cycles. A case study is presented in Section 4 to demonstrate the benefit of the use of the optimization method proposed in this chapter. Finally, the conclusions of the chapter and the recommendations for future work are presented in Section 5.

http://dx.doi.org/10.5772/intechopen.69130

1.1. Refrigeration cycle configuration

1.1.1. Simple vapor-compression cycle

Figure 1(a) shows a simple vapor-compression cycle (VCC), which consists of four components: compressor, condenser, expansion valve, and evaporator. In a simple refrigeration cycle, heat is absorbed from a process stream through evaporation of a liquid refrigerant in an evaporator. The amount of heat transferred to the refrigerant in the evaporator is called the refrigeration load, Qevap. The evaporated refrigerant stream is compressed, and the heat from the refrigerant stream is rejected to the external heat sink. The amount of heat rejected to the external heat sink in the condenser equals the summation of the refrigeration load and the shaft work consumed in the compressor. The VCC assumes isobaric condensation and evaporation, isentropic compression, evaporation of refrigerant to a saturated vapor state, and condensation to a saturated liquid state.

1.1.2. Cascaded refrigeration cycle

Cascade cycles are usually applied in two cases [8]: (1) when the temperature range between condensation and evaporation cannot be covered by any single refrigerant and (2) when use of a single refrigerant cycle consumes more work than a cascade cycle.

Cascaded cycles are composed of two or more refrigeration cycles, where each cycle employs a different refrigerant. The low temperature cycle and a high temperature cycle, as shown in **Figure 1(b)**, are connected to each other through a heat exchanger, which acts as an evaporator

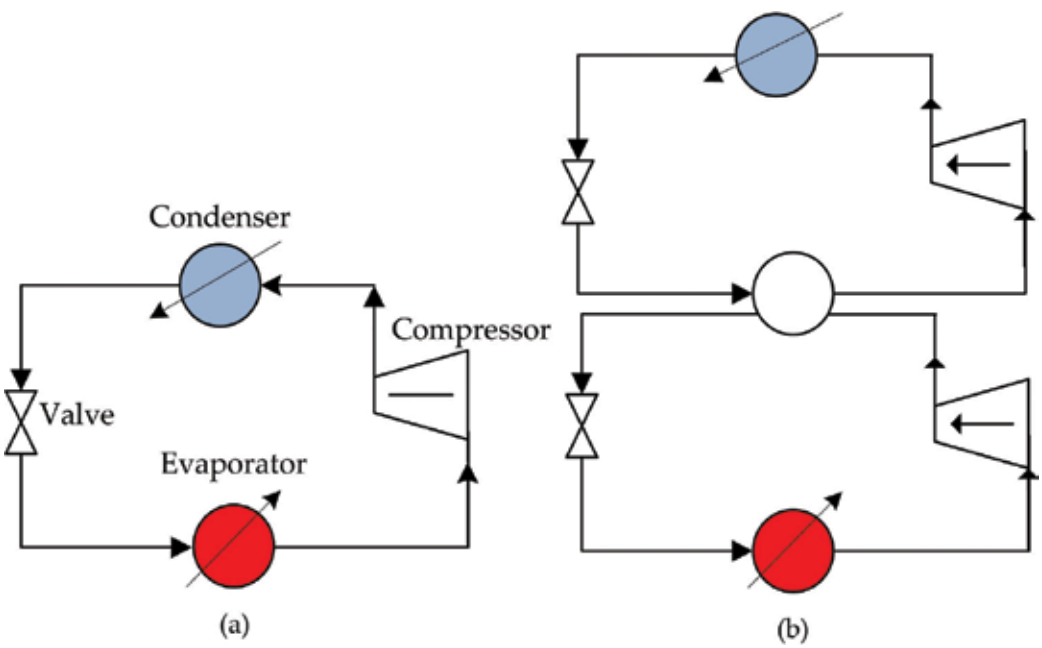

Figure 1. (a) Simple vapor-compression cycle; (b) cascade refrigeration cycle.

for the high temperature cycle and a condenser for the low temperature cycle. The partition temperature, which is the temperature of the evaporator of the upper cycle, is an important design parameter. It influences the total shaft work requirement of the cycle as will be seen in Section 1.2.1.

1.1.3. Multi-stage refrigeration cycle

A multi-stage cycle is normally implemented when the pressure ratio between the heat rejection and heat absorption pressures is high and when cooling is required at different temperature levels. For example, in a two-level cycle, illustrated in **Figure 2(a)**, the cooling duty is satisfied at two different evaporation temperatures using a single refrigerant expanded to two different pressure levels. Introducing two cooling levels reduces the refrigerant flow in the low temperature cycle that in its turn reduces the overall power requirement of the cycle [2].

1.1.4. Decomposing of complex refrigeration cycle

Decomposing a complex cycle into an assembly of simple vapor compression cycles is an alternative approach for predicting the power demand of a complex cycle. For example, a

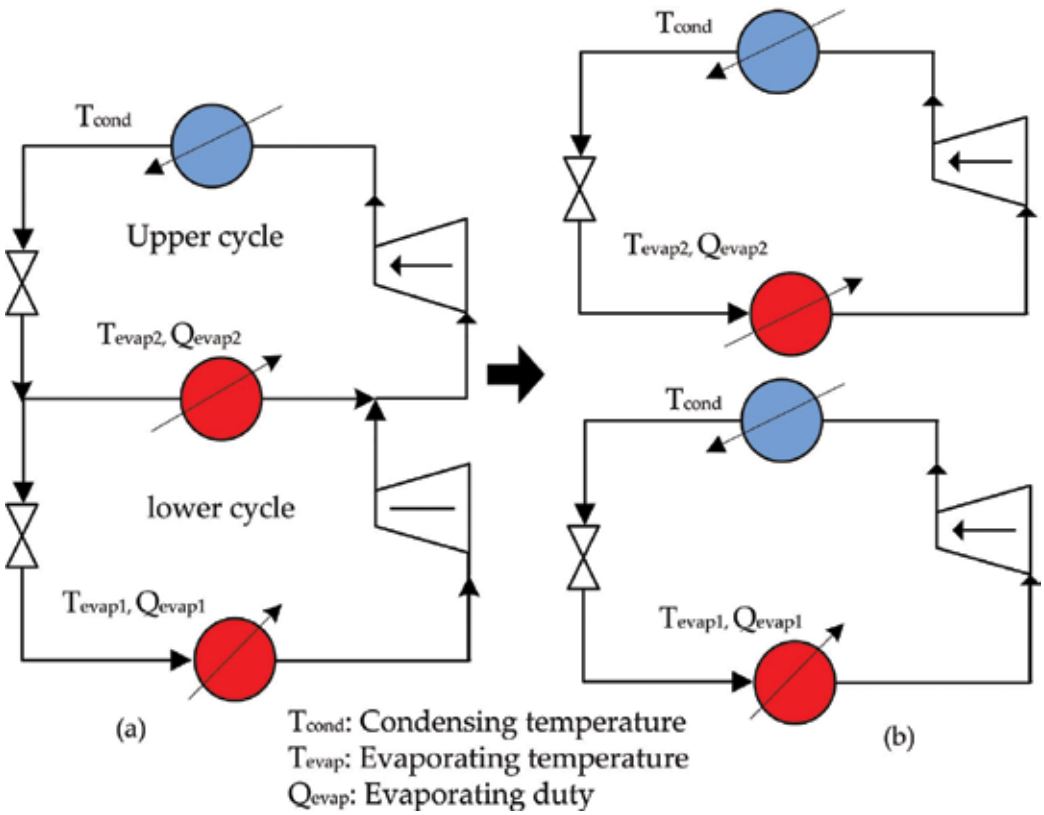

Figure 2. (a) Multi-level refrigeration cycle—two heat sources and a single heat sink; (b) decomposition into simple cycles.

multi-stage cycle with multi-refrigeration levels and a single rejection level can be decomposed into simple cycles, as shown in **Figure 2(b)**. The multi-stage cycle, such as the one shown in **Figure 2(a)**, is decomposed into two simple cycles operating in parallel. One simple cycle operates between level 1 and ambient with cooling load given by the evaporator for level 1. The other simple cycle operates between level 2 and ambient with cooling load given by the evaporator for level 2 [2].

The decomposition approach constitutes a useful for the synthesis, analysis, and design of complex refrigeration system. The main advantage of decomposing approach is that power requirement can be predicted easily using a shortcut method and various design options can be screened quickly. However, some errors might arise when the complex cycle is compared with the decomposed simple cycles. This error is caused by the mixing effects at the inlet to the compressor in the case of a cycle with multiple refrigeration levels or the inlet to the expander for a multi-rejection level cycle [9].

1.2. Thermodynamic performance of refrigeration system

The performance of a refrigeration system can be characterized by an actual coefficient of performance $\mathrm{COP_{act}}$ that is defined as the ratio of the heat absorbed Q_{evap} to the shaft work consumed W:

$$\mathrm{COP_{act}} = \frac{Q_{\mathrm{evap}}}{W} \tag{1}$$

An ideal refrigeration cycle could be based on a Carnot cycle, for which the ideal coefficient of performance $\mathrm{COP_{id}}$ can be defined by:

$$\mathrm{COP_{id}} = \frac{T_{\mathrm{evap}}}{T_{\mathrm{cond}} - T_{\mathrm{evap}}} \tag{2}$$

Where T_{evap} is the evaporating temperature (K) and T_{cond} is the condensing temperature (K).

As a rule of thumb, the shaft work can be approximately estimated with a coefficient of performance ratio, η, typically equal to 0.6 [1, 2].

$$W = \eta \frac{Q_{\mathrm{evap}}}{\mathrm{COP_{id}}} \tag{3}$$

The next section examines the possibility of using the typical value for η (0.6) to calculate the shaft work requirement of a cascade refrigeration cycle.

1.2.1. Example 1: performance and shaft work evaluation of a cascade refrigeration cycle

This example evaluates the coefficient of performance ratio and the shaft work requirement of a cascade refrigeration cycle for a range of condensing temperatures (40, 30 or 20°C), cooling duty of 523 kW, and evaporation temperature of −82°C. In the cascaded refrigeration cycle, as

shown in **Figure 1(b)**, ethylene and propylene are used in the lower and upper cycles, respectively.

In this example, the total shaft work requirement will be calculated using rigorous simulation and compared with the shaft work predicted using Carnot model (η = 0.6). Aspen HYSYS is applied for simulation of the cycles with physical properties calculated by choosing Soave-Redlich-Kwong as the fluid package. In the simulation, the partition temperature T_{part} between the two cycles is optimized to minimize the total shaft work of the cascaded cycle. T_{part} is allowed to change between the lowest temperature that the upper cycle can operate at, which is the normal boiling point for the refrigerant of the upper cycle, and the maximum temperature at which the lower cycle can reject the heat. At each partition temperature, the total shaft work of the cascaded cycles is calculated by adding the shaft work consumption of the upper cycle and the lower cycle. Then, the optimal partition temperature is identified by optimizing the shaft work as shown in **Figure 3**.

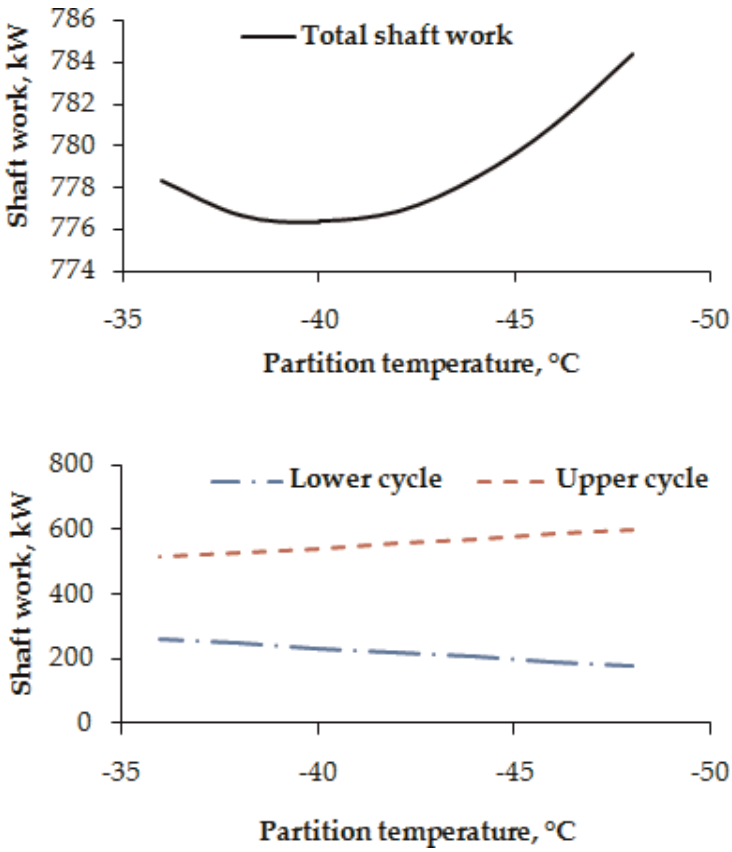

Figure 3. Calculation the optimal partition temperature of ethylene-propylene cascade cycle (T_{evap} = −82°C, T_{cond} = 40°C and Q_{evap} = 523 kW).

Q_{evap} (kW)	T_{evap} (°C)	T_{cond} (°C)	T_{part} (°C)	COP_{id}	COP_{act}	η	Shaft work (kW)		%Error
							(HYSYS)	(η = 0.6)	
523	−82	40	−40	1.57	0.67	0.43	776	556	28
		30	−44	1.71	0.79	0.46	663	510	23
		20	−47	1.88	0.92	0.49	570	464	19

Table 1. Comparison of total shaft work calculated by rigorous simulation and Carnot model using fixed value of coefficient of performance ratio, η.

Results in **Figure 3** show that the optimum partition temperature is closest to the first evaporation level of the upper cycle rather than the last evaporation level of the lower cycle; a similar conclusion was reported by Lee [8].

In **Table 1**, it may be seen that the coefficient of performance ratio (η) is below 0.6, which is the typical value for η [2]. In terms of shaft work requirement, the results in **Table 1** show that the error is significantly larger if the 'typical' ratio of 0.6 is used to predict shaft work requirement of the refrigeration cycle. Therefore, using a single value for the efficiency factor η is not the correct way to evaluate the refrigeration system performance. Section 2 proposes a new shortcut approximation of COP_{act} [3].

2. New shortcut model for refrigeration cycle

This section presents the approach that is used in building a new refrigeration model for predicting the coefficient of performance of a refrigeration cycle [3]. The first step starts with generating performance data using a rigorous simulation package, Aspen HYSYS, where it is assumed that the detailed thermodynamic and unit operation models provide a relatively realistic representation of the refrigeration cycle. Inputs to the simulation software include the refrigerant evaporating temperature, process cooling duty and refrigerant condensing temperature. Rigorous simulations of refrigeration cycles are carried out with the following assumptions: (1) Soave-Redlich-Kwong equation of state is used to calculate thermodynamic and physical properties, (2) a centrifugal compressor that has an adiabatic efficiency of 75% compresses the refrigerant, (3) let-down valves are adiabatic, (4) there is negligible pressure drop in heat exchangers and pipe work and there are no heat gains or losses, (5) the refrigerant leaves the condenser as a saturated liquid and leaves the evaporator as a saturated vapor, (6) the temperature difference between the process source stream temperature and the evaporating temperature is 5°C, and (7) the condensing temperature is variable, to account for heat rejection to ambient media or other heat sinks. The simulation outputs include the compressor power demand and the refrigerant condenser duty. The simulation is repeated for an appropriate range of operating conditions (evaporation and condensing temperatures). The inputs and outputs are then used to correlate the actual COP with the ideal COP. A simple linear relationship between COP_{id} and COP_{act} is obtained, as shown in equations below, for a simple refrigeration cycle using ethylene or propylene as a refrigerant [3].

For ethylene,

$$COP_{act} = 0.741COP_{id} - 0.81 \quad (4)$$

For propylene,

$$COP_{act} = 0.758COP_{id} - 0.747 \quad (5)$$

For ethylene-propylene cascade cycle,

$$COP_{act} = 0.596COP_{id} - 0.213 \quad (6)$$

The potential benefit of the linear model is that it is the fast and easy evaluating refrigeration power demand, as will be illustrated in the following example.

2.1. Case study 1: Evaluation of multi-level refrigeration cycles using decomposition approach and the new refrigeration model

This case explores the use of the new refrigeration model for estimating the power demand in two types of multi-level cycle, with propylene as the refrigerant. The model results will be compared with HYSYS simulation results to demonstrate the usefulness of the model for estimating the net power demand in the complex refrigeration cycles. In this work, the Peng-Robinson equation of state will be used to calculate fluid and thermodynamic properties.

2.1.1. Prediction power requirement in multi-level refrigeration cycle: two heat sources and a single heat sink

The power demand in the multi-level cycle is estimated, for the case data given in **Table 2**, by representing the multi-level refrigeration cycle as a two parallel simple cycle, as shown in **Figure 2(b)**. It is clear from the results in **Table 3** that the refrigeration model is under predicting

	Temperature (°C)	**Duty (kW)**
Heat source 1	−40	3000
Heat source 2	−12.75	3000
Heat sink	30	–

Table 2. Case data – two heat sources and one sink.

Modelling approach	**Shaft work (kW)**	**%Error**
Multi-level cycle (HYSYS)	981 + 2203 = 3184	–
Two simple cycles (shortcut model)	1937 + 922 = 2859	10
Two simple cycles (HYSYS)	1943 + 977 = 2920	8

Table 3. Predicted shaft work requirement for multi-level cycle – two heat sources and a single heat sink using HYSYS and new shortcut model [3].

the compression shaft work requirement by 325 kW. The error between the refrigeration model and HYSYS predictions for the overall shaft work is about 10%. This error occurs because of the mixing of the saturated stream from the low-pressure evaporator with the superheated compressor outlet from the low-pressure compression stage [2]. The superheated inlet conditions to the high-pressure compression stage lead to an overall increase in the power requirement when compared with two simple cycles operating in parallel, as shown in **Figure 2(b)**.

2.1.2. Prediction power requirement in multi-level refrigeration cycle: a single heat source and two heat sinks

The single heat source and two heat sinks cycle can also be presented as a two parallel simple cycle, as shown in **Figure 4(b)**. **Table 4** shows process data for the analyzed case study. The minimum approach temperature is assumed to be 3°C.

The results in **Table 5** show that the error between the power demand predicted by the proposed refrigeration model and that predicted by rigorous simulation software is about 4%. This error comes from the mixing effects at the inlet into the throttle valve, as shown in **Figure 4(a)**. However, this scale of error should be acceptable for preliminary estimation of refrigeration power consumption.

In summary, the case study shows that although there is some error associated with the decomposition approach, the refrigeration model still can predict the power demand within reasonable accuracy. The predicted power demand is shown to be within 10% of that of more accurate simulation models. The simplicity of the refrigeration model enables its use for

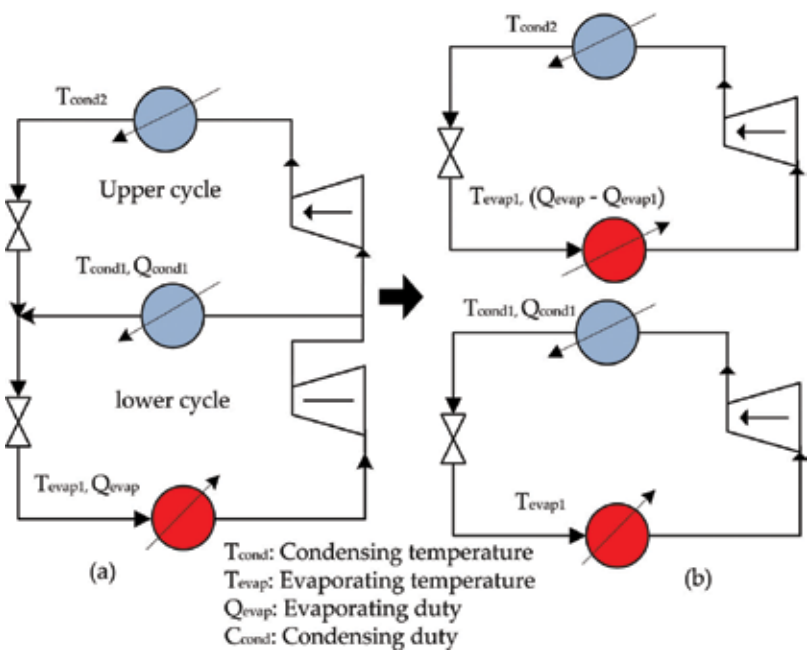

Figure 4. (a) Multi-level refrigeration cycle—a single heat source and two heat sinks; (b) decomposition into simple cycles.

	Temperature (°C)	Duty (kW)
Heat source 1	−40	3000
Heat sink 1	17	2227
Heat sink 2	37	–

Table 4. Case data – one heat source and two sink.

Modelling approach	Shaft work (kW)	%Error
Multi-level cycle (HYSYS)	1615 + 276 = 1891	–
Two simple cycles (shortcut model)	704 + 1112 = 1816	4
Two simple cycles (HYSYS)	727 + 1166 = 1893	−0.11

[1]Relative to complex cycle simulation in HYSYS.

Table 5. Predicted shaft work requirement for multi-level cycle – two heat sinks and a single heat source using HYSYS and new shortcut model[1].

optimizing the design conditions of a complex refrigeration cycle and/or the associated processing conditions, as will be seen in Section 3.

3. Heat-integrated process and refrigeration

For systems working at sub-ambient temperatures, the power demand can be very high; the lower the source temperature, the more complicated the refrigeration system design, the larger the amount of energy consumed. However, there is a great chance to reduce of the compression energy consumption if heat integration technology is applied, such that most appropriate refrigeration levels and their duties are determined to match them against grand composite curve (GCC), as shown in **Figure 5**. The GCC provides the overall source and sink temperature profiles of a process and allows the minimum hot and cold utility requirements to be identified. Also, another key feature of the GCC is that it considers the integration among the process, heat exchanger network, and refrigeration system simultaneously [8]. Therefore, in this work, the GCC has been used in the optimization approach presented in Section 3.1 to find the optimal operating conditions that minimize the compressor energy consumption.

3.1. Calculation procedure for the operational optimization of multi-level refrigeration cycles

This section describes the proposed method for the operational optimization of multi-level refrigeration cycles. In this methodology, it is assumed that the process is designed for maximum heat recovery, the refrigeration rejects the absorbed heat to external cooling utility, e.g., cooling water, the number of cooling levels is given, and the compression shaft work dominates the process economics; thus, minimization shaft power consumption in the refrigeration compressors is set as the objective for optimization.

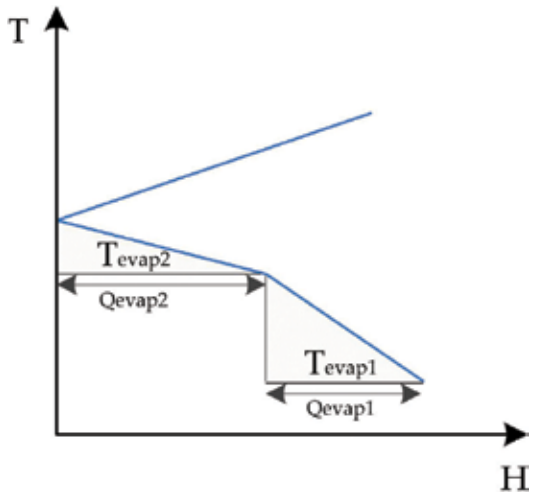

Figure 5. Matching two refrigeration levels against GCC.

The calculation procedure starts with constructing GCC, which is used to identify the total cooling duty Q_e and the lowest refrigeration temperature level. To determine the temperature level (independent variable) and the cooling duty of each level (dependent variables), the part of GCC below the pinch, which is the point where the lowest driving forces between hot and cold streams are located, is modeled as a set of linear functions,

$$H = f(T) \tag{7}$$

$$T = T_{\text{evap}} + \frac{\Delta T_{\min}}{2} \tag{8}$$

$$Q_{\text{evap}_i} = H(T_{\text{evap}_i}) - H(T_{\text{evap}_{i+1}}) \tag{9}$$

$$Q_{\text{evap}_l} = Q_e - \sum_{i=1}^{I-1} Q_{\text{evap}_i} \tag{10}$$

The second step is to decompose the complex refrigeration cycle into simple cycles. This allows the shortcut model to be used for estimating the shaft work requirement of each level. Finally, a nonlinear model is applied to find the optimal cooling temperature levels and duties of each level. The objective function is to:

$$\min\,(W) = \sum_{i=1}^{I-1} \frac{Q_{\text{evap}_i}}{\text{COP}_i}$$

Subject to:

$$\begin{aligned} & T_{\text{evap}_{i+1}} - T_{\text{evap}_i} \geq \Delta T_{\min},\ i = 1 : I-1 \\ & T_{\text{cond}} - T_{\text{evap}_l} \geq \Delta T_{\min} \\ & T^{\text{lb}}_{\text{evap}} \leq T_{\text{evap}_i} \leq T^{\text{ub}}_{\text{evap}} \end{aligned} \tag{11}$$

Where W is the net power demand of the refrigeration cycle, Q_{evap_i} is the cooling duty of ith cooling level, COP_i is the coefficient of performance which is calculated from the developed shortcut model presented in Section 3, T is the shifted temperature, $\Delta T_{\min}$ is the minimum approach temperature, T_{evap_i} is the evaporation temperature of ith cooling level, T_{cond} is the condensing temperature at which the refrigerant being condensed, I is the number of cooling levels, and lb and ub represent the lower and upper bounds, respectively.

The main features of this calculation procedure are: (1) using GCC to determine the temperature level and the duty of each stage; (2) the shaft work required of each stage calculated directly without going through the detailed refrigeration calculations or rigorous simulation; and (3) the constrained optimization problem can be solved easily using a simple optimization algorithm, such that available in MATLAB and Excel (i.e., Excel's Solver). The limitations of this approach can be summarized as follows: (1) the advantage of using economizer in minimizing shaft work consumption cannot be explored because the effect of its use cannot be represented in GCC [7], (2) only pure refrigerants are considered, and (3) heat is rejected to external utility rather than process heat sink streams, so the opportunities of the matching refrigeration system with process sink streams—which can provide significant energy savings—are missing. The implementation of the proposed optimization approach for minimizing the overall shaft work requirement of a complex refrigeration cycle is illustrated in Section 4.

4. Case study 2: cold-end process of an ethylene plant

This case aims to illustrate how the new refrigeration model can be used to estimate the power demand in a multi-level cascade cycle. A second aim is to illustrate the performance of the proposed optimization model in minimizing the net power demand.

The complex refrigeration cycle in the ethylene-propylene cascade refrigeration cycle from the cold-end process of an ethylene plant is selected for analysis. Case study data are given in **Table 6**. **Figure 6(a)** shows the process flow diagram of the ethylene-propylene cascaded refrigeration cycle. **Figure 6**(b) shows the refrigeration cycle matched against the grand composite curve of the stream data presented in **Table 6**. **Table 7** gives the corresponding cascaded refrigeration cycle details, including two propylene cooling levels in the upper cycle and three ethylene cooling levels in the lower cycle.

4.1. Prediction power requirement in multi-level refrigeration cycle

For the cascaded cycle, the low temperature cycle and the high temperature cycle are treated as individual complex refrigeration cycles. The power demand in the three-level ethylene cycle is estimated by representing the three-level refrigeration cycle as a three parallel simple cycle. The power demand in the high temperature cycle is estimated by representing the two-level refrigeration cycle as a two parallel simple cycle. The refrigerant data in **Table 7** are used in the refrigeration model to predict the power demand at each compression stage.

	Supply temp. (°C)	Target temp. (°C)	Duty (kW)
H1	−14	−15	3780
H2	−22	−23	15,911
H3	27	−95	18,985
C1	23	78	7296
C2	7	8	3634
C3	−1	0	14,651
C4	−27	23	6373
C5	−27	23	185

Table 6. Process stream data for case study 2 [10].

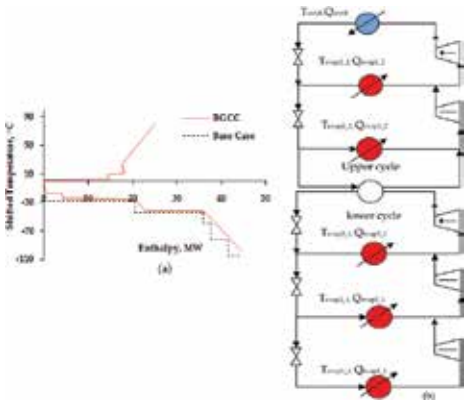

Figure 6. Balanced grand composite curve for case study 1 (a) and its refrigeration cycle (b).

	Temperature (°C)	Duty (kW)
Ethylene refrigeration level 1	−104.1	3113
Ethylene refrigeration level 2	−82.9	3890
Ethylene refrigeration level 3	−58.3	1713
Propylene refrigeration level 1	−44	15,395
Propylene refrigeration level 2	−28	20,482

Table 7. Refrigerant data for ethylene-propylene cascade refrigeration cycle.

For the purpose of comparison, the refrigeration cycle was also simulated in HYSYS software. The fluid package chosen in the simulator for determining thermodynamic properties was the Peng-Robinson equation of state. In this case, it is assumed that the compression efficiency is 80% and all the absorbed heat is rejected to cooling water at 23°C. Also, for the heat exchangers, a 5°C minimum temperature approach is specified, while it is assumed that there

is no pressure drop in both heat exchangers and piping [10]. The partition temperature, which is the temperature of the evaporator of the upper cycle, was set at −44°C.

Table 8 presents the results of the predicted power demand for complex cycle using HYSYS and the new refrigeration model. The error between the refrigeration model and HYSYS predictions for net power demand prediction is about 10% in the lower cycle and −2% in the upper cycle. As can be seen from the HYSYS simulation results for the three parallel cycles, this error arises mainly from the mixing effect at the inlet to the compressor.

4.2. Optimization operating conditions in multi-level refrigeration cycle

This section only explores the optimization of the evaporating temperatures in the lower refrigeration cycle presented in **Figure 6**(**b**). This is because the temperature differences between the heat source temperature profile of the process (i.e., the GCC) and the evaporation temperature of refrigeration levels in the upper cycle are small, as shown in **Figure 6**(**a**). This small temperature difference leads to slight improvement on the energy efficiency of the upper cycle [10].

In this work, the deterministic method (generalized reduced gradient (GRG)) will be used to search for the optimal solution of the objective function. In order to test the prediction accuracy of the proposed method, the results of the proposed method will also be compared with the published results of Oh et al. [10], in which genetic algorithm (GA) was employed to search for the optimal operating conditions of multi-level refrigeration cycle.

The decision variables manipulated for the optimization and the upper and lower bounds are listed in **Table 9**.

The optimal results for the three-level refrigeration cycle using ethylene as a refrigerant are summarized in **Table 10**. The results show that a significant decrease in the overall compression duty of the refrigeration cycle (9%) over the base case is obtained due to the reduction of the temperature lift (the temperature difference between the evaporator and condenser).

Low temperature cycle		
Modeling approach	**Power demand (kW)**	**Error**
Complex cycle (HYSYS)	780 + 1794 + 1615 = 4189	–
Three simple cycles (shortcut model)	2794 + 1620 + 230 = 4644	−10.8%
Three simple cycles (HYSYS)	2393 + 1541 + 228 = 4161	0.67%
High temperature cycle		
Complex cycle (HYSYS)	4218 + 21,810 = 26,028	–
Two simple cycles (shortcut model)	17,863 + 8669 = 26,532	−2%
Two simple cycles (HYSYS)	17,362 + 8656 = 26,018	0.04%

Table 8. Predicted power demand for cascade cycle using HYSYS and new model.

Decision variable	Lower bound	Upper bound
T_{evap_2}	−91.45	−66.13
T_{evap_3}	−76.32	−46.19

Table 9. Optimization variables and their constraints for case 2.

Low temperature cycle		Base case	Optimized case	
			Oh et al. [10] (Complex cycle)	This work (Three simple cycle)
Level 1	Pressure (kPa)	101.3	127.7	127.7
	Temperature (°C)	−104	−100	−100
	Cooling duty (kW)	3113		2221
	Shaft power (kW)	780		1717
Level 2	Pressure (kPa)	300	288.4	264.3
	Temperature (°C)	−82.9	−84.89	−85.67
	Cooling duty (kW)	3890		2847
	Shaft power (kW)	1794		1333
Level 3	Pressure (kPa)	800	649.1	574.8
	Temperature (°C)	−58.3	−66.62	−67.31
	Cooling duty (kW)	1713		3648
	Shaft power (kW)	1615		829
Net power demand (kW)		4189	3560	3828
Saving relative to base case (%)		—	15	9

Table 10. Comparison between the optimization results of the proposed model and the published results [10].

It is clear from the results that GRG has good performance (in terms of getting closer to the optimal solution) and less computationally expensive compared to GA. The results in **Table 10** show that insignificant difference between the results from the proposed model and those obtained from the published results of Oh et al. [10], where the deviation between the results is only 1% both for the evaporation temperature of cooling level 2 and for the evaporation temperature of cooling level 3. The differences between the results of the proposed model and those of Oh et al. [10] are mainly due to using the decomposition approach, which is used to predict the coefficient performance of the refrigeration cycle.

5. Conclusions

This chapter introduces a new refrigeration model and proposes a systematic methodology for operational optimization of multi-level refrigeration cycle. The methodology applies NLP model to minimize the overall power demand of the refrigeration cycle and uses GCC and

linear refrigeration model that is based on regression from rigorous simulations. The GCC is used to obtain cooling duty of each level, while the linear refrigeration model is used to predict the actual coefficient performance of the complex refrigeration cycle that is decomposed into assembly simple cycles. The refrigeration model requires only condensing and evaporating temperatures. The effectiveness of the proposed optimization approach has been demonstrated on the case study of its application to ethylene cold-end process. The results of the case study demonstrate that the refrigeration model can predict the power demand within 10% of rigorous simulation. The optimization algorithm can find a close optimum solution within very short time (less than a second). Also, the results reveal that 9% saving in shaft power demand can be achieved by optimizing the operating conditions. The difference between the optimal operating conditions (i.e., the evaporation temperatures) found by GA and GRG is 1%. Although these findings support the validity of the refrigeration model, and the reliability and computational efficiency of the optimization approach in finding a close optimal solution, there are some factors that need to be considered in the future. These factors include the trade-offs between capital and operating costs, the opportunities for rejecting heat to a cold heat sink within the process rather than an external cooling utility, and the use of mixed refrigerant (the advantage of using mixed refrigerant can be explored by using a refrigeration database that includes the power demand at various operating conditions).

Author details

Asma Etoumi

Address all correspondence to: etomi2006@yahoo.com

Libyan Petroleum Institute, Tripoli, Libya

References

[1] Dimian MC. Integrated Design and Simulation of Chemical. 1st ed. Amsterdam, the Netherlands: Elsevier; 2003. 698 p. DOI: 10.1016/S1570-7946(03)8002-6

[2] Smith R. Chemical Process Design and Integration. 1st ed. Chichester, UK: John Wiley and Sons, Ltd; 2005. 714 p. DOI: 10.1012/ie0496131

[3] Etoumi A, Jobson M, Emtir M. Shortcut model for predicting refrigeration cycle performance. Chemical Engineering Transactions. 2015;**45**:217–222. DOI: 10.3303/CET1545037

[4] Tahouni N, Bagheri N, Towfighi J, Panjeshahi MH. Improving energy efficiency of an olefin plant: A new approach. Energy Conversion and Management. 2013;**76**:453–462. DOI: 10.1016/j.enconman.2013.07.066

[5] Branan CR. Rules of Thumb for Chemical Engineers: A Manual of Quick, Accurate Solutions to Everyday Process Engineering Problems. 4th ed. Burlington, USA: Gulf Professional Publishing; 2005. 496 p. DOI: 10.1016/B978-075067856-8/50011-6

[6] Shelton MR, Grossmann IE. A shortcut procedure for refrigeration systems. Computers and Chemical Engineering. 1985;**9**(6):615–619. DOI: 10.1016/0098-1354(85)87017-4

[7] Montanez-Morantes M, Jobson M, Zhang N. Operational optimization of centrifugal compressors in multilevel refrigeration cycles. Computers and Chemical Engineering. 2016;**85**:188–201. DOI: 10.1016/j.compchemeng.2015.11.006

[8] Lee GC. Optimal design and analysis of refrigeration systems for low temperature processes [dissertation]. UK: The University of Manchester; 2001. 186 p

[9] Wang J. Synthesis and optimization of low temperature gas separation processes [dissertation]. UK: The University of Manchester; 2004. 236 p

[10] Oh JS, Binns M, Park S, Kim JK. Improving the energy efficiency of industrial refrigeration systems. Energy. 2016;**112**:826–835. DOI: 10.1016/j.energy.2016.06.119

Chapter 2

Electrocaloric Cooling

Gunnar Suchaneck, Oleg Pakhomov and Gerald Gerlach

Additional information is available at the end of the chapter

http://dx.doi.org/10.5772/intechopen.68599

Abstract

The *electrocaloric effect* describes a reversible temperature change in dielectric materials submitted to an applied electric field. Adiabatic polarization raises their temperature, and adiabatic depolarization lowers it, analogous to temperature changes that occur when a gas is compressed or expanded. For refrigerator application, the reverse Brayton cycle is currently the most promising for practical implementation. The electrocaloric effect provides a large material efficiency. However, existing refrigerator prototypes lack from the absence of efficient heat switches for thermal linkage to the load and the heat sink. Cooling power densities of a few W/cm^2 and temperature spans in the order of 20 K (in regeneration systems) are achievable at a cycle time of 100 ms.

Keywords: electrocaloric effect, thermodynamic cycles, coefficient of performance, refrigeration devices

1. Introduction

For almost 150 years, refrigeration applications were solved by means of vapour compression. While the most efficient fluids for this approach are based on chlorofluorocarbons, hydrochlorofluorocarbons and hydrofluorocarbons, they come with the severe drawback of contributing to global warming and ozone depletion. Therefore, in 1987, the Montreal Protocol issued a ban on these chemicals providing regulations for phasing them out. Promising natural alternative substances are impractical due to their toxicity (ammonia) or—in particular—their flammability (propane) [1].

Vapour compression refrigerators (VCRs) are operated as reverse Rankine cycles. They use a circulating liquid refrigerant as a medium. The refrigerant is: (i) adiabatically compressed, (ii) condensed at constant pressure undergoing a phase transition (thereby rejecting heat to the heat sink), (iii) adiabatically throttled in an expansion valve and (iv) evaporated at constant

pressure undergoing the reverse phase transition (thereby absorbing heat from the load). The amount of transferred heat is determined by the latent heat of the first-order phase transition. Similarly, in solid-state electrocaloric (EC) cooling, the adiabatic compression/expansion of the refrigerant is analogous to adiabatic polarization/depolarization, while the isobaric processes are replaced by isofield ones. Contrary to VCR, where the adiabatic expansion of the vapour is thermodynamically irreversible, the EC and the magnetocaloric (MC) effects are thermodynamically reversible processes that could reach the limit of the Carnot efficiency. This is another aspect making them promising for future application.

Electric fields required for the EC refrigeration cycle can be supplied much easier and less expensively than the high magnetic fields required for the MC refrigeration [2]. Other advantages in comparison with MC cooling are higher power densities due to potentially higher cycle frequencies, smaller mass of the device, compactness, potential cost reduction, independence on risks of rare-earth materials supply, etc. [3]. Moreover, electrical energy for EC cooling can be provided by stationary or mobile solar cells and by electric vehicle batteries. This opens up completely new possibilities for an environment-friendly industrialization of developing countries.

EC materials provide a solid-state cooling technology without polluting liquid refrigerants and no or almost absent moving parts (pump and motion of a pumped heat transfer fluid). Generally, EC material (refrigerant) converts the electrical input work

$$W = \int E dD, \tag{1}$$

into cooling or heating. Here, E is the electric field and D is the dielectric displacement. The latter is a vector field describing the electrical effect of free and bound charges in materials. Compared to VCR, the E plays the role of pressure and D plays the role of volume in vapour compression.

More detailed descriptions can be found in a number of recent reviews of the EC effect [2, 4, 5] and its application in refrigerators [3, 6, 7], and a book on this topic [8].

2. Electrocaloric effect

An electric field E applied to a dielectric material induces a change in dielectric displacement and, thus, a change in temperature and entropy in the material. The EC effect is a reversible temperature change of a material that results from an adiabatic application of an electric field. It was derived by Lord Kelvin based on the assumption of reversibility of the pyroelectric effect from thermodynamics in 1878 [9]: *If the preceding explanation of pyroelectricity be true, it must follow that a pyroelectric crystal moved about in an electric field will experience cooling effects or heating effects … in virtue of the wholly latent electric polarity of a seemingly neutral pyroelectric crystal (that is to say, a crystal at the surface of which there is an electrification neutralizing for external space the force due to its internal electric polarity), the same cooling and heating effects will be produced by moving it in an electric field, as similar motions would produce in a similar crystal which, by having been heated in hot water, dried at the high temperature, and cooled, is in a state of pyroelectric excitement*.

The first experimental investigations of the EC effect in Rochelle salt, KH_2PO_4, $BaTiO_3$ and $SrTiO_3$ date back to 1930 [10], 1950 [11], 1952 [12] and 1956 [13], respectively. However, the EC effect values reported since that time (at maximum 2.5 K in $Pb_{0.99}Nb_{0.02}(Zr_{0.75}Sn_{0.20}Ti_{0.05})O_3$ ceramics [14]) were too small for practical use.

EC cooling has regained attention in 2006, when Mischenko et al. could show that large electrical fields can be applied to antiferroelectric $PbZr_{0.95}Ti_{0.05}O_3$ thin films [15]. They observed that—close to the ferroelectric Curie temperature of 222°C—a field change from 77.6 to 29.5 V/μm induced an adiabatic temperature change of 12 K as it was determined from the integrated pyroelectric effect. Recently, another group showed that a lead-free stack of 63 $BaTiO_3$ thick films provides an EC temperature change of 7.1 K at an applied field of 80 V/μm [16]. The thickness of the individual layers deposited by tape casting and electrically contacted by inner Ni electrodes amounted to ca. 3 μm. In Ref. [17], commercially available multilayer capacitors (MLCs) even of 200 ceramic layers ($BaTiO_3$-based Y5V formulation) each 6.5 μm in thickness were used as a refrigerant [17]. Here, an EC temperature change of 0.5 K was obtained at 30 V/μm. The MLC concept was developed by Herbert [18] and introduced in the early 1980s by Murata Manufacturing Co. for the fabrication of base metal monolithic capacitors [19]. MLCs are now in mass production (some 5×10^{11} pieces per year) by means of sheeting green ceramic tapes and screen-printing technology [20]. However, they are not optimized for EC applications. Commercial EC devices are still not available.

EC devices are driven by an electric field strength. That means that a voltage has to be applied. In this case, the independent thermodynamic parameters are temperature T and electric field E. According to the second law of thermodynamics, an infinitesimal amount of heat dQ transferred into the system by an entropy change dS is then given by

$$dQ = TdS = T\left[\left(\frac{\partial S(E,T)}{\partial T}\right)_E dT + \left(\frac{\partial S(E,T)}{\partial E}\right)_T dE\right], \tag{2}$$

where S is the entropy per unit volume. Following the definition of volumetric specific heat at constant E, c_E, the first term in parentheses can be replaced by

$$\left(\frac{\partial S(E,T)}{\partial T}\right)_E = \frac{c_E(E,T)}{T}. \tag{3}$$

The value of $c_E(E,T)$ is usually represented by the zero-field value in the temperature range of interest $c = c(T)$. With regard to Maxwell´s equations, entropy S and dielectric displacement D are coupled [21]

$$\left(\frac{\partial S}{\partial E}\right)_T = \left(\frac{\partial D}{\partial T}\right)_E = \pi_E, \tag{4}$$

where π_E is the pyroelectric coefficient at constant electric field. Considering now a ferroelectric material exhibiting below T_C a remnant polarization P_r and an induced polarization $\varepsilon\varepsilon_0 E$, and a dielectric displacement of

$$D(T,E) = \varepsilon_0 \varepsilon(T,E)E + P_r(T), \tag{5}$$

Eq. (2) takes the form:

$$dQ = c_E dT + T\left(\frac{\partial P_r(T)}{\partial T} + \varepsilon_0 E \frac{\partial \varepsilon(T,E)}{\partial T}\right)_E dE. \tag{6}$$

Thus, the EC temperature change is given by two terms [22]:

$$\Delta T_{EC} = -\frac{T}{c_E}\int_{E_1}^{E_2}\left(\frac{\partial P_r(T)}{\partial T} + \varepsilon_0 E \frac{\partial \varepsilon(T,E)}{\partial T}\right)_E dE. \tag{7}$$

In the ferroelectric phase, below T_C, the contributions of spontaneous and induced polarization partially compensate each other, because in this temperature region the temperature coefficients behave oppositely: $\partial\varepsilon/\partial T > 0$ and $\partial P_r/\partial T < 0$. In $SrTiO_3$ ceramics below the temperature of maximum dielectric permittivity, in antiferroelectrics with $\langle P_r \rangle = 0$, and in some relaxors with $\partial Pr/\partial T > 0$, a negative electrocaloric effect can be obtained below T_C, that is, the sample is cooled during adiabatic electric field application.

Figure 1 compares the ΔT_{EC} values of $BaTiO_3$ above T_C ($P_r \rightarrow 0$) calculated from Eq. (7) [23] with available experimental data [12, 16, 24, 25]. Well-known examples of EC materials driven above the temperature of maximum dielectric permittivity are polyvinylidene fluoride terpolymers and irradiated copolymers, both exhibiting relaxor behaviour. Here, assuming a dielectric permittivity

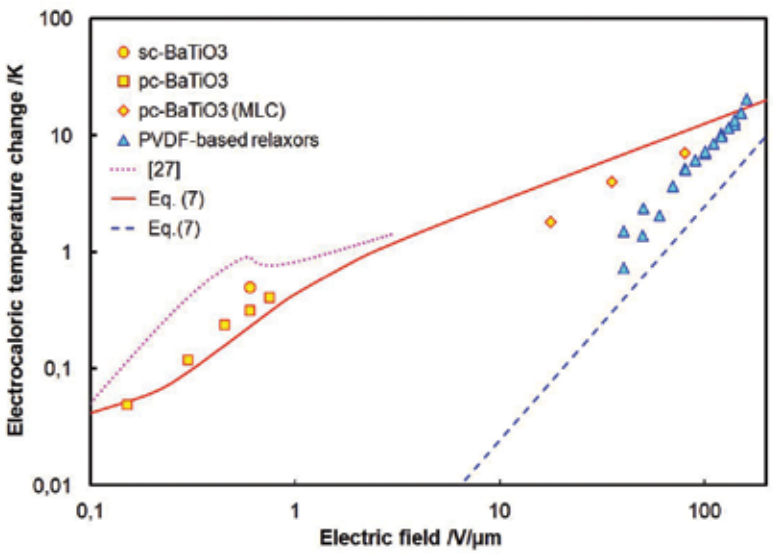

Figure 1. ΔT_{EC} of $BaTiO_3$ [23] (solid line) and PVDF-based relaxor polymers (dashed line) as a function of E calculated for $P_r = 0$ following Eq. (7) in comparison to ΔT_{EC} determined along the coexistence curve of the ferroelectric-paraelectric phase transition [27]. Experimental data of single crystal (sc), polycrystalline (pc) $BaTiO_3$, and PVDF-based polymers were taken from Refs. [12, 16, 24, 25, 28], respectively.

independent on electric field, our calculations revealed that suitable for application ΔT_{EC} values appears only at large electric fields. This is a problem since rapidly rising electric fields favour electrical breakdown of polymers. Moreover, the field dependence of ΔT_{EC} is very different to $BaTiO_3$, but similar to relaxor PLZT in Ref. [26].

In the presence of a first-order phase transition induced by an electric field $E_{PT} < E_2$, an additional entropy ΔS_{PT} change occurs at the phase transition temperature T_{PT} which is originated from the latent heat L

$$\Delta S_{\mathrm{PT}} = \frac{L}{T_{\mathrm{PT}}}. \tag{8}$$

Along the coexistence curve between two phases of the considered constituent, E is no longer an independent parameter. Therefore, it should be substituted by D. The slope of the coexistence curve on the E-T diagram is then given by the Clapeyron equation [29]

$$\frac{dE_{PT}}{dT} = \frac{\Delta S_{PT}}{\Delta T} = \frac{L}{T\Delta D}. \tag{9}$$

In the case of ferroelectrics, where dielectric displacement D approximately equals the polarization P, this yields a ΔT_{EC} of [4]

$$\Delta T_{\mathrm{EC,PT}} = \frac{T}{c_p} \cdot \frac{dE_{\mathrm{PT}}}{dT} \cdot \Delta P, \tag{10}$$

where ΔP is the jump of polarization at the phase transition, and c_P is the volumetric-specific heat at constant P. **Table 1** lists the Clausius-Clapeyron contribution to the EC effect of some typical ferroelectrics.

The EC effect of a first-order phase transition increases along the coexistence curve up to the tricritical point. With further increase of the applied field, it decreases it again [27]. Thus, the Clausius-Clapeyron contribution is substantial only for bulk ceramic-based EC devices driven at moderate electric fields.

Considering the entropy change $\Delta S = S(0, T) - S(E, T)$ for a system of N dipolar entities, each having Ω discrete equilibrium orientations, a physical upper bound on the EC effect was derived in Ref. [35]:

$$\Delta T_{\mathrm{EC,max}} = \frac{T \cdot ln\Omega}{3\varepsilon_0 \cdot c \cdot C_{\mathrm{CW}}} P_s^2, \tag{11}$$

where C_{CW} is the Curie-Weiss constant and P_s the polarization at saturation when all dipoles are aligned along the field. Values of P_s might be obtained from hysteresis loops in the saturation regime. Values of C_{CW} can be derived from the asymptotic behaviour of the linear dielectric susceptibility in a Curie-Weiss-plot $\varepsilon \propto C/(T - T_0)$ with $T_0 < T_C$. T_0 is the Curie-Weiss temperature, i.e. the temperature of the appearance of a metastable paraelectric phase in the ferroelectric one. The upper limit $\Delta T_{\mathrm{EC,max}}$ of lead-based relaxors estimated in this manner

Composition	T_{PT}, °C	$\Delta T_{EC,PT}$, °C	Ref.
$PbTiO_3$	493	10	[4]
$KNbO_3$	435	6	[4]
$PbZrO_3$	230	13	[4]
$Pb(Zr_{0.95}Ti_{0.05})O_3$	230	12	[4]
$Pb_{0.99}Nb_{0.02}(Zr_{0.75}Sn_{0.20}Ti_{0.05})O_3$	163	3.0	[4]
[111] $0.705PbMg_{1/3}Nb_{2/3}O_3$-$0.295PbTiO_3$	127	0.55	[4]
$BaTiO_3$	120	1.5	[4]
P(VDF-TrFE)68/32	~105	~12	[30] (Suppl.)
P(VDF-TrFE)65/45	81	9.5	[8], p.112
P(VDF-TrFE)55/45	~65	~4[1]	[30] (Suppl.)
$0.87PbMg_{1/3}Nb_{2/3}O_3$-$0.13PbTiO_3$	18	0.2	[31]
$0.9PbMg_{1/3}Nb_{2/3}O_3$-$0.1PbTiO_3$	5	0.8	[32, 33]
$PbSc_{0.5}Ta_{0.5}O_3$	2	1.6	[4]
$0.95PbMg_{1/3}Nb_{2/3}O_3$-$0.05PbTiO_3$	−28	0.13	[33, 34]
[111] $PbMg_{1/3}Nb_{2/3}O_3$	−55	0.33	[34]
$NH_4H_2PO_4$	−123	8.2	[4]
KH_2PO_4	−153	0.7	[4]

[1]Calculated using Eq. (12).

Table 1. EC temperature change corresponding to the latent heat calculated using Eqs. (9) or (10) from experimental values.

amounts to about 10 K. The EC temperature of a first- or second-order phase transition deduced from the specific heat curves yields:

$$\Delta T_{EC} = \int_{T_1}^{T_2} \left[\frac{c_p(T)}{c_p^{ph}(T)} - 1 \right] dT, \tag{12}$$

where $c_p{}^{ph}$ is the portion of volumetric-specific heat at constant pressure p due to lattice vibrations. For a second-order phase transition in PZT thin films, ΔT_{EC} amounts to 4.0–5.3 K at 665 K [36]. A phase-transition independent upper bound of the EC effect was proposed in Ref. [37] based on the fact that only a certain energy density might be stored in a dielectric—equivalent to a limit in electrostatic pressure. Electrical breakdown of metal oxide dielectrics is fixed by the arising local electric field and the chemical bond strength leading to $E_{max} \propto \varepsilon^{-1/2}$, with E_{max} the dielectric strength of the EC material [38]. According to Eq. (7), this results for $P_r \rightarrow 0$ in:

$$\Delta T_{EC,max} < -\frac{\varepsilon_0 T}{2c} \cdot \frac{1}{\varepsilon(0,T)} \frac{\partial \varepsilon(0,T)}{\partial T} \cdot \varepsilon(0,T) E_{max}^2. \tag{13}$$

For a relaxor ferroelectrics exhibiting a huge temperature dependence of dielectric permittivity $\frac{1}{\varepsilon(0,T)} \frac{\partial \varepsilon(0,T)}{\partial T} \approx 10^{-2} K^{-1}$ [39], we estimate an ultimate EC temperature change of $\Delta T_{EC,max} \approx 50 K$.

Our estimation explains the high values of the EC effect previously obtained in relaxor lead-lanthanum zirconate-titanate thin films [26].

3. Thermodynamic cycles

3.1. Carnot cycle

An EC refrigerator working under the Carnot cycle will reach the highest efficiency possible. The Carnot cycle describes a reversible change of an ideal gas, which allows to convert a given amount of thermal energy into work, or, conversely, to provide cooling using a given amount of work. It consists of four steps of operation: two adiabatic and two isothermal ones. During the adiabatic steps, no heat is transferred while the refrigerant absorbs heat from the load at its minimum temperature and expels heat to the heat sink at its maximum temperature in the isothermal steps.

The EC Carnot cycle is demonstrated in **Figure 2**. The cycle starts from point 1 where the electric field on the EC material is E_1. In steps 1–2, the electric field is increased adiabatically to E_3. Here, the entropy of the EC material stays constant, and therefore, the temperature increases. At point 2, the EC material starts to experience an isothermal process. The electric field will be increased until it reaches its maximum value E_4 at point 3. In order to conserve isothermal conditions, heat should be simultaneously rejected to the heat sink. In the adiabatic steps 3–4, the electric field is decreased to E_2 while the temperature of the EC material decreases until reaching point 4. In the second isothermal steps 4–1, the electric field decreases to E_1 while heat should be absorbed from the load. Thus, the Carnot cycle requires a minimum of four different electric fields. Since the heat rejected to the heat sink amounts to $Q = T_1 \Delta S$, the cooling power depends significantly on the chosen working point (cf. cycles 1-2-3-4 and 5-6-7-8).

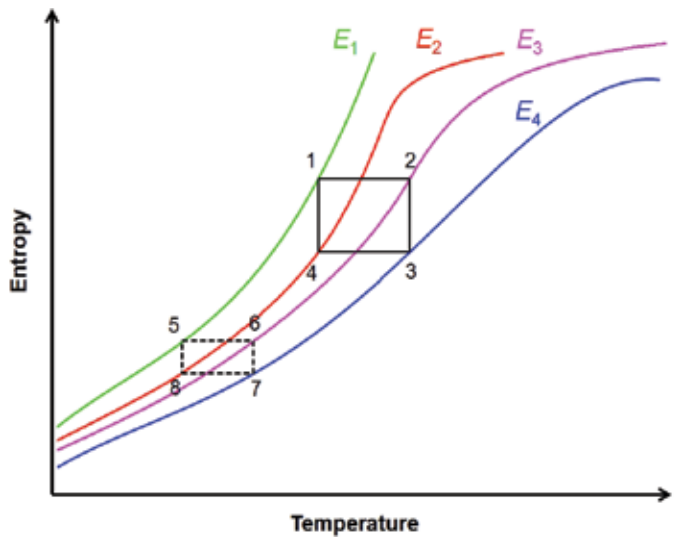

Figure 2. Reverse Carnot cycle for EC refrigeration.

The implementation of the Carnot cycle into a practical refrigeration system is challenging, since the isothermal steps and the transition from an adiabatic process to an isothermal one are not easy to realize. In the two isothermal steps, the refrigerant is in thermal contact with the load or the heat sink, respectively. Here, the rate of electrical field change is limited by the relatively large thermal relaxation time of the thermal interfaces (heat switch or heat transfer agent) of the system. This significantly lowers cycle time. Moreover, the maximum temperature span $T_{span} = T_l - T_s$ of the whole refrigerator will be less than the ΔT_{EC} of the EC material. On the one hand, a small temperature span provides large cycle efficiency (cf. Eq. (14)). The temperature span $T_l - T_s$ might be increased by means of a cascaded structure of m units where the unit n ejects heat to unit $n + 1$, while this unit absorbs heat from unit n ($1 < n < m$) covering the desired $T_l - T_s$. Such a cascade system does not require large ΔT_{EC}. However, in order to reach high efficiency, the heat ejected from the previous step should be completely absorbed by the following step. In general, since the EC-induced entropy change is not a constant, and the specific heat of the EC material also changes with temperature, this requirement is hard to meet. Consequently, the performance of the cascaded refrigerator is further reduced.

The coefficient of performance *COP* is defined as the ratio between the useful heating or cooling provided to work required. Considering an ideal Carnot cycle, the corresponding COP_C can be written as

$$COP_C = \frac{T_s}{T_l - T_s}, \tag{14}$$

where T_s and T_l indicate the temperature of heat sink and load, respectively. COP_C establishes an upper bound for the *COP*. Since the EC effect is a thermodynamically reversible process, EC refrigerators could reach the limit of the Carnot efficiency. The relative efficiency of a refrigerator with respect to an ideal Carnot cycle is defined as

$$\Phi = \frac{COP}{COP_C}, \tag{15}$$

where Φ is determined by the EC material hysteresis, the heat losses of the heat transfer processes through heat switches or a regenerator, the thermal resistance of the heat switches, the regenerator efficiency (the ratio of actual heat exchange in the regenerator to an ideal one), the heat flow from the environment to the load, the deviation of the isothermal steps from the ideal case, Joule heating at the contacts, etc. The total efficiency is then the product of separate efficiency coefficients. The current state-of-the-art commercial vapour compression cycle has a *COP* of about 3.6 [7].

3.2. Alternative refrigeration cycles

Similar to MC cooling, also alternative refrigeration cycles might be employed for EC refrigeration. The Stirling and Ericsson cycles were considered in Ref. [40]. The Stirling refrigeration cycle consists of two isothermal and two isopolarization steps, while the Ericsson refrigeration cycle consists of two isothermal and two isofield steps. The heat is released and absorbed in the two

http://dx.doi.org/10.5772/intechopen.68599

isothermal steps. In the Stirling cycle, polarization would change during heating and cooling due to a strong temperature dependence of the dielectric permittivity of polar dielectrics. Therefore, this cycle is not suitable for EC refrigeration from an experimental point of view. The Ericsson cycle is more readily applicable than other thermodynamic cycles such as the Stirling cycle. An isofield condition is easily realized keeping the EC material connected to the voltage source. The Ericsson cycle requires heat regeneration, i.e. the heat rejected from the hot refrigerant is intermittently stored in a thermal transfer medium, before it is transferred to the cool refrigerant. The efficiency of the regenerator is significantly affected by the heat transfer conditions (heat transfer surface, heat transfer coefficient, boundary layers, heat conduction, fluid viscosity, etc.). Generally, the coefficient of performance of a ferroelectric Ericsson refrigeration cycle is smaller than that of a Carnot cycle for the same temperature range [40].

The Olsen cycles was proposed for application in pyroelectric energy harvesting [41]. Therefore, it will not be considered in this work. It replaces adiabatic polarization and depolarization of a ferroelectric by corresponding isothermal steps.

A gas refrigeration cycle where a gas is compressed and expanded, but does not change phase, is called Bell-Coleman cycle. It consists of two adiabatic (compression and expansion) and two isobaric processes (heat addition and heat rejection). This cycle corresponds also to the reverse Brayton cycle widely used for subcooling in the liquid nitrogen industry. For EC refrigerators, even the reverse Brayton cycle is predominantly chosen [42–44]. It includes the following steps (**Figure 3**):

1. Adiabatic polarization by increasing the electric field to a value E_2, the EC material experiences EC heating ($+\Delta T_{EC}$).

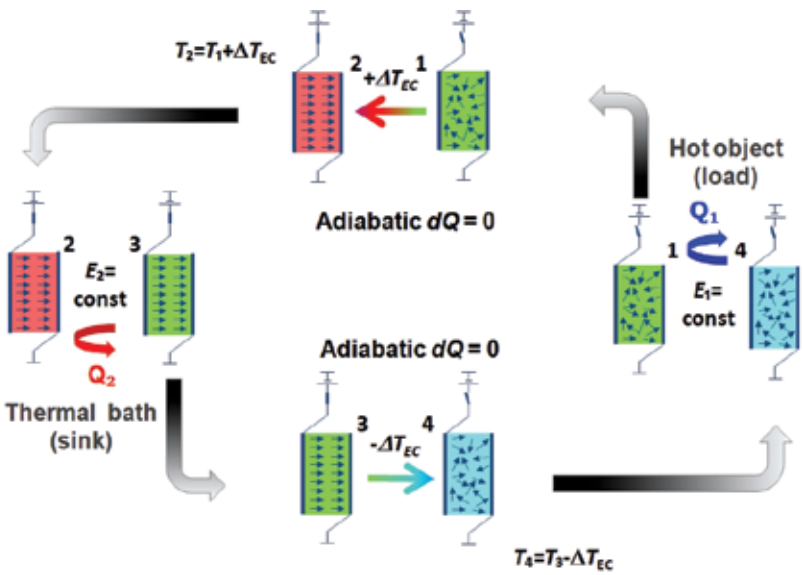

Figure 3. Reverse Brayton cycle for EC refrigeration.

2. Heat rejection: heat rejection to a heat sink under a constant electric field E_2.
3. Adiabatic depolarization by decreasing the electric field to a value E_1, e.g. zero, the material experiences EC cooling by $(-\Delta T_{EC})$.
4. Heat absorption from a load under the constant electric field E_1 returning to the initial state.

The amount of heat transferred from the load to the heat sink per cycle and per unit volume is given by

$$q = c(E_2) \cdot (T_2 - T_3), \tag{16}$$

where $c(E_2)$ is the volumetric-specific heat at $E = E_2$. The cooling power is then $\langle \dot{q} \rangle = q/\tau_c$ with τ_c the cycle time. The difference between the Brayton and Ericsson cycles is that the Brayton cycle uses adiabatic steps instead of using isothermal ones. Compared to the Carnot cycle, the mean temperature during heat rejection to the heat sink will be less than T_2, whereas the mean temperature during heat absorption from the load is higher than T_4. For an ideal gas and a specific heat independent on temperature, the relative refrigerator efficiency amounts to $\Phi \approx 1/4$ [45]. Ferroelectrics themselves exhibit a strong temperature dependence of the volumetric-specific heat, particularly in the vicinity of the ferroelectric-paraelectric phase transition. The relative refrigerator efficiency then comes out as

$$\Phi = \frac{c(E_2)(T_3 - T_2)}{c(E_1)(T_4 - T_1) - c(E_2)(T_3 - T_2)}. \tag{17}$$

This means that it is determined by the ratio $c(E_1)/c(E_2) > 1$. Consequently, it leads to $\Phi < 0.25$. Here, Φ is also largely affected also by the ratio of T_{span} to ΔT_{EC}, i.e. $(T_2 + T_3)/2 \sim \Delta T_{EC}$, which are functions of the EC material, the EC element design and the thermal interfaces. However, this estimation does not account for the losses described in detail below. With regard to losses, Φ is limited to a value of approximately 10–15%, which is comparable to thermoelectric energy converters. Efficiencies of $\Phi \geq 0.5$ have been reported in literature for a micro-EC cooling module comprising a micro-electromechanical heat switch [46], a chip scale EC oscillatory refrigerator (ECOR) [28] and a EC refrigerator with intrinsic regenerator [47]. It seems that such a Φ value originates from unreasonably large values of $COP > 8$.

Considering only heat losses caused by heat switches, the maximum relative efficiency of EC refrigerators is given by [48]

$$\Phi_{switch} = \left(\frac{\sqrt{K} - 1}{\sqrt{K} + 1} \right)^2, \tag{18}$$

where $K = \kappa_{on}/\kappa_{off}$ is the conductivity contrast of the heat switches and, κ_{on} and κ_{off} are the thermal conductivities of the heat switch in the on and off states, respectively. Thus, if $K > 10$, then EC cooling exceeds the efficiency of thermoelectric cooling. For $K > 100$, it offers an

efficiency comparable to magnetic cooling (about 70%) with much smaller and cheaper equipment. With regard to the thermal conductivity of the EC element κ_{EC} [23], the thermal contrast is

$$K' = K \cdot \frac{\kappa_{off} + \kappa_{EC}}{\kappa_{on} + \kappa_{EC}}. \tag{19}$$

For applications, usually $\kappa_{EC} \approx \kappa_{on} \gg \kappa_{off}$ holds.

To cyclically store and release energy to the refrigerant, cyclic operating EC systems require a regenerator. In vapour compression refrigeration, the refrigerant is also the circulating fluid. Similarly, an EC material is used as both the refrigerant and the regenerator. However, an exchange fluid is needed to transport heat to and from the refrigerant since the refrigerant is a solid. Such an active EC regenerator (AER) consists of a porous structure of an EC material and voids or channels through which the heat transfer fluid can flow [42]. Regenerators are also a source of heat loss [40].

4. Optimal EC materials and optimal operational parameters

4.1. EC figure of merit

One way to characterize the performance of devices is the derivation of appropriate figures of merits *FOM*, that is, of appropriate combinations of physical properties affecting device efficiency. The EC device performance is determined by (i) the performance of the refrigeration cycle, (ii) the refrigeration capacity (*RC*) and (iii) the heat transfer efficiency. The different design of EC refrigerators makes a general treatment difficult. Therefore, we will consider first a *FOM* of cooling power based on materials performance instead of system performance. Our *FOM* accounts only for the thermal resistance at the interfaces of the EC material. It does not take into account the thermal mass of the heat switch or the heat transfer agent. Moreover, we assume that the heat transfer does not limit device efficiency, i.e. in case of a heat switch the thermal contrast becomes infinite: $K \to \infty$ (cf. Eq. (18)). We denote this model as an ideal EC element.

In order to characterize the maximum potential of the refrigerant for each cooling technology, an energy conversion efficiency originating from the material, COP_{mat}, was derived in Ref. [7]. It does not include the system details such as limitations in the driving system efficiency (from compressor, motor, etc.), system dynamics, regenerator effectiveness, heat or mass transfer and component geometries. Therefore, it can be regarded as the maximum potential the material has for the cooling technology. In the case of EC cooling, COP_{mat} yields [7]:

$$COP_{mat,EC} = \frac{T_s \Delta S - A_{EC}}{(T_l - T_s)\Delta S + 2A_{EC}}, \tag{20}$$

where A_{EC} is a materials constant appearing for hysteresis and dielectric losses. In Eq. (20), $T_s \Delta S$ represents the heat transferred from the load to the heat sink within one refrigeration cycle and $(T_l - T_s)\Delta S$ the work supplied by the EC material within this cycle. For $A_{EC} \to 0$,

Eq. (20) turns into Eq. (14) describing a thermodynamically reversible process. The COP_{mat} of EC materials (~0.35) is inferior to the ones of MC (~0.86) and elastocaloric materials (~0.65) which both exhibit a much larger latent heat of the corresponding first-order phase transitions [7]. Actually, EC refrigerators benefit much less from the large entropy change induced by driving the material through the phase transition by means of applying of releasing relatively small fields (cf. **Table 1**).

Eq. (20) includes a device-related parameter—the temperature span $(T_l - T_s)$, a thermodynamic parameter ΔS and a physical parameter A_{EC}. For practical use, it would be extremely helpful to implement a refrigerant materials criterion which characterizes the efficiency of the physical cooling process and which is therefore independent on the performance of different thermodynamic cycles. For this purpose, COP_{mat} may be written as [7]

$$COP_{\mathrm{mat}} = COP_C \cdot \Phi_{\mathrm{mat}}. \tag{21}$$

where Φ_{mat} is the dimensionless material efficiency:

$$\Phi_{\mathrm{mat}} = 1 - \frac{\varepsilon\varepsilon_0 E^2 \cdot tan\delta}{c\Delta T_{\mathrm{EC}}}, \tag{22}$$

where tanδ is the sum of dielectric and hysteresis losses during E cycling. The temperature difference $\Delta T* = \Delta T_{\mathrm{EC}} - (T_l - T_s)$ of the heat transfer steps was replaced by its maximum value ΔT_{EC} since we consider the maximum cooling power (cf. Eq. (26)). Then Φ_{mat} becomes independent on cycle parameters, and it receives its minimum value. The second term on the right-hand side of Eq. (22) represents the inverse of the EC efficiency, i.e. the ratio between the heat transferred from the load to the heat sink and the dissipated electrical energy, introduced in Ref. [49].

The RC is a measure of how much heat can be transferred between the load and the heat sink in one ideal refrigeration cycle [50]:

$$RC = \int_{T_1}^{T_2} \Delta S dT \approx \Delta S \cdot \delta T = \frac{c\Delta T_{\mathrm{EC}}}{T}\delta T, \tag{23}$$

where δT is the full width at half maximum of the ΔS versus T curve. Estimations of δT for different EC materials were given in Ref. [51]. Another physical estimate is the distribution width of the local Curie temperatures considered in Refs. [22, 37].

Complete heat transfer from and to the surroundings requires a Fourier number $Fo = \alpha t/d^2 > 1$, where α is the thermal diffusivity, t is the time and d is the thickness of the EC material [46]. Since power is the subject of interest, we have to consider the Fourier number per cycle time τ_c

$$\frac{Fo}{\tau_c} = \frac{\alpha}{d^2} = \frac{\kappa}{cd^2}, \tag{24}$$

with κ is the thermal conductivity. The FOM of an ideal EC element proposed in Ref. [37], combines the materials efficiency Φ_{mat}, the refrigeration capacity RC and the Fourier number per cycle time:

$$FOM = \frac{1}{1-\Phi_{\mathrm{mat}}} \cdot RC \cdot \frac{Fo}{\tau_c} = \frac{\kappa c \cdot \Delta T_{\mathrm{EC.}}^2 \cdot \delta T}{\varepsilon\varepsilon_0 \cdot tan\delta} \cdot \frac{1}{T \cdot E^2 d^2} \cdot \tag{25}$$

This *FOM* consists of a term describing the properties of the EC material and a term of operational parameters applied to the material. It increases not only with the square of the EC coefficient ($\Phi \propto [\Delta T_{\mathrm{EC}}/\Delta E]^2$), but also with increasing EC efficiency ($\Phi \propto c\Delta T_{\mathrm{EC}}/\varepsilon\varepsilon_0 E^2 \tan\delta$), increasing *COP* of the EC effect ($\Phi \propto \Delta T_{\mathrm{EC}}/T$) (the latter two values were proposed separately as EC figures of merit in Refs. [49, 52], respectively), and increasing heat transfer rate ($\Phi \propto \kappa/d^2$). The larger the *FOM*, the better the cooling performance will be. For an ideal refrigerant, *FOM* becomes infinite: $FOM \rightarrow \infty$.

4.2. Best performing EC materials

The most studied and best performing EC materials are currently polyvinylidene fluoride $(\text{-}CH_2\text{-}CF_2\text{-})_n$ terpolymers (P(VDF-TrFE-CFE)) and irradiated copolymers (P(VDF-TrFE)) as well as solid solutions of lead magnesium niobate and lead titanate ((1-*x*)PMN-*x*PT) [2]. Moreover, lead-free perovskite relaxors $BaZr_xTi_{1-x}O_3$ (BZT) provide a ΔT_{EC} value over a broad temperature range sufficient for practical cooling applications [51]. Here, data are available solely for comparably low electric fields (up to 14.5 MV/m). Recently, a large ΔT_{EC} of 45 K was obtained for $Pb_{0.88}La_{0.08}Zr_{0.65}Ti_{0.3}5O_3$ thin films on a $Pt/TiO_2/SiO_2/Si$ substrate at an electric field of 125 V/μm [26].

The general requirements to an EC refrigerant are:

- large and reversible polarization change,
- suitable temperature range of high EC response,
- slim or absent *P-E* hysteresis (coercive field *Ec* => 0),
- small specific heat and large thermal conductivity for fast heat transfer and
- large resistivity, i.e. small Joule heating.

Table 2 compares material characteristics [2, 5, 6, 8, 26, 51, 53], the materials efficiency Φ_{mat}, Eq. (22), and the figure of merit, Eq. (25), of promising EC refrigerants. For comparison, a thickness of 100 μm was chosen. To account for the field dependence of the dielectric permittivity ε was estimated by averaging in the given electric field region. The values of Φ_{mat} exceed significantly the ones known for Brayton engines (0.6–0.8). The only exception is the MLC due to its comparable low value of ΔT_{EC}. MLCs are still not optimized for EC application. The actual *FOM* depends on how much of the potential δT will be really used and on the field dependence of ε. The latter problem is absent in ferroelectric polymers.

4.3. Cooling power of an ideal EC element

The cooling power of an ideal EC element is given by $\dot{q} = C_{\mathrm{EC}}\Delta T/\tau_c$, where C_{EC} is its heat capacity and $\Delta T* = \Delta T_{\mathrm{EC}} - (T_l - T_s)$ is the temperature difference of the heat transfer steps. When the cycle time τ_c is associated by a constant factor m with the thermal time constant $\tau_{RC} = R_{th}C_{\mathrm{EC}}$ of the EC element, the heat capacity cancels out. Consequently, $\dot{q}$ is determined

Refrigerant	T, K	ΔT_{EC}, K	ΔE, V/μm	c, MJ/m^{3}K	ε	κ, W/mK	δT, K	tanδ	Φ_{mat}	*FOM*, mW/cm^3
P(VDF)-based polymers	305	20	200	2.7	60	0.2	50	0.15	0.941	1.111
$BaTiO_3$	400	1.5	1	4.2	5000	2.6	5	0.05	0.9996	13.875
$BaTiO_3$	295	0.5	30	2.5	500	2.6	60	0.07	0.554	0.119
$BaZr_{0.2}Ti_{0.8}O_3$	310	4.5	15	3.4	800	2.6	30	0.05	0.994	21.739
0.7PMN-0.3PT	420	2.5	10	2.8	6000	1.5	100	0.08	0.949	1.765
0.9PMN-0.1PT	350	5	90	3	1250	1.3	100	0.1	0.986	0.311
PLZT8/65/35	385	2.5	10	3	5000	2.3	80	0.1	0.991	1.320
PLZT8/65/35	318	40	120	3	1000	2.3	80	0.07	0.963	20.295

Table 2. Material characteristics, the materials efficiency Φ_{mat} and the figure of merit selected EC refrigerants.

by the ratio of ΔT^* to the total thermal resistance R_{th} of the device. Taking into account that there are two heat transfer steps (heat absorption and heat rejection) with equal time constants and equal heat fluxes within both steps, the average cooling power per cycle yields [44]

$$\langle \dot{q} \rangle \approx \frac{\Delta T^* [1 - \exp(-m)]}{2mR_{th}}, \tag{26}$$

where $R''_{th} = \mathrm{A} \cdot R_{th}$ is the area-specific thermal resistance given in m^2/KW. For thermal time constants with $m > 2$ (two isothermal steps at least with a duration τ_{RC}), the EC material's temperature decays to almost the steady-state value. Here, the cooling power increases linearly with frequency f. At smaller values of m, a temperature offset appears decreasing the effective ΔT^*. The maximum specific cooling power is obtained at a value of $m = \ln 2 \approx 0.7$ yielding

$$\langle \dot{q} \rangle_{\max} = \frac{0.36 \Delta T^*}{\sum_i R''_{th,i}}. \tag{27}$$

Table 3 compiles estimated specific cooling powers of hypothetical EC devices in dependence on the dominating thermal resistance of possible heat-releasing parts.

4.4. Cooling power of the refrigeration system

An EC refrigerator, i.e. a heat pump, is able to transport thermal energy against a temperature gradient from T_l to T_s where $T_l > T_s$. Here, the heat flows from the load to the EC layer and from the EC layer to the heat sink. Both are controlled by thermal connections that have to be opened and closed appropriately as the layer is heated or cooled. Heat is transferred from the load or to the heat sink either

i. via controlled heat switches [58] as well as uncontrolled thermal rectifiers, or

ii. by pumping a gaseous or liquid heat transfer agents through the solid refrigerant [59].

The heat switch or the heat transfer (HT) agent acts as an additional cycle-average thermal mass C_{HT} of the system. Correspondingly, the cycle time $\tau_c \sim R_{th}(C_{EC} + C_{HT})$ is increased.

Performance-limiting component	R''_{th}, m²/KW	$\dot{q}$, W/cm²	Reference
Thermal switch, MEMS (poly-Si-Si_3N_4)	1.67×10^{-5}	11	[54]
Thermal switch, Hg-droplet array	1.10×10^{-6}	164	[55]
Solid-liquid hybrid thermal interface	1.3×10^{-5}	13.9	[56]
Liquid-droplet -mediated interface	$6.7–3.2 \times 10^{-5}$	2.7–5.6	[56]
MLC, Ni-electrode	1.76×10^{-5}	10	[17]
MLC, Ag-electrode	3.86×10^{-6}	47	[17]
Liquid hexane flow	(calc.) 1.4×10^{-4}	~1	[57]
	10^{-3} (exp.)	0.36	

$\Delta T^* = 5$ K, $m = \ln 2$.

Table 3. Specific cooling power of EC devices in dependence on the dominating thermal resistance.

Usually, $C_{HT} > C_{EC}$, i.e. the cycle time is primarily determined by C_{HT}. Thus, the response times of the heat switches or the gas/liquid delivery systems limit significantly the cycle time of EC refrigerators. The thermal time constants of releasable solid-solid, liquid-solid and solid-liquid (hybrid)-solid contacts are 350, 135 and 75 ms, respectively [56]. In an AER, a secondary heat transfer agent (gas or fluid) is used to transfer heat from the cold to the hot end of the regenerator. The heat transfer agent pumped through the EC material substantially enhances the heat flow and, thus, increases the specific cooling power as well as the device efficiency. Here, the Biot number $Bi = d/(\kappa \cdot R''_{th,b})$, characterizing the ratio of the thermal resistances of the EC material volume and the boundaries, will be small for thicknesses d below 100 μm. Assuming a uniform heat flux across the interface, a height of a very long rectangular duct of 0.5 mm and a thermal conductivity of the heat transfer agent of 0.15 W/mK (silicon oil), the corresponding heat transfer coefficient $h = 1/R''_{th,b}$ yields a value of $h \approx 1250$ W/m²K. At $Bi <$ 0.1, the temperature of the EC element during heat transfer remains nearly constant, enabling a lumped system approximation [60]. The time constant amounts then to $\tau_i = c \cdot d/h$. It is in the order of the response time of piezoelectric valves for gas or liquid supply amounting to a few milliseconds [61]. **Table 4** compiles the time constants of hypothetical thermal interfaces and the corresponding operational frequency limits. Note that oxide thermal rectifiers made of two oxides with different thermal conductivities [62] possess a thermal contrast of $K = 1.43$ which is still too low for EC applications.

Thermal switch	τ, *ms*	f_{max}, Hz
Al-Si solid-solid contact	350[1]	0.5
Liquid-droplet-mediated interface	135[1]	1.2
Solid-liquid hybrid thermal interface	75[1]	2.2
Active EC regenerator	~10[2]	17

[1]Ref. [56].
[2]Calculated for $d = 5$ μm.

Table 4. Time constants of thermal interfaces and the associated frequency limit of EC devices.

Currently, the operational frequency of EC refrigerators is limited to about 10 Hz providing cooling powers of a few W/cm^2.

5. Device prototypes

EC refrigerator based on $SrTiO_3$ was initially proposed for cryogenic application, particularly in the 4–15 K temperature range [13, 63]. In a completely solid-state EC device, the electric field and magnetothermal heat switches were cycled in a proper time sequence [63]. However, no cooling power and device efficiency were reported.

For switching from a heat-conducting to a heat-insulating state near room temperature, EC elements are placed between a pair of thermoelectric elements (Peltier elements), serving as heat switch [58]. The first switch is in thermal contact with the heat sink and the second one with the load. During the adiabatic steps, both heat switches are turned off. After the EC material was adiabatically polarized (heated), the first heat switch is turned on, transferring heat from the EC element to the heat sink. The second heat switch stays turned off. After adiabatic depolarization (cooling), the second heat switch becomes active and heat is transferred from the load to the EC element. The first heat switch stays turned off. A device prototype in this configuration using Peltier elements in the passive mode was characterized in Ref. [64]. The thermal contact conductance of Peltier elements was about 1000 W/m^{2}K, i.e. they do not provide an advantage compared to laminar liquid flow of a heat transfer agent [57].

For EC micro-refrigerators, heat switches were fabricated by micro-electromechanic systems (MEMS) technology [43, 46, 65]. For fast heat exchange, laterally interdigitated electrodes were considered in Ref. [46]. The weak point of such a design is the comparably high thermal resistance at the interfaces to the load and the heat sink (cf. **Table 3**).

Liquid crystals were proposed as prospective heat switches [66, 67]. The operation of a thin film EC refrigerator comprising such liquid crystal heat switches was theoretically investigated in Ref. [48]. Although a thermal contrast of up to about 25 was reported for liquid crystals [68], no devices were realized yet.

A fluid-based approach uses electrohydrodynamic (EHD) flows in thin films of dielectric fluids [69]. In this case, the thermal contrast $K = 4.7 \pm 1.1$ yields a relative efficiency $\Phi_{switch} = 0.18$, which is still too low for practical application.

Table 5 compiles the parameters of EC refrigerators where the transport of thermal energy from the cold to the hot side of the system is carried out by means of heat switches. The tables illustrate that commercial multi-layer capacitors described above are an attractive EC component in proof-of-concept refrigerator prototypes. MLCs are extremely reliable. They combine a suitable thermal mass with an operating voltage in the order of 100 V as well as with the high dielectric strength obtained in thin layers (typically <10 μm) [70]. MLCs can be stacked in series to achieve a higher T_{span}. Moreover, MLC arrays can be operated between a common heat source and sink to increase cooling power.

Refrigerant	Heat switch	T, K	E, MV/m	ΔT_{EC}, °C	f, Hz	$\dot{q}$, W/cm^2	Φ	Ref.
$SrTiO_3$	Magnetothermal	10	2	0.3				[63]
n/a	Electrostatic MEMS-actuator	313	–	10		3–6	0.32	[46]
$BaTiO_3$ (MLC)	Electrostatic actuator with liquid thermal interface	300	40	0.5[1]	0.22			[43]
0.7PMN-0.3PT	Passive Peltier element	348	1.2	2.0[1]	0.42	0.035[2]		[64]
$BaTiO_3$ (MLC)	MEMS-shape Si with liquid lubricant	300	27.7	0.5[1]	0.33	0.036	0.46[2,3]	[65]
n/a	Liquid crystal		100	10		5.7[2]	0.18[2,3]	[48]
						≤150[2]	≤0.44[2,3]	
$BaTiO_3$ (MLC)	Hydrofluoroethers	298	~50	0.6[1]	0.25		0.14[2,3]	[69]

[1]Experimental value.
[2]Our estimate.
[3]Calculated using Eq. (18).

Table 5. Characteristics of EC refrigerators comprising heat switches.

A compromise between low thermal interface resistance and a quick heat transfer is a regenerator system, i.e. a heat exchanger where the heat is intermittently stored in a thermal storage medium. In the 1980s, EC cooling near 300 K was demonstrated at an operating frequency of $f = 0.4$ Hz using a regenerator of helium or liquid pentane that flowed back and forth between 0.3-mm-thick $PbSc_{0.5}Ta_{0.5}O_3$ plates [57, 59, 71]. The plates were rendered alternately hot and cold by electrically cycling the phase transition. The cooling power was still low at about 7.7 kg/W. Prototypes with up to 750 plates were built. In order to maintain a high temperature span in a wide temperature range, a cascade concept was realized exploiting the shift of the temperature of maximum EC activity of ceramics tailored by different sintering temperatures. A 10-fold cascade provided a temperature span of 10 K. The same operational principle can be realized using micro-electromechanical systems technology [72]. Here, the heat transfer liquid (Galden HT-70) is pumped back and forth by two diaphragm actuators, which are driven electrostatically. A small-scale EC cooling device based on an active EC regenerator with silicon oil or water as heat transfer fluids is described in Ref. [42].

The heat regeneration process is commonly used to increase the temperature span in cooling devices. Experimentally obtained regeneration factors (ratio between the temperature span established across the device and ΔT_{EC}) are ca. 2 [71] and ca. 3.7 [42], respectively. Simulations predict an improvement by a factor of 5–6 [71] and, by optimizing also the heat transfer agent, up to a factor of 10 [42]. Thus, temperature spans of up to 20 K seem to be technically possible.

Regeneration can be realized also by heat exchange directly between EC elements that are rotating in opposite directions with different applied fields. A corresponding rotary EC refrigerator is described in Ref. [47]. It consists of stacked EC rings where each EC ring is composed of N_s (for example, $N_s = 16$) thermally separated EC elements. The EC rings rotate coaxially with the same rotary speed, but the rotation directions are opposite between neighbouring rings. Every

two neighbouring EC rings are directly contacted to facilitate the heat exchange with each other. Heat exchangers with high thermal conductivity are placed at the circumference at opposite sides of the device to absorb or reject heat. Simulation results showed a cooling power density of 37 W/cm^3 for a T_{span} of 20 K for a cooling device made of P(VDF-TrFE-CFE) terpolymer.

The electrocaloric oscillatory refrigeration device (ECOR) adapts a concept known from thermoacoustic cooling [28, 73]. It consists of an EC element and a solid-state regenerator. The length of the EC module is slightly shorter than that of the regenerator, so that the EC module can move back and forth on the regenerator. Thereby, a temperature gradient is established within both and heat is transported from one side to the other. The solid-state regenerator

Refrigerant	Configuration	T, K	E, MV/m	ΔT_{EC}, °C	f, Hz	$\dot{q}$, W/cm^2	Φ	Ref.
PST	AER		1.5	0.9	4	0.05		[59]
			3[1]	1.5[1]	5			
		260–280	6	3		0.36		[57]
		280–300	1.5	0.9			0.42	[71]
P(VDF–TrFE–CFE) 59.2/33.6/7.2	Fluid-based micro-scale refrigerator	300	150	16	10	3	0.31	
			50		10	0.173		[72]
			50		20	2		
0.9PMN-0.1PT	Small scale AER		115	1.5	1.25			[42]
			87	1.25				
		300	57		0.75			
			50	0.9[1]	0.75			
			25	0.6[1]				
Ba(Zr,Ti)O_3 (MLC)			20	0.54[1]	0.02	0.006[1]		[73]
		298			5	0.083		
					0.02			
					5			
n/a	EC refrigerator with internal regenerator	323	150	14.6	1.25	~4	0.57	[47]
P(VDF-TrFE) 68/32 (irrad.)	Chip scale EC oscillatory refrigerator (ECOR)		50		0.5			[74]
			80	2.2[1]	0.5			
			100		0.5			
		308	100		1			
			100		3			
			150		0.5			
			160	21[1]	10	5.4	0.5	[28]

[1]Experimental value.

Table 6. Characteristics of EC refrigerators using regeneration.

might possess an anisotropic thermal conductivity highly reducing heat conduction losses. A 1 cm long device can provide a cooling density of 9 W/cm^3. The weak point of this design is the friction during the relative motion between EC element and regenerator.

Table 6 illustrates the characteristics of EC refrigerators using regeneration. Although the cooling power of experimental prototypes is still very low, modelling based on experimental results predicts cooling powers of a few W/cm^2.

6. Conclusions

EC cooling is an environment-friendly caloric energy conversion technology. Cooling power densities of a few W/cm^2 and temperature spans in the order of 20 K (in regeneration systems) are achievable at a cycle time of 100 ms. Currently, EC cooling does not represent an alternative for the full replacement of vapour compression. It can be assumed that it will rather penetrate niche markets in the future such as small, compact, local and all-solid-state refrigerators. Although the reverse Brayton thermodynamic cycle is actually the most suitable for practical implementation, further research on more efficient cycles is required. EC cooling processes possess a large materials efficiency and are thermodynamically reversible. At present, the bottleneck of EC refrigerators is the heat transfer process needed to absorb heat from the load and reject it to the heat sink. Most attractive for applications are all-solid-state devices including Peltier elements as thermal switches and active electrocaloric regenerators using a liquid heat transfer agent.

Author details

Gunnar Suchaneck[1]*, Oleg Pakhomov[2] and Gerald Gerlach[1]

*Address all correspondence to: gunnar.suchaneck@tu-dresden.de

1 TU Dresden, Solid State Electronics Laboratory, Dresden, Germany

2 ITMO National Research University (ITMO University), St. Petersburg, Russia

References

[1] Calm JM. Comparative efficiencies and implications for greenhouse gas emissions of chiller refrigerants. International Journal of Refrigeration [Revue Internationale Du Froid]. 2006;**29** (5):833–841. DOI: 10.1016/j.ijrefrig.2005.08.017

[2] Valant M. Electrocaloric materials for future solid-state refrigeration technologies. Progress in Materials Science. 2012;**57**(6):980–1009. DOI: 10.1016/j.pmatsci.2012.02.001

[3] Ožbolt M, Kitanovski A, Tušek J, Poredoš A. Electrocaloric vs. magnetocaloric energy conversion. International Journal of Refrigeration [Revue Internationale Du Froid]. 2014;**37** (January 2014):16–27. DOI: 10.1016/j.ijrefrig.2013.07.001

[4] Birks E, Dunce M, Sternberg A. High electrocaloric effect in ferroelectrics. Ferroelectrics. 2010;**400**(1):336–343. DOI: 10.1080/00150193.2010.505854

[5] Alpay PS, Mantese J, Trolier-McKinstry S, Zhang Q, Whatemore RW. Next generation electrocaloric and pyroelectric materials for solid-state electrothermal energy interconversion. MRS Bulletin. 2014;**39**(12):1099–1109. DOI: 10.1557/mrs.2014.256

[6] Ožbolt M, Kitanovski A, Tušek J, Poredoš A. Electrocaloric refrigeration: Thermodynamics, state of the art and future perspectives. International Journal of Refrigeration [Revue Internationale Du Froid]. 2014;**40**(April 2014):174–188. DOI: 10.1016/j.ijrefrig.2013.11.007

[7] Qian S, Nasuta D, Rhoads A, Wang Y, Geng Y, Hwang Y, et al. Not-in-kind cooling technologies: A quantitative comparision of refrigerants and system performance. International Journal of Refrigeration [Revue Internationale Du Froid]. 2016;**62**:177–192. DOI:10.1016/j.ijrefrig.2015.10.019

[8] Correia T, Zhang Q, editors. Electrocaloric Materials: New Generation of Coolers. Berlin-Heidelberg: Springer; 2014. p. 253. DOI: 10.1007/978-3-642-40264-7

[9] Thomson W. On the thermoelastic, thermomagnetic and pyroelectric properties of matter. Philosophical Magazine Series 5. 1878;**5**(28):4–27. DOI: 10.1080/14786447808639378

[10] Kobeko P, Kurtschatov J. Dielektrische Eigenschaften der Seignettesalzkristalle. Zeitschrift für Physik. 1930;**66**(3):192–205. DOI: 10.1007/BF01392900

[11] Baumgartner H. Elektrische Sättigungserscheinungen und elektrokalorischer Effekt von Kaliumphosphat KH_2PO_4. Helvetica Physica Acta. 1950;**23**(6/7):651–696. DOI: 10.5169/seals-112128

[12] Roberts S. Adiabatic study of 128°C transition in barium titanate. Physical Review. 1952;**85**(5):925–926. DOI: 10.1103/PhysRev.85.925.2

[13] Gränicher H. Induzierte Ferroelektrizität von $SrTiO_3$ bei sehr tiefen Temperaturen und über die Kälteerzeugung durch adiabatische Entpolarisierung. Helvetica Physica Acta. 1956;**29**(3):210–212

[14] Tuttle BA, Payne DA. The effect of microstructure on the electrocaloric properties of Pb(Zr, Sn,Ti)O_3 ceramics. Ferroelectrics. 1981;**37**(1):603–606. DOI: 10.1080/00150198108223496

[15] Mischenko AS, Zhang Q, Scott JF, Whatmore RW, Mathur ND. Giant electrocaloric effect in thin film $PbZr_{0.95}Ti_{0.05}O_3$. Science. 2006;**311**(5765):1270–1271. DOI: 10.1126/science.1123811

[16] Bai Y, Zheng G-P, Ding K, Qiao L, Shi S-Q, Guo D. The giant electrocaloric effect and high effective cooling power near room temperature for $BaTiO_3$ thick film. Journal of Applied Physics. 2011;**110**(9):094103. DOI: 10.1063/1.3658251

[17] Kar-Narayan S, Mathur ND. Direct and electrocaloric measurements using multilayer capacitors. Journal of Physics D-Applied Physics. 2010;**43**(3):032002. DOI: 10.1088/0022-3727/43/3/032002

[18] Herbert JM. Thin ceramic dielectrics combined with nickel electrodes. Proceedings of the Institution of Electrical Engineers. 1965;**112**(7):1474–1477. DOI: 10.1049/piee.1965.0237

[19] Sakabe Y, Minai K, Wakino K. High-dielectric constant ceramics for base metal monolithic capacitors. Japanese Journal of Applied Physics. 1981;**20**(Suppl. 20-4):147–150. DOI: 10.7567/JJAPS.20S4.147

[20] Kishi H, Mizuno Y, Chazono H. Base-metal electrode-multilayer ceramic capacitors: Past, present and future perspectives. Japanese Journal of Applied Physics. 2003;**42**(Part 1, Number 1):1–15. DOI: 10.1143/JJAP.42.1

[21] Lines ME, Glass AM. Principles and Application of Ferroelectrics and Related Materials. 1st ed. Oxford: Clarendon Press; 1977. p. 148. ISBN: 0486648710

[22] Suchaneck G, Gerlach G. Electrocaloric cooling based on relaxor ferroelectrics. Phase Transitions. 2015;**88**(3):333–341. DOI: 10.1080/01411594.2014.989225

[23] Suchaneck G, Gerlach G. Requirements to (Ba,Ca)(Zr,Ti)O_3 electrocaloric materials. In: 2013 Joint IEEE International Symposium on Application of Ferroelectrics and Workshop on Piezoresponse Force Microscopy (ISAF/PFM); 21–25 July 2013; Prague: IEEE; 2013. pp. 244–247. DOI: 10.1109/ISAF.2013.6748680

[24] Karchevskii AI. Electrocaloric effect in polycrystalline barium titanate. Soviet Physics Solid State. 1962;**3**:2249–2254

[25] Bai Y, Zheng G-P, Shi S-Q. Kinetic electrocaloric effect and giant net cooling of lead-free ferroelectric refrigerants. Journal of Applied Physics. 2010;**108**(10):104102. DOI: 10.1063/1.3511342

[26] Lu SG, Rožič B, Zhang QM, Kutnjak Z, Li X, Furman E, et al. Organic and inorganic relaxor ferroelectrics with giant electrocaloric effect. Applied Physics Letters. 2010;**97**(16): 162904. DOI: 10.1063/1.3501975

[27] Novak N, Pirc R, Kutnjak Z. Impact of critical point on piezoelectric and electrocaloric response in barium titanate. Physical Review B. 2013;**87**(10):104102. DOI: 10.1103/PhysRevB.87.104102

[28] Li X, Gu H, Qian X, Zhang Q. Compact cooling devices based on giant electrocaloric effect. In: 13th IEEE Intersociety Conference on Thermal and Thermomechanical Phenomena in Electronic Systems (ITherm); 30 May–1 June 2012; San Diego, CA (USA), IEEE; 2012. pp. 934–937. DOI: 10.1109/ITHERM.2012.6231525

[29] Clapeyron MC. Mémoire sur la puissance motrice de la chaleur. J. de l´École polytechnique. 1834;**23**:153–190. ark: /12148/bpt6k4336791/f157

[30] Neese B, Chu B, Lu S-G, Wang Y, Furman E, Zhang QM. Large electrocaloric effect in ferroelectric polymers near room temperature. Science. 2008;**321**(5890):821–823. DOI: 10.1126/science.1159655

[31] Peräntie J, Hagberg J, Uusimäki A, Jantunen H. Field induced thermal response and irreversible phase transition enthalpy change in $Pb(Mg_{1/3}Nb_{2/3})O_3$-$PbTiO_3$. Applied Physics Letters. 2009;**94**(10):102903. DOI: 10.1063/1.3098067

[32] Peräntie J, Tailor HN, Hagberg J, Ye Z-G. Electrocaloric properties in relaxor ferroelectric (1-x)$Pb(Mg_{1/3}Nb_{2/3})O_3$-x$PbTiO_3$ system. Journal of Applied Physics. 2013;**114**(17):174105. DOI: 10.1063/1.4829012

[33] Mohammadi S, Khodayari A, Ahmadi A. Electrocaloric response of ferroelectric material applicable as electrothermal transducer. Advances in Materials Science and Engineering. **2013**;2013:858656. DOI: 10.1155/2013/858656

[34] Kutnjak Z, Blinc R, Ishibashi Y. Electric field induced critical points and polarization rotation in relaxor ferroelectrics. Physical Review B. 2007;**76**(10):104102. DOI: 10.1103/PhysRevB.76.104102

[35] Pirc R, Kutnjak Z, Blinc R, Zhang QM. Upper bounds on the electrocaloric effect in polar solids. Applied Physics Letters. 2011;**98**(2):021909. DOI: 10.1063/1.3543628

[36] Suchaneck G, Gerlach G, Deyneka A, Jastrabik L, Davitadze ST, Strukov BA. Phase transitions of self-polarized PZT thin films. MRS Proceedings. 2002;718:718-D8.4. DOI: 10.1557/PROC-718-D8.4

[37] Suchaneck G, Gerlach G. Lead-free relaxor ferroelectrics for electrocaloric cooling. Materials Today: Proceedings. 2016;**3**(2):622–631. DOI: 10.1016/j.matpr.2016.01.100

[38] McPherson J, Kim J-Y, Shanware A, Mogul H. Thermochemical description of dielectric breakdown in high dielectric constant materials. Applied Physics Letters. 2003;**82**(13):2121–2123. DOI: 10.1063/1.1565180

[39] Yu Z, Ang C, Guo R, Bhalla AS. Ferroelectric-relaxor behavior of $Ba(Ti_{0.7}Zr_{0.3})O_3$ ceramics. Journal of Applied Physics. 2002;**92**(5):2655–2657. DOI: 10.1063/1.1495069

[40] He J, Chen J, Zhou Y, Wang JT. Regenerative characteristics of electrocaloric Stirling or Ericsson refrigeration cycles. Energy Conversion and Management. 2002;**43**(17):2319–2327. DOI: 10.1016/S0196-8904(01)00183-2

[41] Olsen RB, Biscoe JM, Bruno DA, Butler WF. A pyroelectric energy converter which employs regeneration. Ferroelectrics. 1981;**38**(1):975–978. DOI: 10.1080/00150198108209595

[42] Plaznik U, Kitanovski A, Rožič B, Malič B, Uršič H, Dmovšek S, et al. Bulk relaxor ferroelectric ceramics as a working body for electrocaloric cooling device. Applied Physics Letters. 2015;**106**(4):043903. DOI: 10.1063/1.4907258

[43] Jia Y, Ju YS. A solid-state refrigerator based on the electrocaloric effect. Applied Physics Letters. 2012;**100**(24):242901. DOI: 10.1063/1.4729038

[44] Suchaneck G, Gerlach G. Materials and device concepts for electrocaloric refrigeration. Physica Scripta. 2015;**90**(9):094020. DOI: 10.1088/0031-8949/90/9/094020

[45] Kirillin VA, Sytchev VV, Sheindlin AE. Engineering Thermodynamics. 1st ed. Moscow: Mir Publishers; 1976. p. 560.

[46] Ju SY. Solid-state refrigeration based on the electrocaloric effect for electronics cooling. Journal of Electronic Packaging. 2010;**132**(4):041004. DOI: 10.1115/1.4002896

[47] Gu H, Qian X-S, Ya H-J, Zhang QM. An electrocaloric refrigerator without external regenerator. Applied Physics Letters. 2014;**105**(16):162905. DOI: 10.1063/1.4898812

[48] Epstein RI, Malloy KJ. Electrocaloric devices based on thin-film heat switches. Journal of Applied Physics. 2009;**106**(6):064509. DOI: 10.1063/1.3190559

[49] Defay E, Crossley S, Kar-Narayan S, Moya X, Mathur ND. The electrocaloric efficiency of ceramic and polymer films. Advanced Materials. 2013;**25**(24):3337–3342. DOI: 10.1002/adma.201300606

[50] Gschneider Jr KA, Pecharsky VK, Tsokol AO. Recent developments in magnetocaloric materials. Reports on Progress in Physics. 2005;**68**(6):1479–1539. DOI: 10.1088/0034-4885/68/6/R04

[51] Qian X-S, Ye H-J, Zhang Y-T, Gu H, Li X, Randall CA, et al. Giant electrocaloric response over a broad temperature range in modified $BaTiO_3$ ceramics. Advanced Functional Materials. 2014;**24**(9):1300–1305. DOI: 10.1002/adfm.201302386

[52] Guzmán-Verri GG, Littlewood PB. Why is the electrocaloric effect so small in ferroelectrics? APL Materials. 2016;**4**(6):064106. DOI: 10.1063/1.4950788

[53] Suchaneck G. Upper bounds in electrocaloric cooling. In: 2016 Joint IEEE International Symposium on Application of Ferroelectrics, European Conference on Polar Dielectrics, and Piezoelectric Force Microscopy Workshop (ISAF/ECAPD/PFM); 21–25 August 2016; Darmstadt. Piscataway, NJ: IEEE; 2016. p. 4. DOI: 10.1109/ISAF.2016.7578104

[54] Cho J, Richards C, Bahr D, Jiao J, Richards R. Evaluation of contacts for a MEMS thermal switch. Journal of Micromechanics and Microengineering. 2008;**18**(10):105012. DOI: 10.1088/0960-1317/18/10/105012

[55] Song W-B, Sutton MS, Talghader JJ. Thermal contact conductance of actuated interfaces. Applied Physics Letters. 2002;**81**(7):1216–1218. DOI: 10.1063/1.1499518

[56] Jia Y, Ju YS. Solid-liquid hybrid thermal interfaces for low-contact pressure thermal switching. Journal of Heat Transfer. 2014;**136**(7):074503. DOI: 10.1115/1.4027205

[57] Sinyavsky YV, Brodyansky VM. Experimental testing of electrocaloric cooling with transparent ferroelectric ceramics as a working body. Ferroelectrics. 1992;**131**(1):321–325. DOI: 10.1080/00150199208223433

[58] Mathur N, Mishenko A., inventors; Cambridge University Technical Services, assignee. Solid state electrocaloric cooling devices and methods. World Intellectual Property Organization patent application WO 2006056809 A1; 2006 June 1.

[59] Sinyavsky YV, Pashkov ND, Gorovoy YM, Lugansky GE, Shebanov L. The optical ferroelectric ceramic as working body for electrocaloric refrigeration. Ferroelectrics. 1989;**90**(1):213–217. DOI: 10.1080/00150198908211296

[60] Bergman TL, Lavine AS, Incropera FP, DeWitt DP. Fundamentals of Heat and Mass Transfer. 7th ed. Hoboken, NJ: John Wiley & Sons Inc.; 2011. p. 1048. ISBN: 978-0470501979

[61] Rogge T, Rummler Z, Schomburg WK. Polymer micro valve with a hydraulic piezo-drive fabricated by AMANDA process. Sensors and Actuators A. 2004;**110**(1–3):206–212. DOI: 10.1016/j.sna.2003.10.056

[62] Kobayshi W, Teraoka T, Terasaki I. An oxide thermal rectifier. Applied Physics Letters. 2009;**95**(17):171905. DOI: 10.1063/1.3253712

[63] Radebaugh R, Lawless WN, Siegwarth JD, Morrow AJ. Electrocaloric refrigeration at cryogenic temperatures. Ferroelectrics. 1980;**27**(1):205–211. DOI: 10.1080/00150198008226100

[64] Chukka R, Vandrangi S, Shannigrahi S, Chen L. An electrocaloric device demonstrator for solid-state cooling. Europhysics Letters. 2013;**103**(4):47011. DOI: 10.1209/0295-5075/103/47011

[65] Wang YD, Smullin SJ, Sheridan MJ, Wang Q, Eldershaw C, Schwartz DE. A heat-switch-based electrocaloric cooler. Applied Physics Letters. 2015;**107**(13):134103. DOI: 10.1063/1.4932164

[66] Epstein RI, Malloy KJ. inventors; Epstein RI, Malloy KJ, assignee. Electrocaloric refrigerator and multilayer pyroelectric energy generator. United States patent application US20100037624 A1; 2010 February 18

[67] Epstein RI, Malloy KJ. inventors; Stc. Unm, assignee. Electrocaloric refrigerator and multilayer pyroelectric energy generator. United States patent application US20130074900 A1; 2013 March 28

[68] Carr EF. Electrohydrodynamics and the heat switch. Molecular Crystals and Liquid Crystals. 1991;**2002**(1):1–6. DOI: 10.1080/00268949108035653

[69] Hehlen MP, Mueller AH, Weisse-Bernstein NR, Epstein RI. Electrocaloric refrigerator using electrohydrodynamic flows in dielectric fluids. In: Epstein RI, Seletskiy DV, Sheik-Bahae M, editors. Proceedings of SPIE 8638, Laser Refrigeration of Solids VI. Bellingham, WA: SPIE; 2013. p. 86380D. DOI: 10.1117/12.2004009

[70] Milliken AD, Bell AJ, Scott JF. Dependence of breakdown field on dielectric (interelectrode) thickness in base-metal electroded multilayer capacitors. Applied Physics Letters. 2007;**90**(11):112910. DOI: 10.1063/1.2713780

[71] Sinyavsky YuV. Electrocaloric refrigerators: A promising alternative to current low-temperature apparatus. Chemical and Petroleum Engineering. 1995;**31**(6):295–306. DOI: 10.1007/BF01148217

[72] Guo D, Gao J, Yu Y-Y, Santhanam S, Slippey A, Fedder GK, et al. Design and modeling of a fluid-based micro-scale electrocaloric refrigeration system. International Journal of Heat and Mass Transfer. 2014;**72**(May 2014):559–564. DOI: 10.1016/j.ijheatmasstransfer.2014.01.043

[73] Sette D, Asseman A, Gérard M, Strozyk H, Faye R, Defay E. Electrocaloric cooler combining ceramic multi-layer capacitors and fluid. APL Materials. 2016;**4**(9):091101. DOI: 10.1063/1.4961954

[74] Gu H, Qian X, Li X, Craven B, Zhu W, Cheng A, et al. A chip scale electrocaloric effect based cooling device. Applied Physics Letters. 2013;**102**(12):122904. DOI: 10.1063/1.4799283

Chapter 3

Food Chilling Methods and CFD Analysis of a Refrigeration Cabinet as a Case Study

Radu Roşca, Ioan Ţenu and Petru Cârlescu

Additional information is available at the end of the chapter

http://dx.doi.org/10.5772/intechopen.69136

Abstract

This chapter presents the most significant facts about food chilling. For food chilling, the chilling medium in mechanically cooled chillers may be air, water or another secondary cooling agent (slurry ice), or metal surfaces (heat exchangers). Ice chilling is also presented. CFD simulation is applied to a vertical display cabinet with four shelves. In order to evaluate the temperature gradient, the following stages are taken into account: preprocessing—geometry set-up and design of the discretization scheme; processing—introduction of the boundary conditions and calculation; and post-processing—visualization of the velocity and temperature fields.

Keywords: chilling equipment, secondary agents, refrigeration cabinet, CFD simulation

1. Introduction

Refrigeration slows down the chemical and biological processes in foods, such as the accompanying deterioration and the loss of quality, extending the shelf life of the products, with minimum changes to the sensory characteristics and nutritional properties.

Temperatures in the range of 0–5°C slow down the development and growth of microorganisms, but some pathogenic agents can grow to large numbers at these temperatures or are still sufficiently virulent to cause poisoning. Because the activity of most of the pathogenic agents is only slowed down and not stopped, long-term storage of refrigerated products can finally

cause food poisoning [1]. In these cases, when a longer preservation period is needed, freezing must be used to minimize any physical, biochemical, and microbiological changes affecting quality during storage. The storage life of fresh perishable foods, such as meats, fish, fruits, and vegetables, can be extended by several days by cooling, and by several weeks or months by freezing [2, 3]. During freezing, most of the water content of the meat, about 80%, solidifies into pure ice crystals, accompanied by a separation of dissolved solids [2, 4].

Chilled foods are commonly grouped into three categories, according to the storage temperature range [1]:

- −1 to +1°C—fresh fish, meats, sausages and ground meats, smoked meats, and breaded fish;
- 0 to +5°C—pasteurized canned meat, milk, cream, yoghurt, prepared salads, sandwiches, baked goods, fresh pasta, fresh soups and sauces, pizzas, pastries, and unbaked dough;
- 0 to +8°C—fully cooked meats and fish pies, cooked or uncooked cured meats, butter, margarine, hard cheese, cooked rice, fruit juices, and soft fruits.

In order to chill fresh foods, it is necessary to remove the sensible heat and also the heat generated by the respiratory activity of vegetables and fruits; in animal tissues, aerobic respiration rapidly declines when the supply of oxygenated blood is stopped at slaughter [1, 4].

2. Cooling rate and duration

Cooling rate may be defined as [4]:

$$w = \frac{dt}{d\tau} \ [^{\circ}\mathrm{C/s}], \tag{1}$$

where dt is the temperature variation during the period $d\tau$.

Several assumptions are taken into account in order to obtain the temperature-time function [4]:

- homogenous product;
- at any moment, the temperature is the same in the entire mass of the product;
- the temperature of the cooling medium is constant;
- there is no mass transfer between the product and the cooling medium.

The assumption that the sensible heat removed from the product equals the convective heat transfer from the product to the cooling medium leads to [4]:

$$m \cdot c \cdot dt = -S \cdot h \cdot (t - t_0) \cdot d\tau. \tag{2}$$

Eq. (2) finally leads to the temperature-time equation:

$$t = t_0 + (t_i - t_0) \cdot e^{-\frac{h \cdot S}{m \cdot c} \cdot \tau}. \quad (3)$$

The chilling duration is [4]:

$$\tau_r = \frac{m \cdot c}{h \cdot S} \cdot \ln \frac{t_i - t_0}{t_f - t_0}. \quad (4)$$

3. Chilling equipment

Food chilling is performed with mechanical refrigeration systems or with ice [4]. The temperature of the product should be lowered as quickly as possible through the critical warm zone (5–10°C), where maximum growth of microorganisms occurs [1, 3, 4].

Batch or continuous operation is possible when using mechanical refrigeration systems, while batch operation is used in the ice chilling systems.

The chilling medium in mechanically cooled chillers may be air, water, or metal surfaces.

3.1. Air chilling

Air chillers use forced convection to circulate cold air at high speed (4 m/s); thus, the thickness of the boundary film is reduced, and the heat transfer rate is increased.

Air chilling of foods is performed in chilling tunnels or chilling rooms; usually, the chilling tunnels operate continuously, while the batch chilling is used for chilling rooms [4].

In a refrigeration tunnel, air circulates longitudinally, transversally, or vertically (**Figures 1** and **2**). Two-phase chilling can also be used in order to speed up the process and limit the evaporative weight losses [4]. **Figure 3** presents the schematic of the two-phase chilling tunnel. In the first

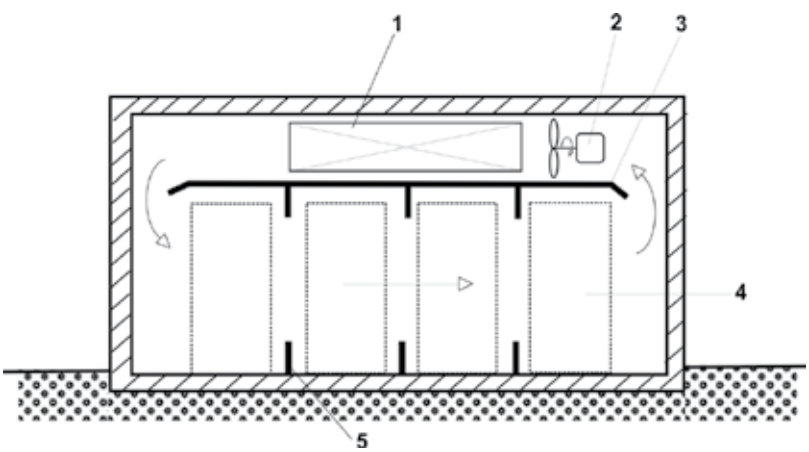

Figure 1. Air chilling tunnel, with longitudinal circulation of the air (vertical cross-section). 1, evaporator; 2, fan; 3, false ceiling; 4, product; 5, baffle.

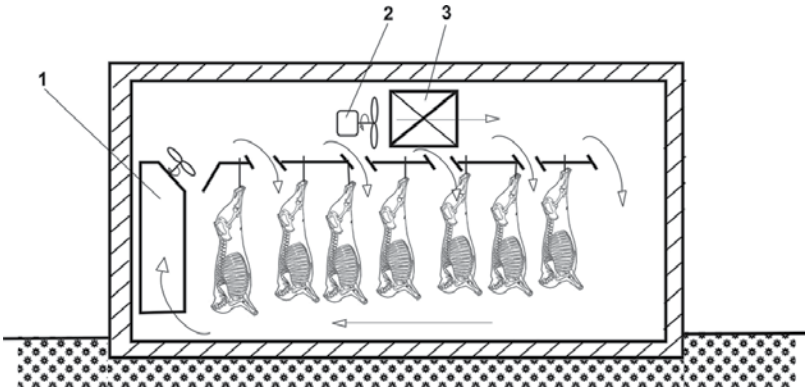

Figure 2. Air chilling tunnel, with vertical circulation of the air (vertical cross-section). 1, 3, evaporators; 2, auxiliary fan.

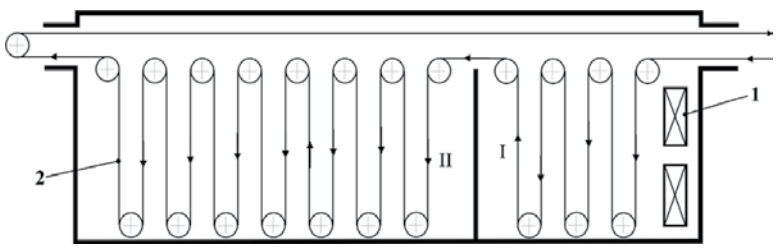

Figure 3. Two-phase chilling tunnel (horizontal cross-section). 1, evaporator; 2, conveyer; I, II, cooling sections.

chilling phase, the air temperature is around −10°C, and its speed is approximately 1 m/s; the products, hanged on the conveyer, travel through section (I) of the tunnel in about 4–5 h. The surface of the products is chilled rapidly in this first section. In the second section of the tunnel (II), air temperature is about 0°C, and its speed is 0.3 m/s; the duration of the chilling process is 10–15 h, until the product reaches a relatively uniform temperature in its entire mass [4]. This system allows the diminishing of the evaporative weight loss compared with the one-phase chilling systems because the surface of the product is quickly cooled in the first phase, and a lower temperature difference between the product and the cooling medium is achieved in the second phase.

Chilling rooms have a lower capacity than chilling tunnels; because of the lower air speed (0.3 m/s), the duration of the chilling process increases. **Figure 4** presents some examples of chilling rooms: the air discharge ducts are placed in the upper side of the room, while the air intake ports are placed in the lower part.

3.2. Chilling with liquid secondary agents

In this case, a chilled secondary agent is used in order to refrigerate the product; the product is sprayed with cold agent or is immersed into the chilling agent [1, 4, 5]. Due to the higher values of the convective coefficients, chilling with cold liquid agents requires less time than air chilling. The procedure is used for chilling poultry, fish, and some vegetable products [4, 5].

http://dx.doi.org/10.5772/intechopen.69136

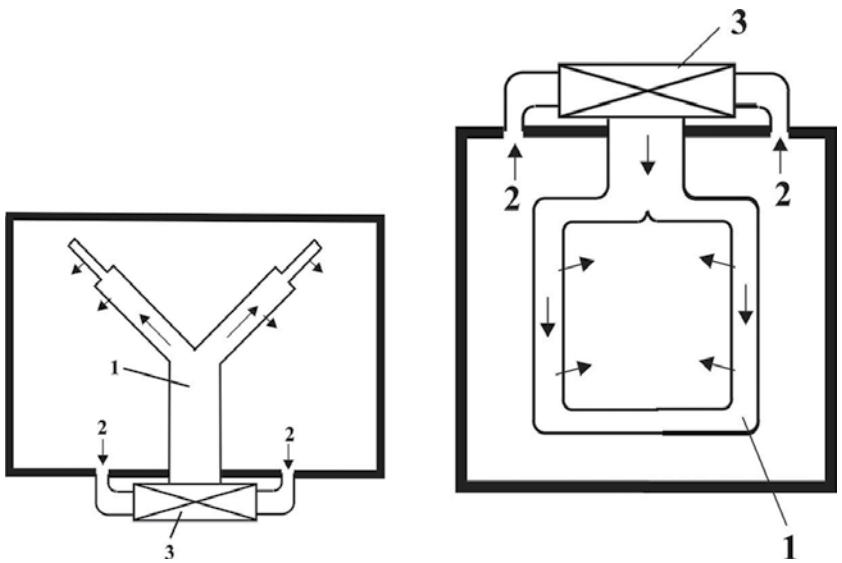

Figure 4. Chilling rooms. 1, discharge duct; 2, intake ports; 3, evaporator and fan.

Depending on the final temperature of the product and on the type of product, chilling may be achieved with water, salt water (brine), or slurry ice; ice or vapor compression refrigeration systems are used in order to cool the secondary agent [4].

Figure 5 presents the schematics of a device for the immersion chilling of poultry [1]; the carcasses are placed on the conveyor (2) and then immersed into the cold agent. The secondary agent is chilled in the heat exchanger (9) by a vapor compression refrigeration system.

Slurry ice is a phase-changing secondary agent, containing small ice crystals (typically 0.1–1 mm in diameter), suspended within a solution of water and a freezing point depressant. Some

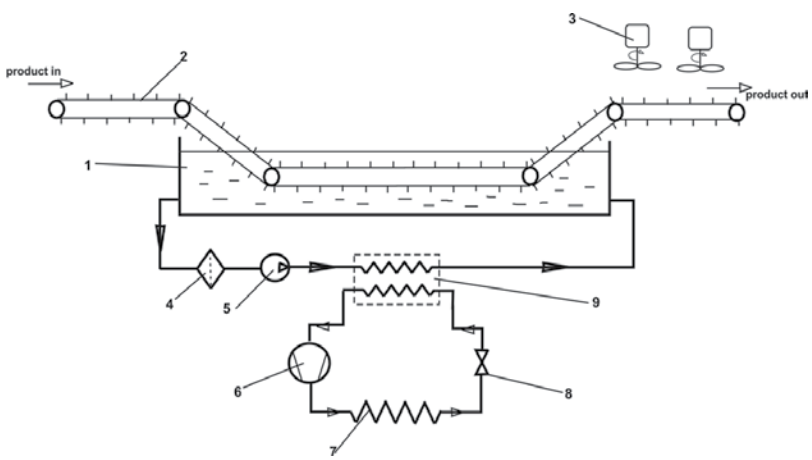

Figure 5. Immersion chilling of poultry. 1, immersion tank; 2, conveyor; 3, fan; 4, filter; 5, pump; 6, compressor; 7, condenser; 8, expansion valve; 9, heat exchanger.

commonly used compounds are salt (sodium chloride), ethylene glycol, propylene glycol, various alcohols (isobutyl, ethanol), and sugar (sucrose, glucose) [6]. This type of ice has many advantages in comparison with the traditional ice (flake ice, shell ice, crushed ice, etc.): it can be used in direct contact with the object to be chilled; due to the large contacting area, it has very good cooling performances; slurry ice can be pumped to the point of use (**Figure 6**), eliminating costly and maintenance intensive rakes, augers, and ice conveying systems [7]; operating at temperatures below the freezing point of water, ice slurry facilitates several efficiency improvements such as lowering the required temperature difference in heat exchangers due to the beneficial thermo-physical properties of ice slurry [6].

Slurry ice is produced in scrapped surface heat exchangers (SSHE); **Figure 7** presents the operating principle of the SSHE for slurry ice. The ice slurry generator consists of a cylindrical metal shell (1). The exterior surface is cooled by the evaporating refrigerant passing through the cooling jacket (2), while water freezes in contact with the cold inner surface of the shell. Spring-loaded rotating blades (4) scrap off the ice crystals formed on the inner cylindrical surface of the metallic shell.

3.3. Ice chilling

This method is used for chilling fish and vegetables [1, 4].

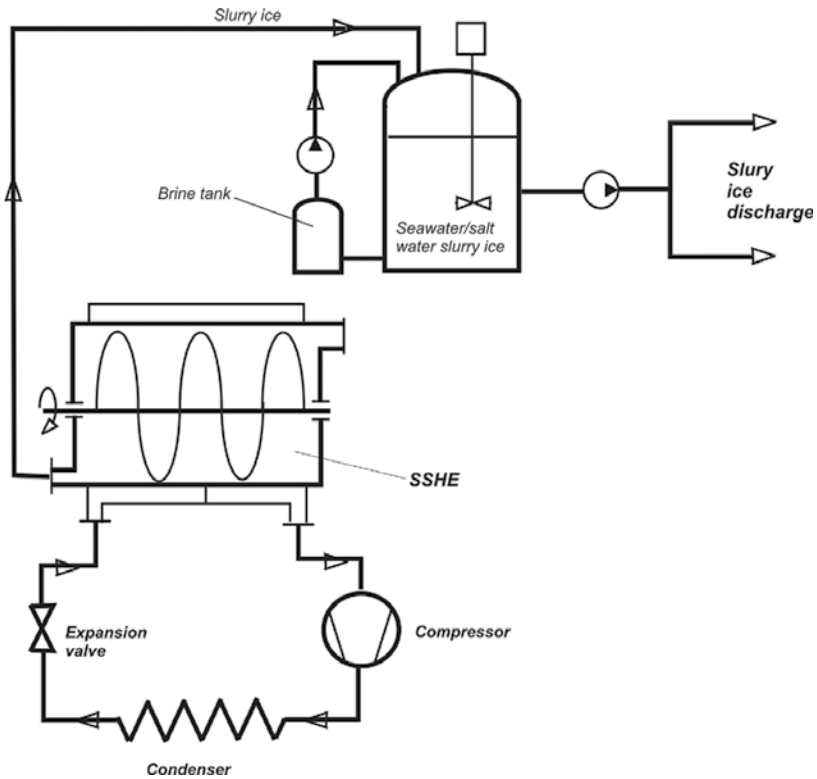

Figure 6. Schematics of a slurry ice installation. SSHE, scrapped surface heat exchanger.

http://dx.doi.org/10.5772/intechopen.69136

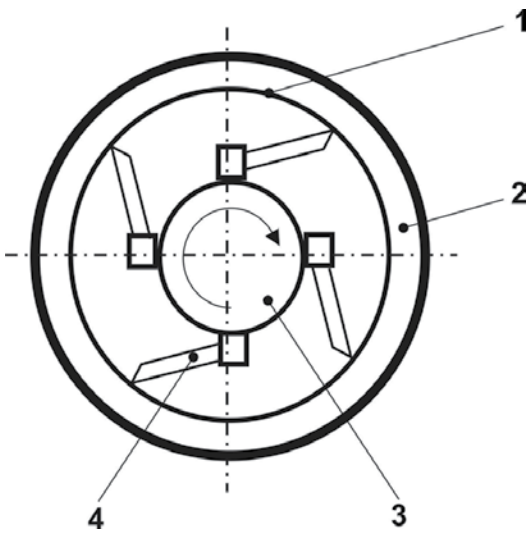

Figure 7. Schematic diagram of the ice slurry generator. 1, cylindrical metal shell; 2, cooling jacket; 3, rotating shaft; 4, blade.

Ice is often produced in the form of lumps or blocks, of various weights, from 10 to 200 kg. Alternatively, ice may be made in the form of smaller pieces (granular ice). Different types of granular ice exist (flake ice, tube ice, plate ice) [4].

In order to obtain ice blocks, the water to be frozen is filled into large metal molds, which are placed in a tank containing refrigerated brine, for up to 24 h. When the ice blocks are completely frozen, they are removed from the freezing tank and dipped into hot water. This melts the surface of the block so that it can be tipped out of its mold. The molds can then be refilled with water and returned to the freezing tanks. The large ice blocks may then be broken down into smaller pieces in an ice-crushing machine (**Figure 8**).

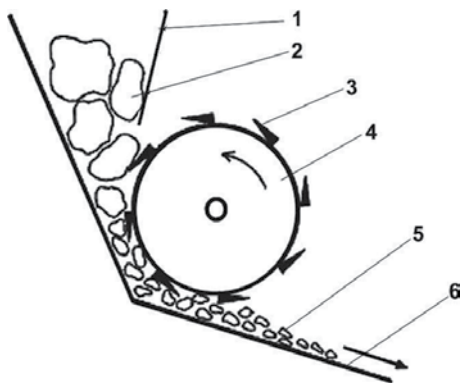

Figure 8. Ice-crushing machine. 1, infeed hopper; 2, large ice chunks; 3, blade; 4, rotating drum; 5, crushed ice; 6, discharge chute.

One of the most common types of granular ice is flake ice, which is obtained by freezing water onto the surface of a rotating, refrigerated drum (**Figure 9**). The water freezes into a 2–3-mm-thick layer of ice, which is then scraped off the drum as flakes of ice.

Storing fish in ice is largely used aboard fishing ships; apart from chilling the fish, ice removes heat from the surrounding structure of the box or storage compartments, absorbs the heat input through the structure from the warm air and sea outside, and removes the heat produced by the spoilage process in the fish themselves [8]. It is therefore essential that plenty of ice is properly distributed throughout the catch to ensure efficient cooling. Ideally, each fish should be in contact only with ice; in practice, there are alternating layers of ice and fish (**Figure 10**). The ice-to-fish ratio is comprised between 1/3 and 1/1; there should be at least 5 cm thick layers of ice (1, 3) between fish and the compartment walls [8]. In order to avoid the lower layers being damaged under the weight of the upper layers, fish must be placed on shelves, in order to keep the depth of the storage compartment (2) lower than 0.5 m [8].

Ice chilling is also used for vegetables and fruits [4]; the products are placed in wooden or cardboard crates, filled with ice. **Figure 11** presents the schematics of an ice-filling machine; the ice flakes flow into the machine hopper (2) through the chute (1) and are poured into the crates through the hopper (4).

3.4. Chilling in tanks and heat exchangers

This chilling method is used for liquid food products (milk, cream, juices, beer, wine, etc.). Refrigerants or secondary cooling agents are used on the cold side of the chilling device, which is operated in batch or continuous mode [4].

In the batch operation mode, the product fed into the tank is cooled using an external cooling jacket or an internal cooling coil. **Figure 12** presents the schematics of a tank equipped with an external cooling jacket (2). The product is fed into the tank through the pipe (7); when the desired final temperature is reached, the product is purged from the tank through the discharge pipe (5).

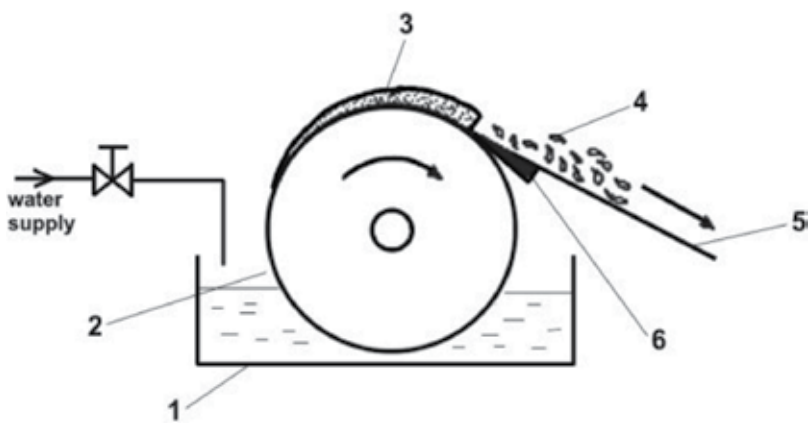

Figure 9. Production of ice flakes. 1, water tank; 2, rotating refrigerated drum; 3, ice layer; 4, ice flakes; 5, ice chute; 6, scrapper blade.

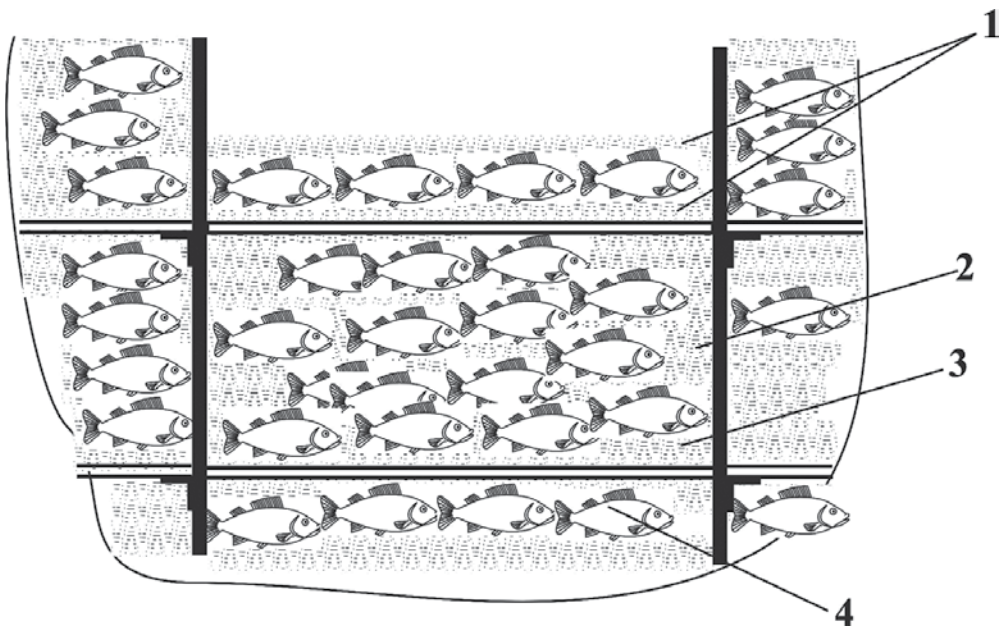

Figure 10. Fish chilling with ice. 1, 3, ice layers; 2, storage compartment; 4, fish.

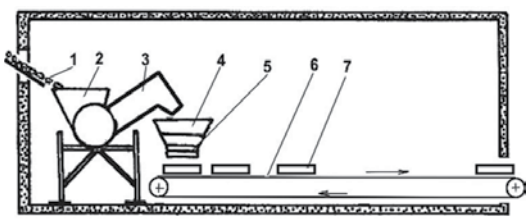

Figure 11. Ice-filling machine. 1, chute; 2, 4, hoppers; 3, flexible hose; 5, flap; 6, discharge conveyer; 7, crates.

Heat exchangers are used in order to continuously chill the liquid products [3, 4]. **Figure 13** presents a double pipe heat exchanger; the cooling medium circulates through the shell (3), while the product circulates through the inner pipe (4). The exchanger contains several sections that are coupled through flanges; the number of sections depends on the final temperature and flow rate of the fluids [9].

3.5. Retail refrigeration cabinets

Retail refrigeration cabinets use cold air circulated through natural or forced convection. The cost of chill storage is high and, in order to reduce costs, large stores may have a centralized plant to circulate the refrigerant to all cabinets; the heat generated by the condensers of the refrigeration system may be used for in-store heating. Computer control of multiple cabinets detects excessive rises in temperature and warns of any requirement for emergency repairs or planned maintenance. Other energy-saving devices include night blinds or glass doors on the front of cabinets to trap cold air.

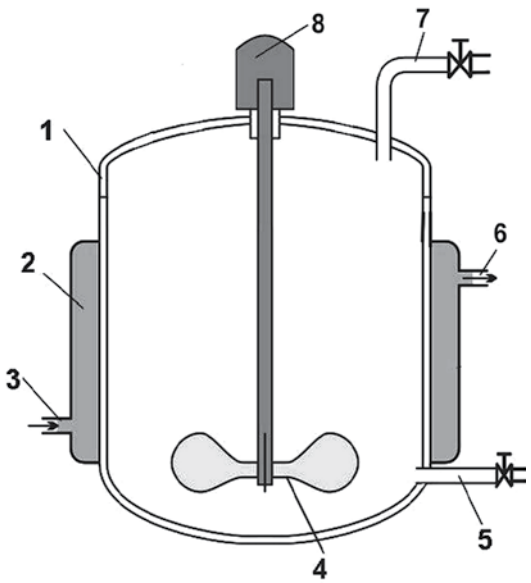

Figure 12. Chilling tank for batch operation. 1, tank; 2, cooling jacket; 3, coolant inlet; 4, stirrer.

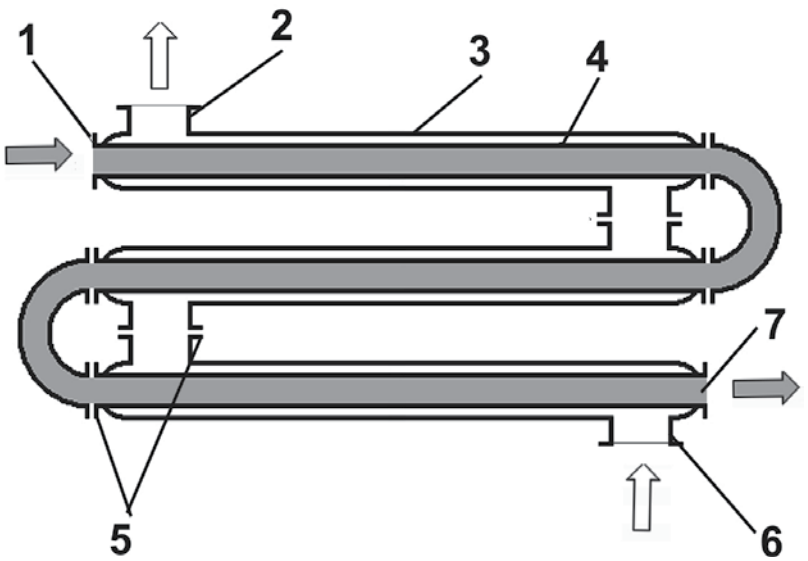

Figure 13. Double pipe heat exchanger. 1, product inlet connection; 2, refrigerant outlet connection; 3, outer shell; 4, inner pipe; 5, flanges; 6, refrigerant inlet connection; 7, product outlet connection.

According to the cabinet geometry, the retail refrigeration cabinets are [10]:

- horizontal, single-deck units;
- vertical, multi-deck units.

http://dx.doi.org/10.5772/intechopen.69136

Horizontal refrigeration cabinets (**Figure 14**) are open-top and are designed for self-service; the wall-site units (**Figure 14a**) allow shopping from one side, while the island type units (**Figure 14b**) are accessible from all sides [2, 10].

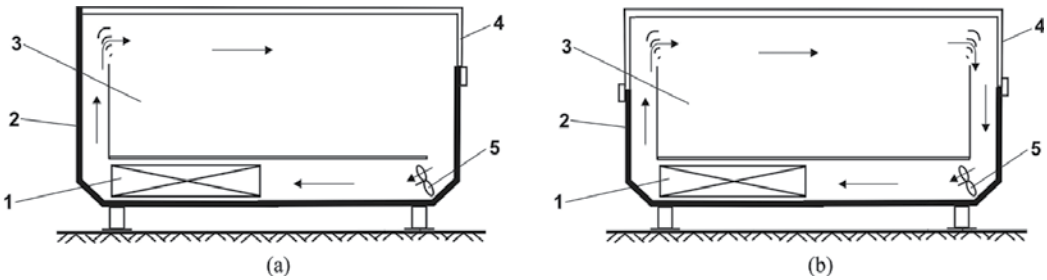

Figure 14. Horizontal refrigeration cabinets. 1, evaporator coil; 2, thermaly insulated case; 3, product loading space; 4, glass panels; 5, fan.

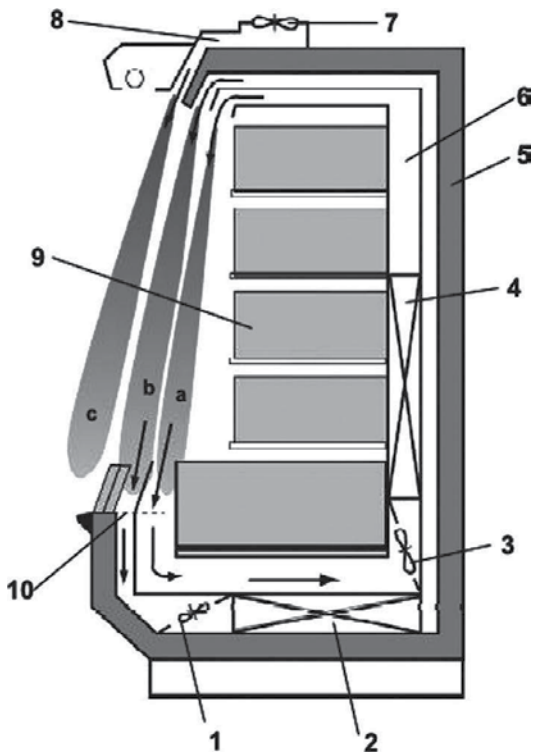

Figure 15. Vertical open front refrigeration cabinet. 1, 3, 7, fans; 2, 4, evaporator coils; 5, case; 6, 8, air channels; 9, products; 10, grills; a, b, c, air curtains.

Axial fans (6) are used to provide air flow over the evaporator coils (1), and grills placed at the upper side of the cabinet deflect the air current from one side of the cabinet to the other, over the stacked products. Due to cold air stratification, air infiltrations from the environment are relatively low; the heating load is due to the radiant heat transfer and conductive heat transfer through the insulated walls of the cabinet case [10].

Vertical multi-deck units have an open front or are provided with a glass front door [2, 10]. The open front refrigeration cabinets (**Figure 15**) use air curtains (a, b, c) in order to prevent the infiltrations of warm air into the cabinet. The axial fans (1) and (3) circulate the cold air over the evaporator coils (2, 4) and produce the stream of air necessary for obtaining the inner air curtains; the outer air curtain (c) is generated by the axial fan (7). Grills are used in order to direct the air flow and obtain the air curtains.

The three air curtains form a very complex system, and the proper design imposes an in-depth understanding of the cabinet's fluid dynamics [2].

Some stores are equipped with combination cabinets (**Figure 16**), comprising an open front vertical cabinet and an open-top, horizontal cabinet [10].

The closed vertical refrigeration cabinets (**Figure 17**) use a glass door (4) in order to contain the products into the refrigerated space and prevent the infiltration of warm air [10].

Table 1 summarizes some characteristics of the retail display cabinets.

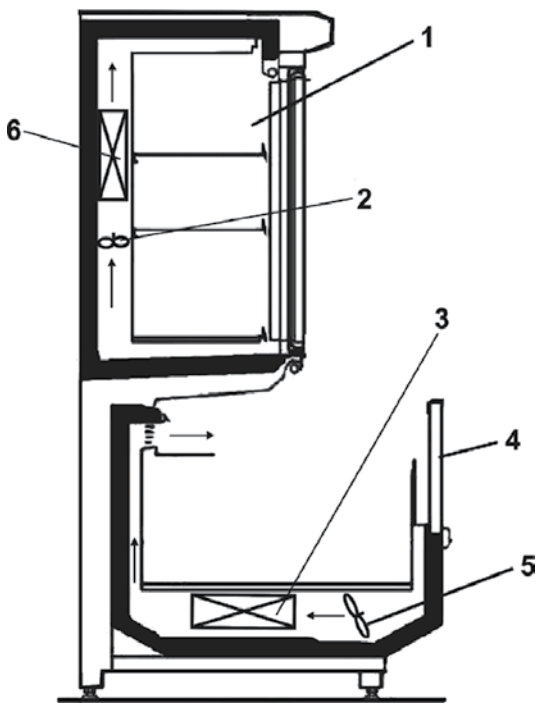

Figure 16. Combination cabinet. 1, vertical, open front, refrigeration cabinet; 2, 5, fans; 3, 6, evaporator coils; 4, horizontal, open type, refrigeration cabinet.

http://dx.doi.org/10.5772/intechopen.69136

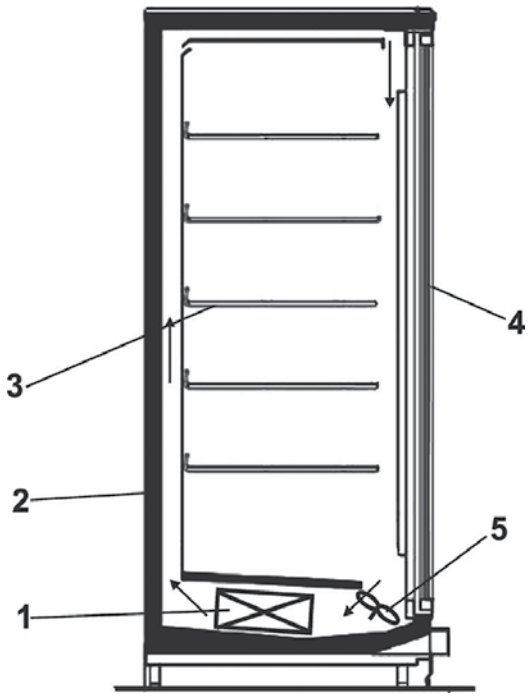

Figure 17. Vertical, closed, refrigeration cabinet. 1, evaporator; 2, case; 3, product shelves; 4, glass door; 5, fan.

Type	Refrigeration load [W/m]	Energy consumption [W/m]	Available volume [m^3/m]
Horizontal, wall site	400–500	250–400	0.2–0.3
Horizontal, island	500–700	350–600	0.3–0.7
Vertical, closed	600–700	400–600	0.7–0.9
Vertical, open, three air curtains	1900–2200	1200–1900	0.7–0.8

Table 1. Characteristics of the retail display cabinets [10].

4. CFD modeling and simulation in a vertical refrigeration cabinet

Vertical refrigerating cabinets are widely used in supermarkets because the products have good storage conditions and are adequately presented to the consumers.

As mentioned above, the open type refrigerating cabinets use one or more air curtains in order to separate the cold interior from the warm surroundings.

The study of air curtains is necessary because these can be easily disrupted by air circulation in front of the cabinet or by the consumers taking foods from the shelves; the disturbing effect increases with the height of the cabinet. The aerodynamic non-homogeneity of the air curtain

increases when the number of "holes" increases, leading to the increase of the temperature inside the display case and of its power consumption; as a result, the products inside the cabinet are stored at temperatures higher that the recommended ones. Moreover, the infiltration of exterior humid air inside the case results in additional ice formation over the evaporator coils, thus reducing the heat transfer and the efficiency of the refrigeration system; therefore, the defrosting cycles become more frequent, further increasing the power consumption.

Some estimations show that 72–75% of the cooling load is used in order to counteract the effect of warm air infiltrations through the air curtain (**Figure 18**) and can reach even 90% if the operating conditions are not suitable [11]; 50% of the power consumption of a supermarket is due to the refrigeration and freezing cabinets.

CFD simulation was applied to a vertical display cabinet with four shelves, and in order to evaluate the temperature gradient, the following stages were taken into account: preprocessing—geometry set-up and design of the discretization scheme; processing—introduction of the boundary conditions and calculation; post-processing—visualization of the velocity and temperature fields.

4.1. CFD simulation and experimental tests

A refrigeration vertical cabinet with four shelves (**Figure 19**) was the basis of the simulation; the dimensions of the cabinet ($L \times W \times H$) are 1900 × 796 × 1911 mm.

The axial fans (2) induce the airflow over the evaporator coil (3), placed at the bottom front part of the cabinet. A limited amount of air is fed into the unit, passing through the perforated plate behind the shelves (4), while the most significant amount of air flows through the horizontal

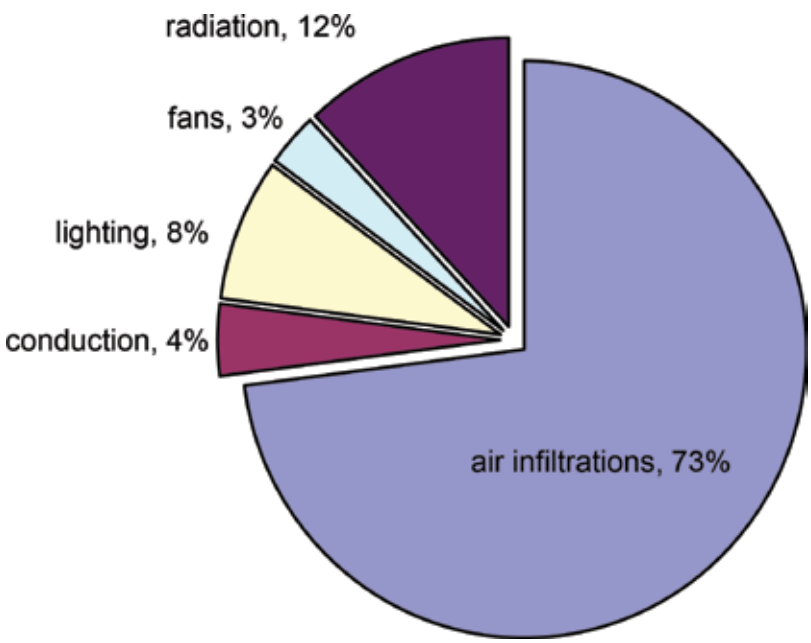

Figure 18. Cooling load components.

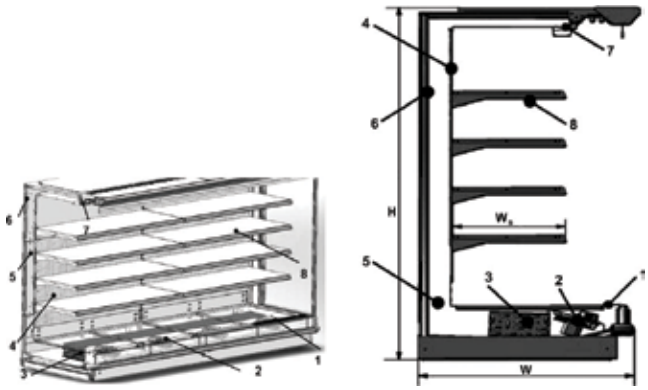

Figure 19. Vertical display cabinet with four shelves. 1, base grill (GRA); 2, fans; 3, evaporator coil; 4, perforated plate; 5, air plenum; 6, thermal insulation; 7, horizontal grill (GPA); 8, shelves.

grill (7), thus creating the air curtain. The air curtain covers the front part of the shelves over their entire length; the air flows downward and is extracted through the base grill (1). The air curtain dimensions are as follows: thickness B = 60 mm; width of the shelves W_s = 350 mm.

The geometry of the air channels was used as a basis for producing the 3D model of the cabinet. The finite volumes discretization of the domain consisted of 1,585,690 nodes, being denser in the lower region of the cabinet (**Figure 20**).

In order to obtain the real boundary conditions, during the experimental tests, the refrigeration cabinet was placed inside a class 3 climatic chamber (according to EN-ISO 23953 and EN 441/4—**Figure 21**), which allowed the adjustment of different parameters of the ambient air (velocity, temperature, and humidity). During the tests, the air flow inside the chamber was parallel with the longitudinal axis of the cabinet, with a velocity of 0.2 m/s.

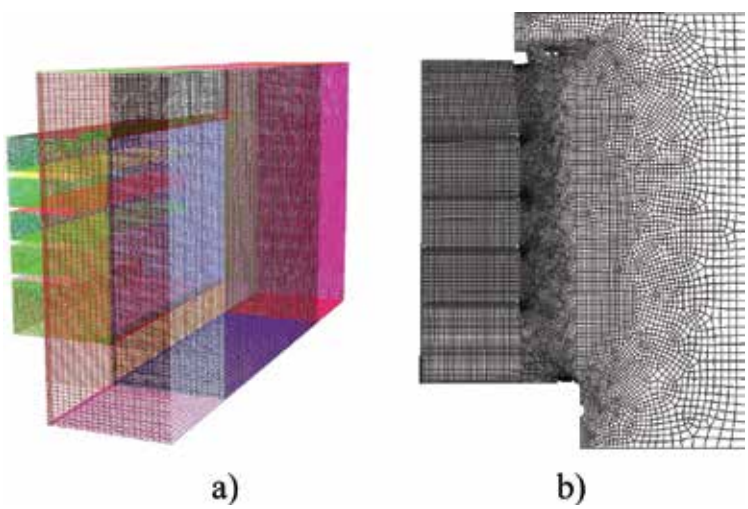

Figure 20. Structured discretization. a, view of the discretization domain; b, cross-section of the discretization domain.

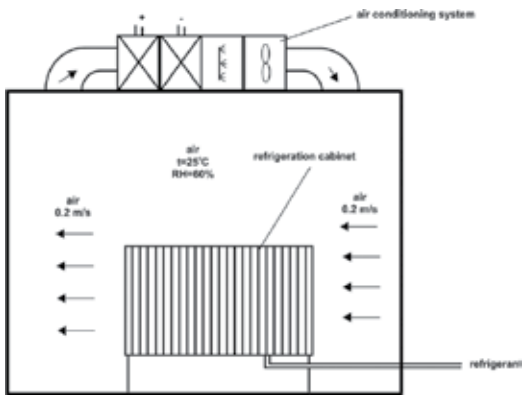

Figure 21. Placement of the vertical refrigeration cabinet inside the climatic chamber.

Table 2 summarizes the transducers used in the experiments; the placement of the temperature, humidity, and velocity sensors in front of each shelf is shown in **Figure 22a**; temperature, humidity, and velocity sensors were also placed at the exit of the horizontal grill (GPA, **Figure 22b**); all the transducers were connected to a central data acquisition unit (**Figure 22c**). The sensors were placed in three vertical planes along the cabinet length: left, middle, and right (1, 2, 3, **Figure 23**).

Transducer type	Model	Purpose	Precision
Temperature	RTD, SEM 105 P	Ambient air temperature measurement	±0.1°C
Temperature	TC with PTFE insulation	Temperature measurement inside the cabinet	±0.2°C
Humidity	SEM 105H-3	Air humidity inside the cabinet and in the climatic test chamber	±0.3%
Velocity	Hot wire sensor, VelociCalc	Measurement of air velocity at the exit of GPA grill	±0.015 m/s

Table 2. Summary of the transducers and their characteristics.

Figures 24 and **25** present the experimental results referring to the air velocity and temperature at the exit from the horizontal grill (GPA). The experimental data were then filtered using a C++ program; **Figures 26** and **27** show the filtered results.

Based on the charts presented in **Figures 26** and **27**, polynomial functions for the velocity and temperature variations were defined as:

a. velocity functions:

- left plane:

$$f(v_1, \tau) = (-1.4 \cdot 10^{16} \cdot v^{10} + 4.4 \cdot 10^{15} \cdot v^9 - 5.6 \cdot 10^{14} \cdot v^8 + 3.9 \cdot 10^{13} \cdot v^7 - 1.6 \cdot 10^{12} \cdot v^6 + 4.1 \cdot 10^{10} \cdot v^5 - 6.1 \cdot 10^8 v^4 + 4.8 \cdot 10^6 \cdot v^3 - 22484 \cdot v^2 + 162.5 \cdot v) + A_1 \cdot \sin(6.283 \cdot \tau / T_1); \quad (5)$$

- middle plane:

$$f(v_2, \tau) = (1.1 \cdot 10^{16} \cdot v^{10} - 4 \cdot 10^{15} \cdot v^9 + 5.6 \cdot 10^{14} \cdot v^8 - 4.3 \cdot 10^{13} \cdot v^7 + 1.9 \cdot 10^{12} \cdot v^6 - 5.2 \cdot 10^{10} \cdot v^5 + 7.7 \cdot 10^8 v^4 - 5.8 \cdot 10^6 \cdot v^3 + 18574 \cdot v^2 + 4.2 \cdot v) + A_2 \cdot \sin(6.283 \cdot \tau / T_2); \quad (6)$$

- right plane:

$$f(v_3, \tau) = (-2.1 \cdot 10^{15} \cdot v^{10} + 6.9 \cdot 10^{14} \cdot v^9 - 9.5 \cdot 10^{13} \cdot v^8 + 7 \cdot 10^{12} \cdot v^7 - 3 \cdot 10^{11} \cdot v^6 + 7.5 \cdot 10^9 \cdot v^5 - 1 \cdot 10^8 v^4 + 8.7 \cdot 10^5 \cdot v^3 - 11436 \cdot v^2 + 167.91 \cdot v) + A_3 \cdot \sin(6.283 \cdot t / T_3). \quad (7)$$

b. temperature functions:

- left plane:

$$g(t, \tau) = t_{1med} + A_{11} \cdot \sin\left(\frac{6.283 \cdot \tau}{T_{11}}\right); \quad (8)$$

- middle plane:

$$g(t, \tau) = t_{2med} + A_{22} \cdot \sin\left(\frac{6.283 \cdot \tau}{T_{22}}\right); \quad (9)$$

- right plane:

$$g(t, \tau) = t_{3med} + A_{22} \cdot \sin\left(\frac{6.283 \cdot \tau}{T_{33}}\right). \quad (10)$$

The above functions were introduced as user defined functions (UDF) into the numeric model.

4.2. The numeric model

The general equation for the incompressible flow of a fluid for a dependent variable Φ ($\Phi = 1$ for the continuity equation; $\Phi = v$ for the momentum equation; $\Phi = t$ for the energy equation) is [12]:

$$\frac{\partial}{\partial x_i}\left(\rho v \phi - \Gamma_\phi \frac{\partial \phi}{\partial x_i}\right) = S_\phi. \quad (11)$$

The model is based on the following assumptions:

- air is considered a perfect gas;
- the latent heat of condensation for the humidity in the air curtain is neglected;
- the air curtain is considered as a jet;
- air velocity and temperature at the horizontal grill are modeled as polynomial functions;
- the effect of air flowing through the holes of the perforated plate behind the shelves is neglected.

The model is based on two equations (one for the turbulent kinetic energy and the other one for the dissipation rate of the turbulent kinetic energy), using the SIMPLE algorithm. The

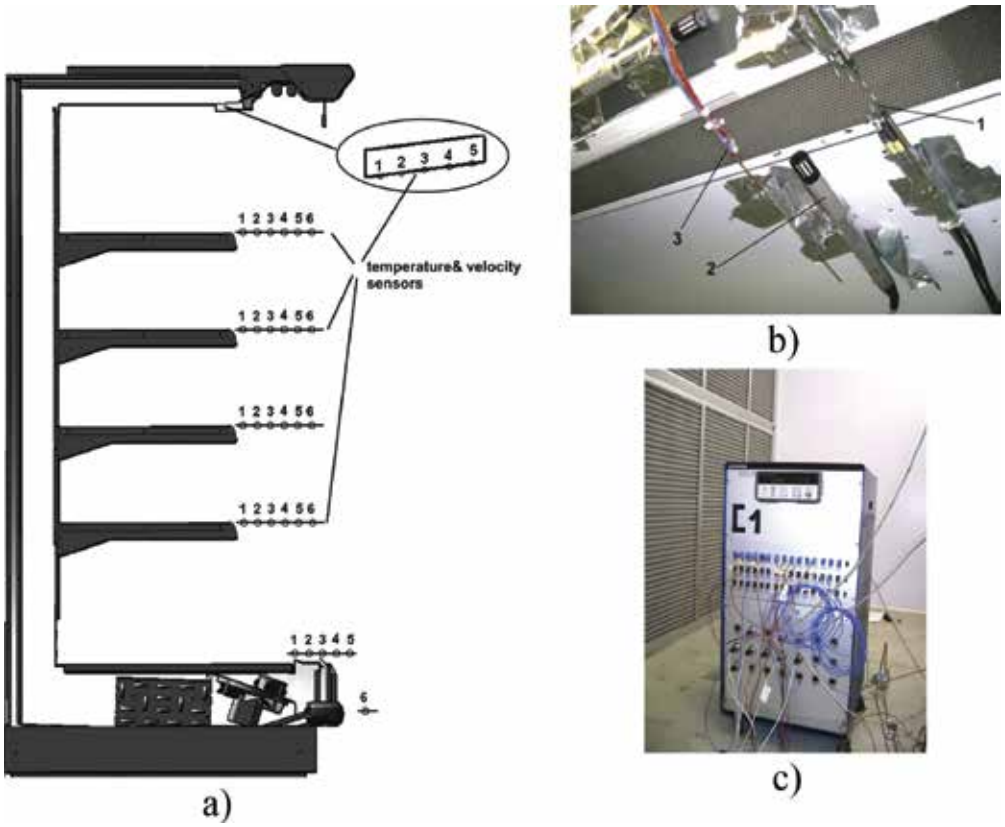

Figure 22. Placement of the sensors and the central data acquisition unit. a, placement of the temperature, humidity, and velocity sensors inside the cabinet; b, placement of the temperature, humidity, and velocity sensors at GPA grill; c, view of the central data acquisition unit.

calculation is an iterative process, using the pressure-velocity coupling algorithm, in which the momentum and continuity equations, based on pressure, is solved simultaneously, and the terms referring to the pressure gradient and mass flow rate are discretized implicitly.

4.3. Boundary conditions

The boundary conditions were imposed by the pre-processing program Gambit and completed with functions and values in the Fluent CFD simulation program [12]. The boundary conditions also took into account the conditions inside the climatic chamber (t_{env} = 25°C, Φ_{env} = 60%, v_{air} = 0.2 m/s, according to EN-ISO 23953); as there are different boundary conditions for the horizontal grill (GPA) and base grill (GRA), these are presented separately.

4.3.1. Boundary conditions for GPA

The velocity and temperature functions, for the three vertical planes considered (left, middle, and right), were the ones presented above. The air turbulence was specified using the turbulence intensity [12]:

$$I_t = 0.16 \cdot \mathrm{Re}_{Dh}{}^{-0.125} \cdot 100. \tag{12}$$

Turbulence intensity at GPA exit had the following values: $I_t = 2.66$ (left plane); $I_t = 1.83$ (middle plane); $I_t = 2.16$ (right plane).

A boundary condition was also imposed for the lateral plane (0, **Figure 23**); here, air velocity was constant over the entire section (0.2 m/s), the flow was laminar, and air temperature was 25°C.

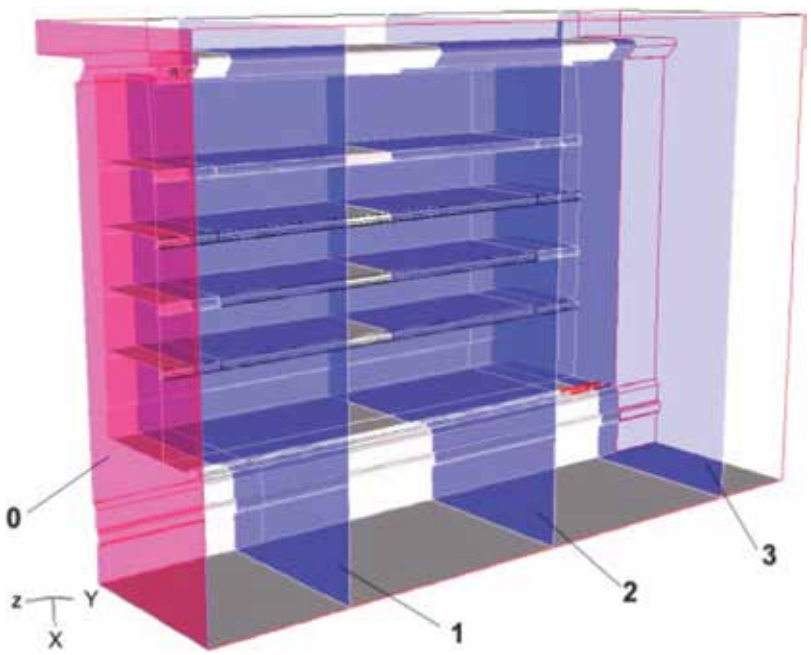

Figure 23. Measuring planes. 0, lateral plane, with air entering at 0.2 m/s; 1, left plane; 2, middle plane; 3, right plane.

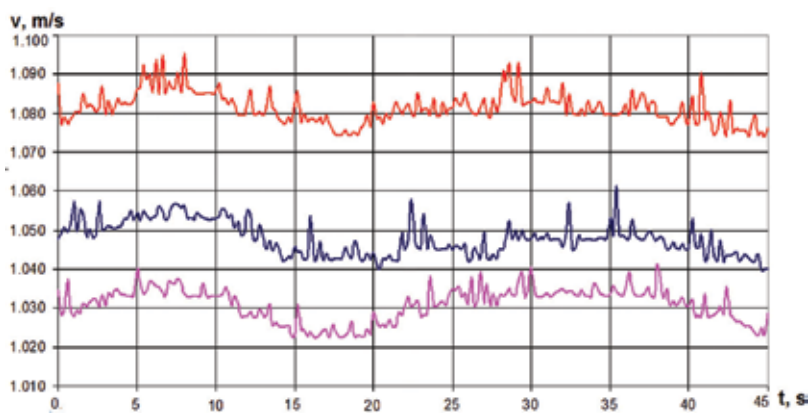

Figure 24. Air velocity at the GPA level.

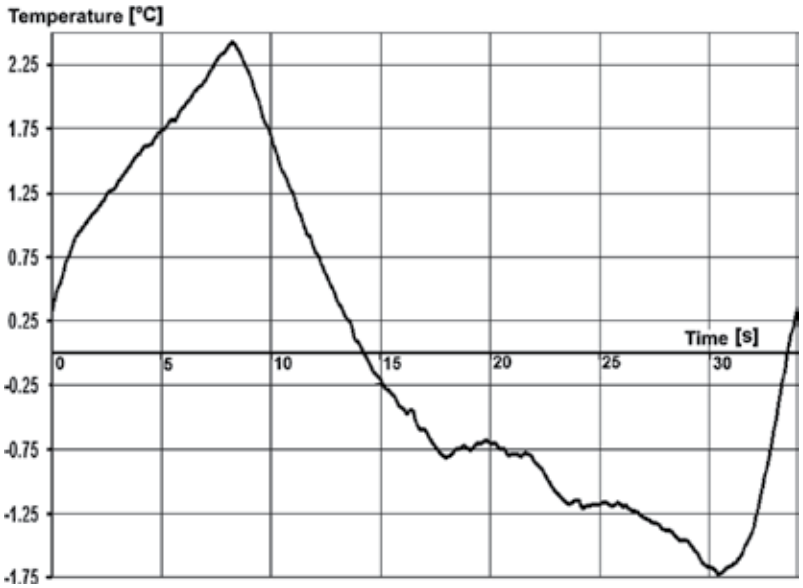

Figure 25. Air temperature at the GPA level.

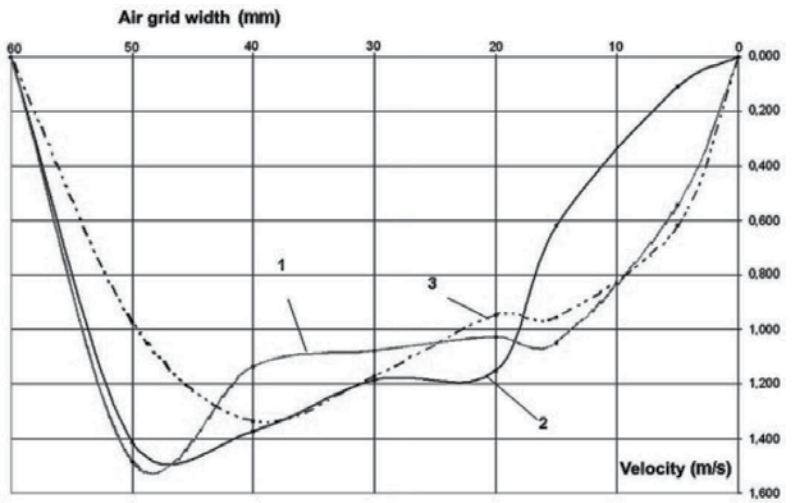

Figure 26. Air velocity profiles, after filtering, for the three vertical planes.

4.3.2. Boundary conditions for GRA

The boundary conditions for the base grill take into account the average experimental values: over the entire length of the grill, air velocity is 1.7 m/s, and air temperature is +9.2°C. The air turbulence parameters were defined as above.

http://dx.doi.org/10.5772/intechopen.69136

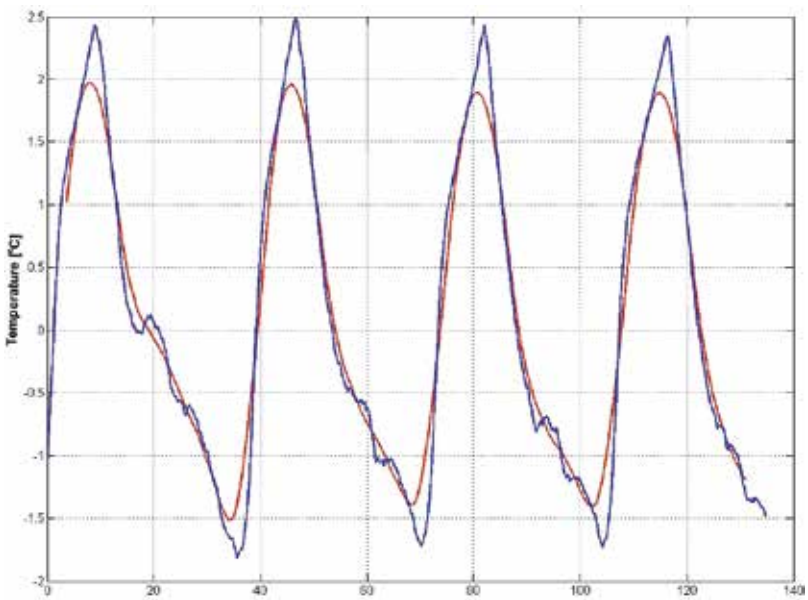

Figure 27. Air temperature profiles, after filtering, for the three vertical planes.

4.3.3. Boundary conditions for heat flow rate

The boundary conditions for the heat flow rate take into account the conductive heat transfer through the cabinet walls and the heat generated by the illumination system of the display case.

The conductive heat transfer was defined using Fourier's law; the overall heat transfer coefficient was calculated based on the thermal conductivity of each individual layer of the respective wall. The conductive heat transfer rates were as follows: 6 W/m^2 for the ceiling of the cabinet; 7 W/m^2 for the bottom of the cabinet; and 7.63 W/m^2 for the side walls.

Fluorescent lamps, type OSRAM L58W20, were used for the illumination of the appliance; the corresponding heat flow rate was 10 W/m^2.

4.3.4. Boundary conditions for the walls

The cabinet walls were modeled only in the wall-air contact areas. The average temperatures were obtained experimentally, as follows: evaporator fins—0.95°C; interior walls +7°C; shelves +5°C.

4.3.5. Product thermal load

According to the EN-ISO 23953 standard, the load is simulated using a gel-type substance (tylose), with thermal properties similar to the ones of beef meat. However, in the present simulation, there was no product load inside the cabinet.

4.4. Processing

In the processing stage, the time step was set at 0.2 s, the number of steps was 1800, and the maximum number of iterations for one step was 10.

The simulation was performed on a Pentium IV, DualCore 6400, 2.4 GHz system with 4 GB RAM; for 6 min of simulation and a total number of 18,000 iterations, the computing time was approximately 12 h.

In order to prevent the equation coefficients from changing too quickly, the change in dependent variables from one iteration to another was slowed by "relaxing" them. Thus, the linear relaxation method was used for the control of the CFD simulation in order to maintain its stability; **Table 3** presents the values of the relaxation factors for the different physical parameters.

Property	Variable	Relaxation factor, α
Pressure	p	0.3
Density	ρ	0.5
Lift force	F	0.5
Momentum	v_i	0.8
Turbulent kinetic energy	k	0.6
Dissipation rate of the turbulent kinetic energy	ε	0.6
Turbulent viscosity	μ_t	0.8
Energy	E	0.7

Table 3. Linear relaxation factors.

In this CFD simulation, the convergence criterion was selected so that the residues remained lower than 10^{-6}.

4.5. Post-processing

Post-processing is the final stage of the CFD simulation, aiming to display the temperature and velocity fields, as well as the streamlines in the simulation domain. This stage is useful in the intermediate phases of the simulation, allowing its calibration based on the experimental data; at the end of the simulation, the final temperature and velocity fields and the streamlines are presented in a graphical form.

Figures 28–30 present the temperature fields in the three vertical planes taken into account (see **Figure 23**); the results show that, for the lower shelves, the temperature is with at least 4°C higher than the one required (5°C, according to ISO 23954-2:2005), which means that this area is not adequate for the storage of refrigerated goods.

Figure 31 presents the velocity field profile in the middle plane, at the exit of the horizontal grill (GPA).

Figure 32 presents the velocity field in the vertical right plane and also in the horizontal plane, in the vicinity of the base air grill (GRA). In the horizontal plane, air velocity was comprised

http://dx.doi.org/10.5772/intechopen.69136

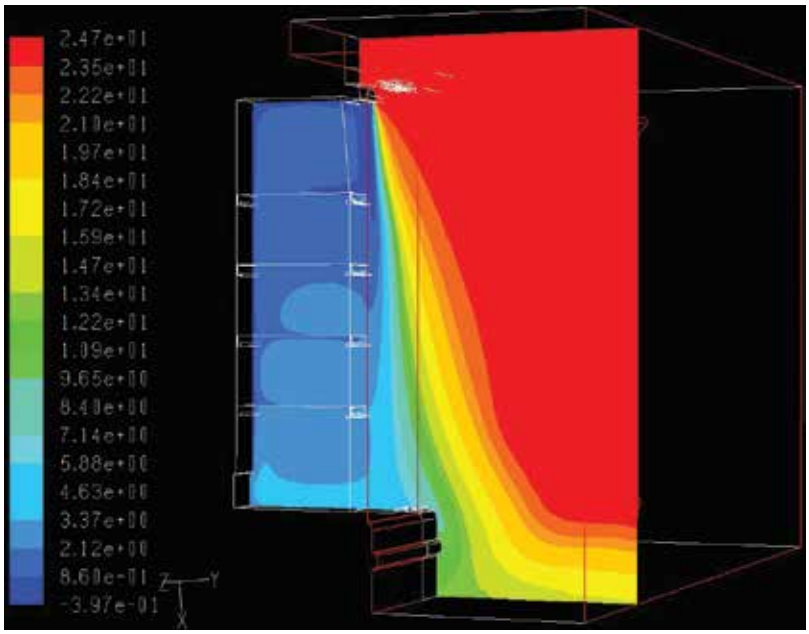

Figure 28. Temperature field in the left plane of the cabinet, at the end of the 6 min simulation [°C].

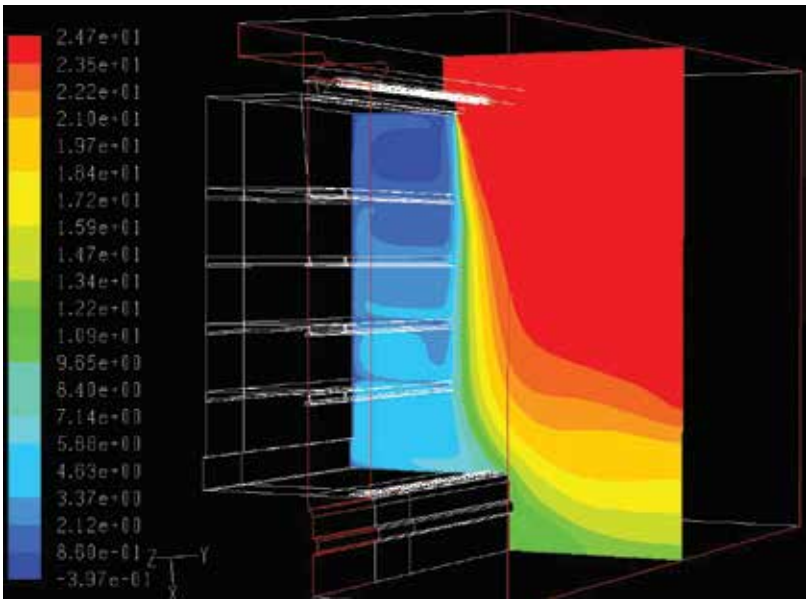

Figure 29. Temperature field in the middle plane of the cabinet, at the end of the 6 min simulation [°C].

between 0.4 and 0.6 m/s; these values were significantly lower than the average value of 1.7 m/s, which was considered as a boundary condition for GRA, showing the non-uniformity of the air curtain in this area.

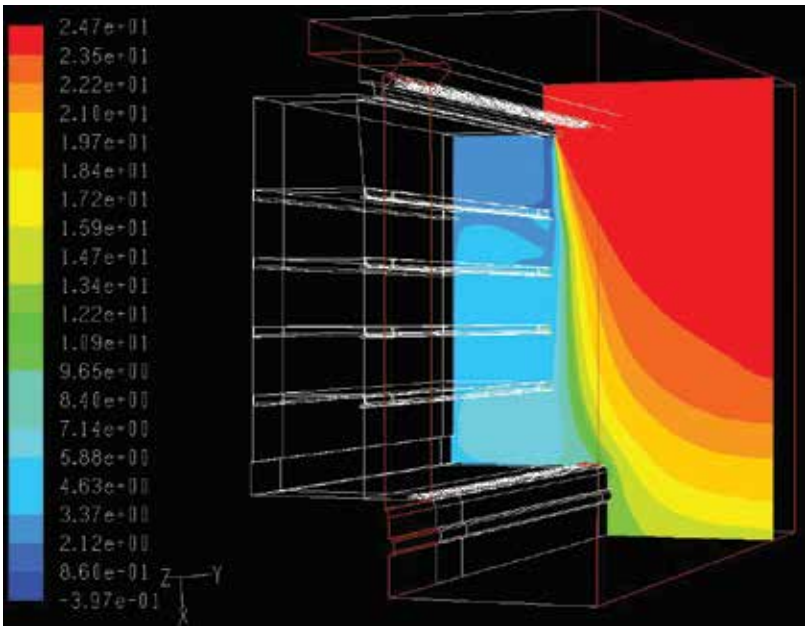

Figure 30. Temperature field in the right plane of the cabinet, at the end of the 6 min simulation [°C].

The streamlines presented in **Figure 33** complete the picture of the air curtain in terms of air velocity, while **Figures 34** and **35** display the streamlines in terms of air temperature; the results can be summarized as follows:

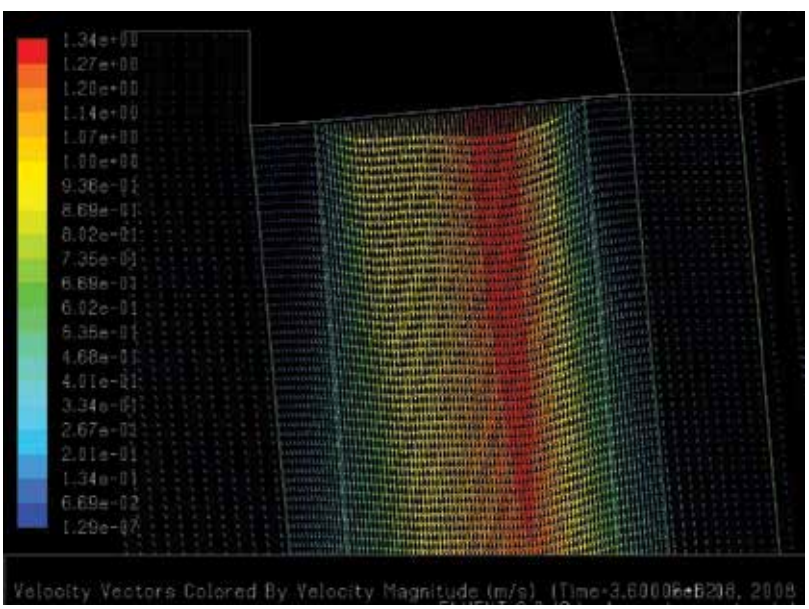

Figure 31. Velocity field profile at GPA, in the middle plane, at the end of the simulation.

http://dx.doi.org/10.5772/intechopen.69136

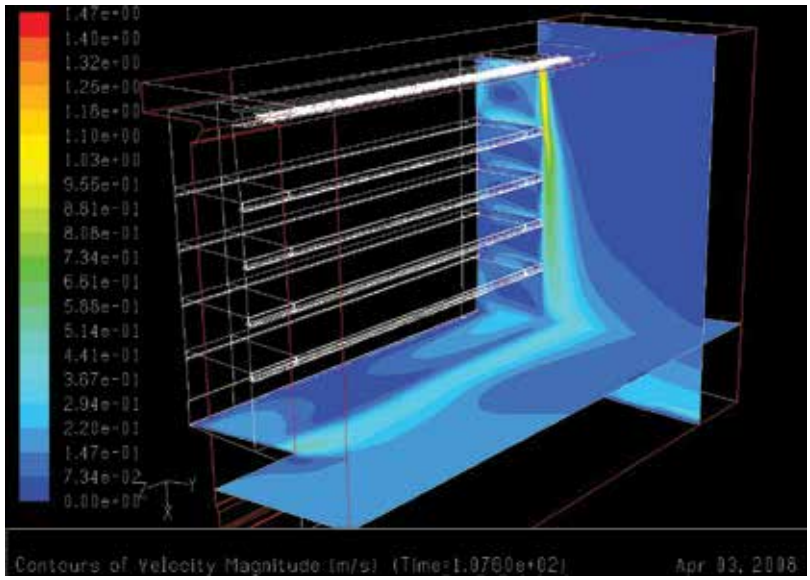

Figure 32. Velocity field profile in the vicinity of GRA and in the vertical right plane.

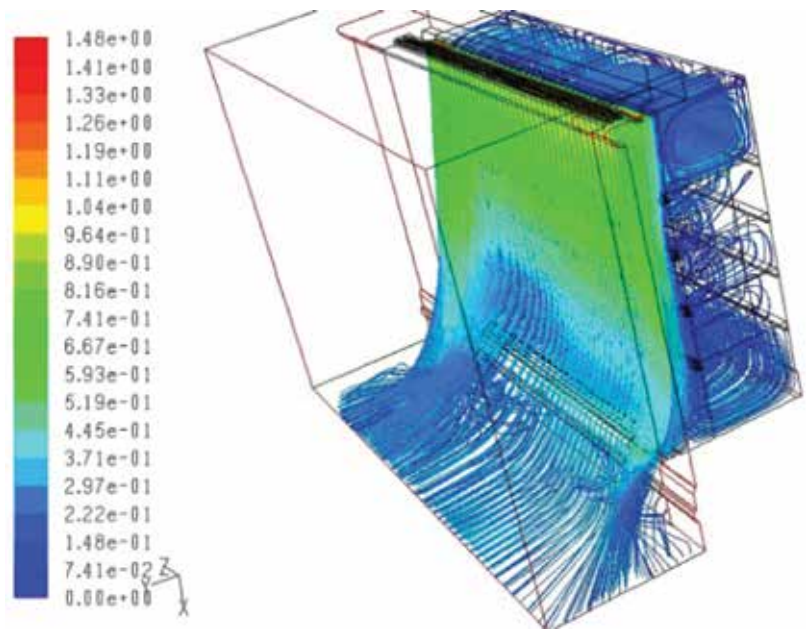

Figure 33. Streamlines for air velocity [m/s].

- the turbulence and temperature are higher at the back of the cabinet;
- the infiltration rate through the air curtain is higher in the lower part of the cabinet, through the left and right planes;
- the temperature difference between the upper and lower shelves is 6°C.

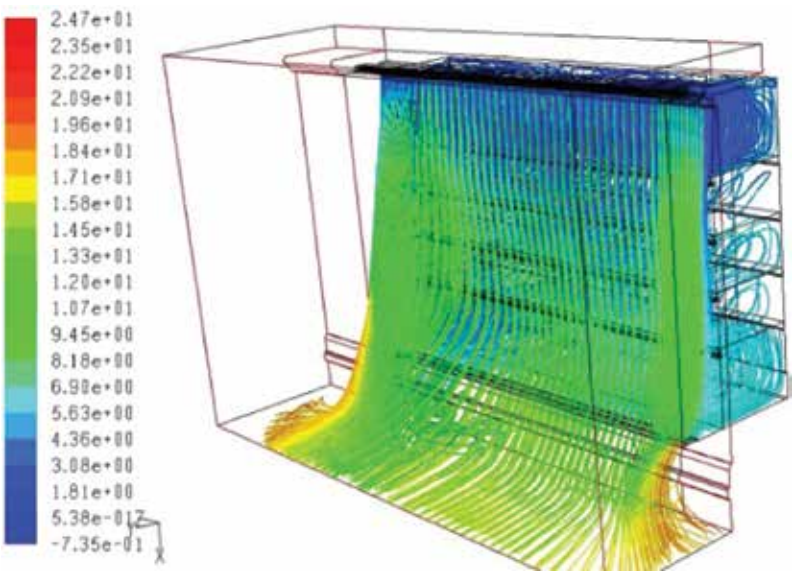

Figure 34. Streamlines for air temperature, front view [°C].

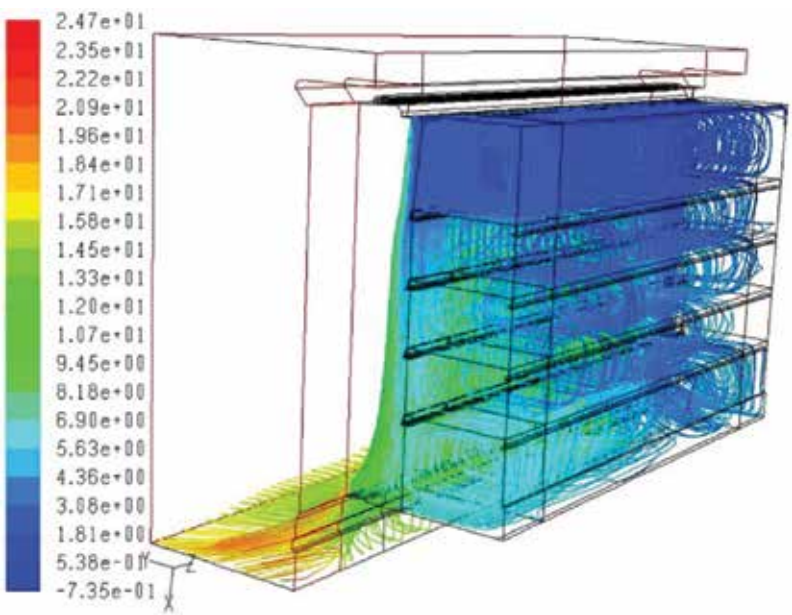

Figure 35. Streamlines for air temperature, rear view [°C].

5. Conclusions

Refrigeration slows down the chemical and biological processes in foods, such as the accompanying deterioration and the loss of quality, extending the shelf life of the products.

Food chilling is performed with mechanical refrigeration systems or with ice; the temperature of the product is lowered to 0–8°C, depending on the type of food. The chilling medium in mechanically cooled chillers may be air, water, or metal surfaces; batch or continuous operation is possible when using mechanical refrigeration systems, while the batch operation is used in the ice chilling systems.

Retail refrigeration cabinets use cold air, circulated through natural or forced convection. The open front refrigeration cabinets use air curtains in order to prevent the infiltrations of warm air into the cabinet; the proper design of the air curtains imposes an in-depth understanding of the cabinet's fluid dynamics.

CFD simulation was applied as a case study for a refrigeration cabinet. The simulation led to the conclusion that, for the lower shelves, the temperature is at least 4°C higher than the one required by standards, while there was a 6°C temperature difference between the upper and lower shelves of the cabinet; in the meantime, the simulation showed the non-uniformity of the air curtain in the vicinity of the base air grill. Turbulence intensity and temperature were higher at the back of the cabinet.

Nomenclature

A_1, A_2, A_3	amplitude of the air velocity functions, m/s
A_{11}, A_{22}, A_{33}	amplitude of the air temperature functions, °C
c	specific heat of the product, J/kg·°C
D_h	hydraulic diameter, m
h	convective heat transfer coefficient, W/m^2·°C
I_t	turbulence intensity
m	product mass, kg
Re_{Dh}	Reynolds number based on the hydraulic diameter
S	product surface, m^2
S_Φ	source term
T_1, T_2, T_3	period of the air velocity functions, s
T_{11}, T_{22}, T_{33}	period of the air temperature functions, s
t	product temperature, °C
t_i	initial product temperature, °C
t_f	final product temperature, °C
t_0	cooling medium temperature, °C
t_{1med}, t_{2med}, t_{3med}	average cabinet temperatures, °C

v	air velocity m/s
w	cooling rate, °C/s
x_i	orthogonal coordinates
α	relaxation factor
Γ_Φ	diffusion coefficient
ν	cinematic viscosity, m^2/s
ρ	density, kg/m^3
τ	time, s
τ_r	chilling time, s
ϕ	dependent variable

Author details

Radu Roşca*, Ioan Ţenu and Petru Cârlescu

*Address all correspondence to: rrosca@uaiasi.ro

University of Agricultural Sciences and Veterinary Medicine "Ion Ionescu de la Brad", Iaşi, Romania

References

[1] Mascheroni H M, editor. Operations in food refrigeration . Boca Raton, FL: CRC Press, Taylor&Francis Group; 2012. p. 383

[2] Sun Da-Wen, editor. Handbook of frozen food processing and packaging. Boca Raton, FL: CRC Press, Taylor&Francis; 2006. p. 723

[3] Fellows P. Food Processing Technology, principles and practice. 2nd edition. Cambridge: CRC Press, Woodhead Publishing Limited; 2000. p. 575

[4] Naghiu Al, Apostu S. Refrigeration and air conditioning techniques in food industry (in Romanian). Cluj-Napoca: 2006. p. 536

[5] James S J, James C. Meat refrigeration. Cambridge: CRC Press, Woodhead Publishing Limited; 2002. p. 347

[6] Singh R, Kachhwaha SS. Experimental studies on a scraped surface ice slurry generator. International Journal of Engineering Science and Innovative Technology. 2013;**2**(4):117–131. Available from: http://www.ijesit.com/Volume%202/Issue%204/IJESIT201304_18.pdf [Accessed: June 10, 2016]

[7] IceSynergy. MaximICE Systems Information [Internet]. 2010. Available from: http://www.icesynergy.com/L2-4-2prod-syst.html [Accessed: 2017-01-20]

[8] Graham J, Johnston WA, Nicholson FJ. Ice in fisheries. FAO Fisheries Technical Paper. 1992;**331**:75. Available from: http://www.fao.org/docrep/T0713E/T0713E00.htm#Contents [Accessed: May 21, 2016]

[9] Funke. Heat Exchanger Systems [Internet]. 2016. Available from: http://en.funke.cn/products_detail/&productId=30.html [Accessed: 2017-01-20]

[10] Kennedy C J, editor. Managing frozen foods. Cambridge: CRC Press, Woodhead Publishing Limited; 2000. p. 286

[11] Faramarzi PER. Efficient display case refrigeration. ASHRAE Journal. 1999;**41**(11):46–54

[12] Fluent Incorporated. Fluent 6.1 User's Guide. Lebanon, New Hampshire: Fluent Incorporated; 2003. p. 1864

Chapter 4

Refrigeration in Winemaking Industry

Ángel Benito Sáez, Eva Navascues Lopez-Cordon,
Fernando Calderón Fernández and
Santiago Benito Sáez

Additional information is available at the end of the chapter

http://dx.doi.org/10.5772/intechopen.69481

Abstract

The effectiveness of winery operations in a wine cellar and their impact on wine quality depend closely on the technology used. A correct application of refrigeration systems is perhaps the best guarantee of a correct processing process. In this work, a review of the refrigeration engineering in warehouse is carried out, calculating the refrigeration needs of each one of the main stages of elaboration, according to the different winemakings. The energy requirements for the cold maceration and debourbage in white winemaking, the cooling of the crushed-grapes in the elaboration of red wine, as well as for the temperature control during fermentation and physical-chemical stabilization of the finished wine are calculated. The main cold production techniques in the winery are also addressed to respond to those needs.

Keywords: winemaking, refrigeration, fermentation, tartaric stabilization, wine refrigeration exchanger

1. Introduction

The temperature control in each one of the winemaking operations is a usual and extended practice. The thermal conditioning of the grapes on their arrival at the winery is already an essential requirement in some wineries, and even the grape harvesting systems are adapted to this factor (early or even night grape harvesting), which is very important in warm regions.

The prefermentation works of cold maceration and debourbage in white winemaking, the pellicular maceration in red wines, the controlled fermentations, as well as the processes of finished wine conditioning require a control and maintenance of their optimum temperatures. **Table 1** shows the most important applications of refrigeration in a warehouse, as well as the optimal temperatures for each operation.

Importance				
Operation	**V. in white wine**	**V. in red wine**	**Optimum temperature**	**Effects on wine/must**
Cold extraction	+	–	−5/−10°C	Must sugar concentration by elimination of frozen water
Cold maceration	++	++	5/10°C	Extraction of aromatic precursors Fermentation delay
Musts Refrigeration	+++	+++	10/18°C	Enable the debourbage in white wines In red wines lower the temperature until the optimum of fermentation
Deboubarge	+++	–	10/15°C	Accelerate the sedimentation process
				Delay the start of fermentation
Pellicular maceration	++	++	<15°C	Extraction of polyphenolic fraction and aromatic precursor in red wines before fermentation
Fermentation thermal control	+++	–	13/20°C	Aromatic enhancement in white wines
				Avoid fermentation stops
Thermal control of fermentation and meccanization	–	+++	25/30°C	Decrease aromatic losses
				Avoid fermentation losses
Cold storage of finished wines	+++	+++	10/15°C	Slow down microorganisms metabolism
				Decrease oxidation and aromatic losses
Amicrobic stabilization	+++	++	<5–10°C	Filtration process improvement
Colloidal stabilization	–	+++	<5–10°C	Hasten unstable coloring matter
Tartaric stabilization	+++	+++	−5/1°C	Hasten tartaric salts of calcium and potassium
				Control the oxidation-reduction process and cession
Aging in oak	+++	+++	15–20°C	Decrease volume losses
				Avoid undesirable microbial development
Second fermentation in bottle	+++		12/15°C	Control the alcoholic fermentation. Refinement of sparkling wine by slow transfer of fermentation and autolysis products.
Bottling	+	+	15°C	Reduce loss of aroma and enable the process
Bottle store	+++	+++	12–18°C	Enhance wine stability

Table 1. Applications of cold engineering in a wine cellar: optimum working temperatures in wine cellars and the effect on must/wine.

2. Refrigerating necessities on prefermentative operations

The temperature control can be done from the first stages of winemaking, by cooling the freshly squeezed grape or the must at the exit of the press. Most authors recommend the entry

http://dx.doi.org/10.5772/intechopen.69481

of red wine vintage at 20°C due to an inlet temperature of 26–28°C, this can lead to a difficult start of fermentation and higher production of volatile acidity [1–3]. The prefermentative maceration applied to certain varieties (Pinot Noir) for the extraction of polyphenols needs to bring the crushed-grapes to temperatures below 13°C, to avoid starting fermentation [4].

In white wines, the pellicular maceration of aromatic grapes (Moscatel, Gewürztraminer, Verdejo, Sauvignon Blanc and Chardonnay) at low temperatures enables the extraction of aromatic compounds. The static debourbage is a slow process, which allows in its course the proliferation of microorganisms. Cold helps to stop or slow the start of fermentation, and the low temperatures increase the speed of sedimentation. Time and temperature are the keys for a quality debourbage. The use of pectolytic enzymes allows a considerable reduction of debourbage times, but on the other hand, the cold slows down the enzymatic phenomena of despectination. Therefore, in the debourbages with addition of enzymes, the temperature of the must should not be less than 10°C [5, 6]. The promptness of enzymatic debourbage is doubled when the temperature rises to 10°C, at the expense of risks of grater microbial proliferation, and is discouraged for vintages with poor sanitary quality. Temperatures under 8°C promote the inactivation of the enzymes and lengthen the fermentative latency phase. In any of the above cases, the refrigeration needs to cool the must or the crushed-grapes to the operating conditions are defined by the fundamental equations of the energy balance (Eq. (1)) [3, 7–10]:

$$\mathrm{d}Q/\mathrm{d}t = m \times C_e \times \Delta t \tag{1}$$

- $\mathrm{d}Q/\mathrm{d}t$ is the cooling capacity per unit of time (kJ/h).
- m is the mass flow of must or crushed-grapes (kg/h). $m = vx_{\rho}$.
- ρ is the density (kg/m^3).
- C_e is the specific heat of the must/crushed-grapes/wine, which according to authors is:
  - C_e = 4.18 kJ/kg °C [11,12].
  - C_e = 3.8 kJ/kg °C for musts with a density of 1090 kg/m^3 [13].
  - C_e = 4.5 kJ/kg °C for wines with a density of 995 kg/m^3 [13].
  - C_e = 3.65 kJ/kg °C for musts and 4.15 kJ/kg °C for wine [14, 15].
- Δt is the (initial temperature–final temperature) of must/crushed-grapes.

3. Refrigeration requirements in prefermentative operations

The fermentation of sugar by the yeast glycolytic allows the cells to transform glucose and fructose into pyruvic acid and this, through an enzymatic complex of carboxylase activity, will be transformed into acetaldehyde, which is finally reduced by the alcohol dehydrogenase into ethanol. This transformation is an exergonic reaction, releasing heat which, when accrues in the must, causes a thermic elevation.

The metabolic activity of the yeasts increases in proportion with the temperature with maximum rates between 25 and 28°C [16]. Temperatures above 32–35°C imply high risks of fermentation stops, as well as further proliferation of acetic and lactic bacteria. Fermentations below 18°C are distinguished by delayed onset (longer latency phase) and very slow fermentation development. In years of warm harvests, in large deposits or cellars in the middle of the season with several fermentation tanks, it is easy for the microbial activity itself to pass through the 35°C barrier, negatively affecting both cellular viability and the sensorial characteristics of the wine [1–3, 16, 17]. On the other hand, fermentations at moderate or even low temperature (below 18°C) allow preserving the aromatic precursors of the grape varieties and stimulating the formation of secondary compounds by yeasts. All this underlines the importance of having a temperature control of fermentation in the wine cellar. It is considered suitable for fermentation of red wines 28–30°C (aid to maceration), while for fermentation of white and rose, temperatures below 22°C are recommended. The cooling of the must or the crushed-grapes, as indicated above, allows the fermentation process to start at the desired temperature in the case of warm harvests. It is an added advantage in the case of a cold debourbage.

The low temperature fermentations (13°C or less) have a great interest for the production of white and rose wines, especially for musts arising from varieties with a great aromatic potential. In addition to avoiding their evaporation, the low temperatures considerably condition the bacteria development, allowing the use of less doses of sulfur dioxide.

It does not happen the same with the yeasts. The low temperatures influence in a different way on the different species which concur in the must. Some yeasts such as *Kloeckera apiculata* dominate fermentation at 13°C, according to Heard and Fleet [18].The survival of non-*Saccharomyces* species affects the production of certain undesirable volatile substances such as acetic acid and ethyl acetate [19]. The temperature affects the biochemical activities of fermentative yeasts, which in turn affects the wine and its composition. The most notable effect of yeast adaptation at low temperatures is the increase in the degree of unsaturation of the fatty acids [20] and the reduction of the synthesis of sterols. Both changes are an important determinant of the membrane fluidity and reduce the transit of nutrients, resulting in an inhibition of fermentative activity.

According to Suárez and Iñigo [1], not all sugar molecules will follow the equation of Gay-Lussac, obtaining two molecules of ethanol and two of CO_2 for each mole of glucose, but depending on the metabolism of the yeast, a certain number of molecules are going to be intended to glycerine and pyruvic acid, which will be the origin of secondary products in wine. As a consequence, the thermal flow originated during fermentation will depend on the importance of these secondary reactions.

Bouffards [21] using a sealed calorimetric chamber determines the heat of fermentation reaction between 83.7 and 100.5 kJ/mol. Subsequently, several authors have established a thermal flow ranking from 71 [22] to 106 kJ/mole [1], according to the purity of the fermentative process and the derivation of the glucose molecules toward other secondary metabolic routes. Assuming the most thermodynamically adverse case and the known parallel reactions always occurring to the alcoholic fermentation, the average mean value of heat flow most widely accepted by the various experts is 100.32 kJ/mole [2, 3, 10, 19, 23].

This heat released by mole of transferred sugar corresponds to the theoretical case of an instant fermentation process. In fact, the process lasts several days in which heat dissipation takes place by contact of the tank walls with the outside and by the release of volatile products released during the transformation. According to this, the data referred to by the authors mentioned above as energy released during the process are modified by a factor corresponding to the rate of consumption of sugars throughout the fermentation process with units of [mole/m^3.h]. This aspect, directly related to the concentration of ethanol and CO_2 produced per unit of time, depends on the physical and chemical conditions of the fermenting must (content in sugars, temperature, acidity, pH and richness in nitrogen sources), operating conditions (yeast morphology population, temperature, agitation and oxygenation) and fermentation time.

To identify and quantify the influence of these factors on the amount of heat energy released throughout the fermentation time, several authors have developed simulations and mathematical models.

Boulton [24] establishes that the loss of heat throughout the fermentation process is defined by Eq. (2):

$$dQ/dt = \Delta H \times dS/dt, \tag{2}$$

- dQ/dt is the energy released per unit of time (kJ/h).
- ΔH is the energy released during fermentation of one glucose mole (kJ/mol).
- dS/dt is the rate of reduction of sugar content by yeast consumption (mol/m^3h).

This quantification system of the energy released during the fermentation process is the most widely accepted by the experts, although there is no consensus regarding the calculation and valuation of the term dS/dt, that is, to say on the system of calculation of the decrease in the concentration of fermentable sugars per unit of time. Several authors propose mathematical models to define this rate of degradation, based on empirical data from different variables.

The model proposed by El Haloui et al. [25] relates the concentration of residual sugars with the volume of CO_2 released, according to Eq. (3):

$$S = 3.92 \times V_{CO_2} + 0.1463 \times S_o - 117 \tag{3}$$

where

S is the sugars consumed in a precise moment (g/L).

V_{CO_2} is the volume of CO_2 produced until that moment (L).

S_o is the initial concentration of sugars (g/L).

The volume of CO_2 released can be calculated by empirical analysis in laboratory scale tests with Muller valve occluded flasks [1] or at the level of experimental microvinifications using CO_2 flowmeters [26, 27].

Afterwards, and based on empirical data, the same authors [28] build a model which relates fermentation curve with the density and initial concentration of sugars in the initial must (Eq. (4)):

$$S = 0.99109 \times S_o - 2.096 \times 10^3 \times d_{30^\circ} \text{ relative must density} - \text{wine at } 30^\circ\text{C} \quad (4)$$

The concentration of residual sugars in each moment of the fermentative process can be calculated, establishing the concentration of glucose-fructose by enzymatic methods or by detection systems based on measurements of radiation in that infrared spectrum.

López and Secanell [15] develop a complex model of the heat evolution curve during fermentation based on physical-chemical parameters such as initial sugar content, total acidity, fermentation temperature and duration of this one. They get expressions such as Eq. (5):

$$\mathrm{d}Q/\mathrm{d}t = \frac{k_1}{k_2 - k_1}(e^{-k_2 t} - e^{-k_1 t}) \quad (5)$$

in which k_1 and k_2 at the same time are constants representing values of activation energy of the fermentative chemical reaction and depend on the temperature and the total acidity of the must. Starting from this equation, the authors calculate the maximum energy evolution during the process according to the following expression (Eq. (6)):

$$Q_{\max} = 100.32/180 \times S_o \times F_c \quad (6)$$

where

S_o is the initial sugar concentration (g/L).

F_c is the correction factor depending on initial concentrations.

Avilés [11] states that the heat developed in fermentation of the must is determined by the probable alcoholic strength of the wine according to Eq. (7):

$$Q =: K \times^\circ A \times L \times P \quad (7)$$

where

K is the heat transfer coefficient for each probable alcoholic strength depending on the material of the fermentation tank (1, 3/2, 2).

°A is the probable alcoholic grade of the wine (%vol/vol).

L is the must volume in fermentation (L).

P is the coefficient of thermal development by the metabolic activity of yeasts.

Starting from a wide series of empirical data, and from the equation raised in 1978, Boulton et al. [10] established that with a fermentation ratio of 2 Brix/day the energy released is approximately 0.46 kJ/L h for white wines, while for red wine with a ratio reaching 6 °Brix/day of sugar consumption, the energy released can be set at 1.36 kJ/L h.

According to the Federation Départamentale des Centres d'Etudes et d'Informations Oenologiques of the Gironde-France, FD-CEIOG [12], the heat released in fermentation is defined by Eq. (8):

$$Q = \rho \times C_e \times D_t \times VF \times V/100.32 \quad (8)$$

ρ is the density of the must-wine (kg/m^3).

C_e is the specific heat of the must-wine (kJ/kg °C).

D_t is the elevation of the temperature by %vol (K%vol). The mean value of D_t is 2.8 K/%vol.

VF is the fermentation rate (%vol/J).

V is the total volume (m^3).

Flanzy [3] established that the released energy during fermentation can be estimated approximately by knowing the concentration of sugars consumed per hour and liter of must, taking into account that one mole of glucose is equal to 180 g (Eq. (9)):

$$Q : (X/180) \times V \times 100.32 \quad (9)$$

X is the concentration of sugars consumed per liter of must and hour (g/L h). The value of X varies according to the activity of fermentation, with mean values of X = 2g/L h for white wines of slow fermentation at a low temperature and of X = 7 g/L h for red wines.
180 g/mole glucose.

V is the total volume of the must to ferment (L).

100.32 kJ/mole glucose.

These mathematical models are difficult to apply in the cellar, so for practical purposes it is more interesting to consider the quantity of sugar consumed per liter of must and per hour. However, there are no reproducible models of the consumption of sugars during fermentation, but the thermodynamic curve of fermentation must be determined for each specific vinification. As an operational parameter for the calculation of cold storage needs of a wine cellar, the maximum value of energy released must be considered (Eq. (10)).

$$Q = \frac{100.32}{180} \times S_o \quad (10)$$

This means that for a must of 12° the heat released is 133 kJ/L of must in fermentation, although for the calculation of cold production equipment it is interesting to refer the total energy produced during fermentation to the duration of the same Q/t.

Part of this energy produced in fermentation is absorbed by the alcohol, the H_2O and the CO_2, which when released into the atmosphere partially or totally cools the system. A total of 180 g of glucose produces 88 g of CO_2 and 92 g of ethanol when they ferment. Each mole of CO_2 formed drags 13.62 kJ for each mole of glucose metabolized. The heat absorbed by the water and the alcohol is determined by the rate of vaporization of the substances, depending on the temperature reached during fermentation and the exterior of the premises [11]. Due to the difficulty of these calculations and the slight thermal decrease, they mean, most authors [2, 3, 10] consider that the heat lost in form of CO_2, ethanol and water equals 10% of the total heat generated.

On the other hand, a certain percentage of the energy released in fermentation is dissipated by the environment, depending on the outside temperature. When the set fermentation temperature is lower than the environment temperature, it produces a thermal transfer from the environment to the tank. The calculation of the energy released or absorbed is based on the conduction/convection heat transfer equations (Eq. (11)) [8–10]:

$$Q = U \times S \times \Delta T \tag{11}$$

U is the heat transfer coefficient. It is a function of the material of constitution of the tank as well as the speed of circulation of the air in the exterior and the presence or not of circulating currents inside the same. According to various authors, the mean value for stainless steel tanks, the static regime of outdoor air and must/indoor wine is U = 16.72 kJ/m^2 H °C [3, 8-10] or U = 4.64 w/m^2.°K [3, 18].

S is the outer surface of the tank in contact with the environment.

ΔT is the temperature difference between the must in fermentation with the exterior (°C or °K).

If fermentation tank (or later of storage) is located outside the winery, the solar thermal input is important in regions with high isolation. In order to calculate the energy input, it is necessary to take into account the degree of incidence of the solar rays on the surface of the deposit. Flanzy [3] considers that this thermal contribution varies between 400 w/m^2 in winter and 800 w/m^2 in summer for northern countries. Generally speaking, in Spain, the values can vary between 700 and 1100 w/m^2, respectively. On the other hand, during the night, a significant cooling of the fermentation mas takes place. In complex calculations, involving many variables not always known, this heat dissipation is not taken into account when calculating the cold storage needs, being a margin of safety of the calculations made.

According to what has been said so far, the heat produced during the fermentation process to be dissipated by the application of cold is (Eq. (12)):

$$Q_{total} = Q_{fermentation} - Q_{dissipated\ by\ CO_2,\ H_2O\ and\ ethanol} \pm Q_{ambient} \tag{12}$$

4. Refrigeration requirements for the chemical stabilization of wines

Freshly fermented wine is a saturated solution of tartaric salts whose solubility depends on the alcoholic strength and temperature. In order to avoid the presence of soaps once the wine is bottled, it is necessary to produce in the winery the insolubility and subsequent precipitation of these tartaric salts, mainly potassium bitartrate and calcium tartrate. For this, the wine is subjected to low temperatures modifying its solubility. This must refrigeration presents other side effects of great importance: precipitation of coloring matter and unstable proteins, insolubilization of colloids and reduction of the wine microbial load and facilitates the subsequent process of microbiological stabilization

According to Boulton [13], Maujean [29] and Moutonet et al. [30, 31], the formation of tartrate crystals follows a kinetic of the form (Eq. (13)):

http://dx.doi.org/10.5772/intechopen.69481

$$[Tartrates]/t = K_v \times N \times (C_a - C_s)^F \tag{13}$$

K_v is the constant that depends on the concentration in salts of the wine and its temperature.

N is the number of existing crystals per ml of wine.

C_a is the concentration of the existing tartrates.

C_s is the concentration of saturation.

F is the conversion factor. It ranges between 5 and 7.

The tartaric stabilization can be carried out discontinuously and continuously. The traditional or continuous stabilization is based on cooling the wine to a temperature close to the freezing temperature set in

$$\text{Ta} = \frac{\text{alcoholic degree } - 1}{2},$$

which means reaching temperatures of −5/−6°C. Once the wine has been cooled at this temperature, it is stored in isothermal tanks and they remain until Tsat control data, conductivity or other stability tests result in the stabilization of the wine [2, 18, 32]. This guard time lasts between 7 and 10 days. The modern stabilization systems, continuous or semicontinuous, are based on the refrigeration of the wine to a temperature close to 0°C or slightly lower (−2.5°C) with addition of microcrystals of tartrates in variable concentration (generally 4 g/L) and continuous stirring contact method. With these procedures, the treatment time is reduced from 7–10 days to 60–90 min [12, 33]. In both cases after the treatment, the wine already treated gives its cooling energy to the wine that enters by a plate exchanger. Subsequently, it is subjected to a process of filtration by earth or plates to eliminate crystals.

The refrigeration capacity required to cool the wine until the stabilization temperature of −5/−6°C (batch system) to −2.5/0°C (continuous system) is defined by the expression (Eq. (14)) [3, 8–10]:

$$\mathrm{d}Q/\mathrm{d}t = m \times C_e \times Dt \tag{14}$$

$\mathrm{d}Q/\mathrm{d}t$ is the cooling capacity per unit of time (kJ/h).

m is the mass flow of wine (kg/h). $m = v \times r$.

v is the volumetric flow rate (m^3/h).

r is the density (kg/m^3).

C_e is the specific heat of the wine that according to author is C_e = 3.99 kJ/kg °C [16]; C_e = 4.18 kJ/kg °C [3, 20]; C_e = 4.5 kJ/kg°C [10].

Dt is the (initial temperature–final temperature) of the wine.

5. Refrigeration production techniques for cooling musts and crushed-grapes in prefermentative operations

For the refrigeration of white wine must, until the temperature of the debourbage or cryomaceration and for the decrease of the temperature of red wine crushed-grapes to the one stablished in fermentation, indirect and direct systems of heat transfer may be used. Among the indirect systems of possible application in the winery, the refrigeration equipment with scraped surface evaporator or with evaporator of concentric tubes and the exchangers are described. As direct methods, CO_2 solids and liquid CO_2, known as carbonic snow, are used.

5.1. Refrigeration of indirect methods

The indirect refrigeration systems most commonly used in the winery are plaque exchangers, tubular exchangers and spiral exchangers. The tubular exchangers consist of a central conduct, of small diameter through which the must or wine circulates, which is concentrically in the interior of a tube of greater diameter through which circulates the refrigerating fluid. The diameter of the inner tube is determined by the viscosity of the fluid flowing through it. Diameters greater than 75–90 mm are recommended for musts and crushed-grapes; for wine, diameters of 50 mm are optimal. The exchange surface and the number of tubes required by the thermal transfer equations will be seen below.

The plaque exchangers consist on fine rectangular surfaces through which the refrigerant and must circulate counterflow. The separation between the plaques does not exceed 10mm and have rough surfaces to create turbulence between the exchange fluids

In the spiral exchangers, the must/crushed-grapes enter at one end and run along a spiral path until it leaves the center axis. At the same time, the refrigerant fluid counterflows on the opposite side.

The cooling power generated by the refrigerant in the heat exchanger is defined by the general energy transfer equation (Eq. (15)) [8, 9, 24]:

$$dQ/dt = \rho \times V \times dT/dt = F_T \times U \times S \times (\Delta T)_{ml} = W \times C_e \times (t_1 - t_2) = W' \times \lambda \qquad (15)$$

where

dQ/dt is the dissipated energy per unit of time (kJ/h).

ρ is the must density (kg/m^3).

V is the tank volume (m^3).

dT/dt is the must temperature variation per unit of time (°C/h).

F_T is the correction factor depending on the must and the refrigeration fluid. It is a measure of the thermal efficiency of the exchange.

U is the global coefficient of heat transfer (w/m^2°C). Characteristics of each type of exchanger and the conditions of vinification and outdoor environment.

S is the exchange surface (m^2).

$(\Delta T)_{\mathrm{ml}}$ is the logarithmic mean temperature difference between glycol water and must (Eq. (16))

$$(\Delta T)_{ml} = \frac{(t_{em} - t_{sa}) - (t_{sm} - t_{ea})}{\ln \frac{(t_{em} - t_{sa})}{(t_{sinm} - t_{ea})}} \tag{16}$$

W is the mass flow of refrigerant (kg/h).

C_e is the specific heat of refrigerant fluid (kJ/kg°C).

t_{em} is the initial temperature of must (°C).

t_{sm} is the final temperature of must (°C).

W' is the vaporization rate of the refrigerant (kg/h).

λ is the latent heat of vaporization of the refrigerant (kJ/kg).

Geankoplis [9] and McCabe et al. [8] propose a formula (Eq. (17)) for the calculation of the thermal transfer coefficient U, the Donohue expression applied for low values of the Reynolds number, *Re*:

$$\frac{UD_o}{k} = 0.2 \left(\frac{D_o \sqrt{G_a} G_m}{\mu} \right)^{0.6} \left(\frac{Ce\mu}{k} \right)^{0.33} \left(\frac{\mu}{\mu w} \right)^{0.14} \tag{17}$$

U is the thermal exchange coefficient (w/m$^{2\circ}$C).

k is the thermal conductivity of the must (w/m$^{2\circ}$C).

D_o is the outer diameter of the tubes (m).

G_a is the mass transfer rate of the glycol water (kg/m^{2}h) equal to m_a/s_b.

G_m is the mass transfer speed of must/crushed-grapes (kg/m^{2}h) equal to $\mathrm{m_m/S_c}$.

$\mathrm{m_a}$, $\mathrm{m_m}$ is the mass per unit of time of glycol water and must in circulation (kg/h).

S_a, S_c is the internal and external contact surfaces as a function of the number of tubes (m^2).

μ: is the must/crushed-grapes viscosity (cP).

C_e is the specific heat of must/crushed-grapes (kJ/kg°C).

μ_{w} is the specific heat of glycol water (kJ/kg°C).

This complex expression is difficult to apply in practice by relying on factors not always known in oenology, so in a generally accepted form empirically obtained values of U are used.

For tubular exchangers used in musts, the value of U is set at 400–1300 w/m$^{2\circ}$C for smooth tubes and at 1700–2400 with rough surface [16], from 500 to 900 w/m$^{2\circ}$C [8], from 600 to 900 w/m$^{2\circ}$C [13], from 750 to 1200 w/m$^{2\circ}$C [34], from 700 to 1100 w/m$^{2\circ}$C [3, 35].

In plate exchangers U = 2900–4800 w/m$^{2\circ}$C [10], at 3500–6500 w/m$^{2\circ}$C [8], from 2400 to 2600 w/m$^{2\circ}$C [10, 13], of 2000 w/m$^{2\circ}$C [3].

In spiral exchangers U = 1700 w/m$^{2\circ}$C [10], of 2000–2100 w/m$^{2\circ}$C [8], from 760 to 1060 w/m$^{2\circ}$C [10, 13, 36].

5.2. Direct refrigeration systems

In direct refrigeration system, two fluids that exchange energy are physically in contact. In oenology, the inert gases N_2 and CO_2 are used as refrigerating fluids, since when vaporizing at low temperatures they absorb heat from the must/crushed-grapes.

Of the two inert gases mentioned above, CO_2 in solid and liquid forms is the most used in oenology, due to its low sublimation temperature at atmospheric pressure –72.4°C, added contribution of inert atmosphere of conservation, possibility of partial freezing of the must with the consequent sugar concentration, ease of handling and no residues.

The cooling capacity provided by CO_2 in solid form is defined by the following expression (Eq. (18)) [4, 8–10, 13]:

$$dQ = \rho \times V \times C_e \times (T_1 – T_2) = M \times (\lambda_{FS} + \lambda_{VP}) \tag{18}$$

If ice is produced due to the freezing of the water from the must to this expression (Eq. (19)), we must add the energy due to the sublimation heat of CO_2:

$$Q_{H_2O} = m \times \lambda_{H_2O},\ resultado : dQ = m \times \lambda_{H_2O} + \rho \times V \times C_e \times (T_1 – T_2) = M \times (\lambda_{FS} + \lambda_{VP}) \tag{19}$$

where

m is the formed ice mass (kg).

λ_{H_2O} is the latent heat of water fusion (0.108 kJ/kg).

ρ: is the must/crushed-grapes density (°C).

V is the must/crushed-grapes volume (m^3).

C_e is the specific heat of must/crushed-grapes (kJ/kg °C).

T_1 is the initial temperature of must/crushed-grapes (°C).

T_2 is the final temperature of must/crushed-grapes (°C).

M is the mass of CO_2 in solid form required for refrigeration (kg).

λ_{FS} is the latent heat of fusion of solid CO_2 (573 kJ/kg).

λ_{VP} is the latent heat of vaporization of liquid CO_2 (393 kJ/kg).

To form 1 kg of ice in the must mass, it is necessary to add 0.58 kg of CO_2 to the freezing temperature of the must (–2.5 to 3.0°C). In the refrigeration of musts, wines and crushed-

grapes, the formation of ice is unadvisable to increase the risk of subsequent physical and chemical instability, so that for the purpose of calculating the cooling power, generally the energetic term Q_{SB} is not taken into account.

According to Boulton et al. [10, 13], in order to reduce the temperature of a white wine must (5°C), it is necessary to use 4.42 kg of solid CO_2 for each hectoliter of must. Geankoplis [9] stablishes that due to the energy losses by the deposit walls, this quantity must increase to 4.6 kg/hl.

The use of CO_2 in liquid form supposes a decrease of the dissipated energy of the deposit in relation to the solid ice, since in the energy transfer equation the latent heat of fusion of CO_2 does not come into play, resulting (Eq. (20)):

$$dQ = m \times \lambda_{H_2O} + \rho \times V \times C_e \times (T_1 - T_2) = M \times \lambda_{VP} \tag{20}$$

As stated above, it is not advisable to form ice from the water of constitution of the must or crushed-grapes, whereby the above expression is modified as follows (Eq. (21)):

$$dQ = \rho \times V \times C_e \times (T_1 - T_2) = M \times \lambda_{VP} \tag{21}$$

ρ: is the must/crushed-grapes density (kg/m^3).

V is the must/crushed-grapes volume (m^3).

C_e is the must/crushed-grapes specific heat (kJ/kg °C).

T_1 is the initial temperature of must/crushedgrapes (°C).

T_2 is the final temperature of must/crushed-grapes (°C).

M is the mass of CO_2 in solid form required for refrigeration (kg).

λ_{VP} is the latent heat of vaporization of liquid CO_2 (393 kJ/kg).

6. Cold production techniques for the control of fermentation temperature

In order to dissipate the energy produced during fermentation in the oenological industry, water spray or shower systems, refrigeration liners and internal plaques or snakes are used. The external exchangers are also used, the description of which has been made in the previous section as it is the most used mechanism in the refrigeration of musts and crushed-grapes in prefermentative operations.

6.1. Water shower

It consists on spraying the walls of the fermentation tank with water from an upper ring connected to a general feed system. A very fine and homogeneous layer of laminar water is generated, which descends through the walls and is normally collected in channels arranged in the lower part of the tank. An automatic control allows the opening and closing of solenoid

valves according to the temperature inside the tank and the preset. The refrigeration mechanism by conduction and convection is based on the removal of energy from the tank by partial vaporization of the circulation system water.

Thermodynamically, it is the most unfavorable refrigeration system and the one that uses the greater volume of water, which supposes a greater environmental cost. These cases are recommended where no refrigerated water is available (below 20°C). For this reason, it is used with efficiency in the control of fermentation in red wine vinifications, not being able to be applied in any case for rose and white wine vinifications.

The refrigeration power of the water curtain is defined by the heat of vaporization of the water at room temperature. The heat of its vaporization is the sum of its sensible heat in liquid state and the latent heat of vaporization corresponding to the change in water-vapor station. For calculation purposes, the refrigeration power of the water due to sensible heat is defined by (Eq. (22)):

$$Qs = U \times S \times (T_{\text{inside tank}} - T_{\text{curtain water}}) \tag{22}$$

where

K is the thermal transfer coefficient. For stainless steel tanks and water circulation in a thin layer laminar regime on the surface, the value of U is of the order of 100 w/m$^{2\circ}$C [3, 7, 8, 35].

S is the surface of the tank in contact with the water curtain.

The refrigeration power due to the latent heat of water vaporization is (Eq. (23)):

$$Q_1 = H \times S \times (T_{air} - T_{wet\ air\ bulb}) \tag{23}$$

where

H is the coefficient of thermal transmission by convection between the water curtain and the tank surface. According to McCabe et al. [8] and Geankoplis [9], Lamúa [37] takes values between 10 w/m$^{2\circ}$C for closed rooms without air circulation and 40 w/m$^{2\circ}$C for exterior conditions subjected to wind action.

S is the surface of the tank in contact with the water curtain.

The wet bulb temperature of the air can be determined on a psychometric diagram and depends on the room temperature and the relative humidity of the air.

Only if the water temperature exceeds the humid bulb temperature of the air, vaporization has place and therefore a dissipation of energy of the tank, since if it is lower a condensation of the air humidity occurs on the tank.

6.2. Refrigerating shirts

The use of refrigeration shirts is currently the most widespread fermentation control system in both white and red winemaking. Traditionally, they have been constructed in stainless steel

and are fixedly arranged in the upper part of the tank, occupying between 15 and 30% of the surface. In the recent years, some manufacturers are using new polymers of medium rigidity and high resistance that makes possible their installation on the tank according to the needs of the campaign. As to their disposition, and in agreement with the results of several investigations that advise for vinifications in red wine the use of fermentation tanks of equal height and base diameter, the shirts are installed covering the greatest part of the side surface of the deposit, reaching in some cases 90% of it. This new system allows a homogeneous control of fermentation, avoiding the problem of the thermal stratification that takes place with large diameters.

Similar to the tubular and plaque exchangers, the exchanged energy is defined by the general energy transfer equation (Eq. (24)) [8, 10, 13, 38]:

$$dQ/dt = \rho \times V \times dT/dt = F_T \times U \times S \times (\Delta T)_{ml} = W \times C_e \times (t_1 - t_2) = W' \times \lambda \qquad (24)$$

dQ/dt is the dissipated energy per unit of time (kJ/h).

ρ: is the must density (kg/m^3).

V is the tank volume (m^3).

dT/dt is the must temperature variation per unit of time (°C/h).

F_T is the correction factor depending on the ratio of the must and coolant velocities. It is a measure of the thermal efficiency of the exchange.

U is the global coefficient of heat transfer (w/m^2°C). The coefficient depends on the type of refrigeration jacket, vinification and exterior environment conditions. Based on empirical data, mean values of 12–60 x/m^2°C are stablished [10, 13]. Other authors raise the value of U to 200–600 w/m^2°C [3] or 600–1000 [39].

S is the shirt surface (m^2).

$(\Delta T)_{ml}$ is the logarithmic mean temperature difference between glycol water and must (Eq. (25))

$$(\Delta T)_{ml} = \frac{(t_{em} - t_{sa}) - (t_{sm} - t_{ea})}{ln \frac{(t_{em} - t_{sa})}{(t_{sm} - t_{ea})}} \qquad (25)$$

W is the mass flow of refrigerant (kg/h).

C_e is the specific heat of refrigerant (kJ/kg °C).

t_{em} is the must initial temperature (°C).

t_{sm} is the must final temperature (°C).

W' is the vaporization rate of refrigerant (kg/h).

λ is the vaporization latent heat of refrigerant (kJ/kg).

Two of the cases that take place, the refrigerating fluid changes of state for example R-717 evaporated to 5–7°C (in that case the fluid temperature is constant) or there is no change of state (glycol water), producing a heating throughout the cooling process. As approximate data, it is considered that water enters between 5 and 7°C and exits between 10 and 12°C.

For the purpose of calculating the equipment of the cold production facility, a simplified equation of the above is used (Eq. (26)):

$$Q_c = U \times S \times (T_{\text{inside tank}} - T_{\text{circulating water}})_{\text{ml}} \tag{26}$$

Since the must/wine inside the tank is in steady state and this heat exchange equation is applied for counter current flowing fluids, the term $(\Delta T)_{\text{ml}}$ is simplified to $(T_{\text{inside tank}} - T_{\text{circulating water}})$.

It should be noted that 50% of the refrigerating protein produced by the shirt dissipates in the environment surrounding the tank if it is not well heat-insulated. In case no insulation is available, the required shirt surface must be doubled, or, if appropriate, the cooling capacity is reduced by half for calculation purposes.

The cooling jackets have very low heat transfer coefficients due to the steady state in which the must/wine is located inside the tank. The effectiveness of the refrigeration decreases proportionally with the diameter of the tank, being considered that for normal temperatures of circulation water limiting diameters of more than 4 m, due to the vertical thermal stratification that occurs [10, 13, 35]. If only large diameter tanks are available, the effectiveness decreases in a high percentage, so to maintain it in appropriate values, very low temperatures are required in the glycolic water, close to 1–2°C. According to Bouton et al. [10, 13], if the diameter doubles the surface of the jacket, it is multiplied by four and the volume of the must/wine is refrigerated by eight, maintaining the ratio surface/volume. As an approximate value and only for approximate calculations, 2 m^2 of cooling jacket per 100 hl of must in fermentation is recommended.

The cooling jackets are used in the tartaric stabilization process of the wines by the system of planting nuclei of crystallization, circulating glycolic water at −7°C to reach temperatures of −1°C.

6.3. Cooling plaques or submerged coils

The coolant fluid flows through an exchanger (plaque or coil) submerged in the must/wine. The refrigeration is based on convection and conduction phenomena.

It is a very economical solution as it does not require special tanks and large accessory installations. It is applied in wine cellars of small and medium capacity that have tanks with volumes never exceeding 300 hl. As an advantage, the possibility of placing them in the zones of maximum thermal generation is at any level and from the beginning of fermentation.

Both plates and coils are constructed of stainless steel and are usually mobile structures that are moved from one tank to another by flexible conducts. Glycol water circulates in its interior at temperatures of 5–7°C or refrigerating fluids with similar evaporating temperature.

The refrigeration capacity generated is calculated in the same way as in the case of outer cooling jackets, taking into account that in this case the exchange surface is double as both sides are in contact with the must/wine (Eq. (27)):

$$Q_c = U \times S \times (T_{\text{inside tank}} - T_{\text{circulating water}})_{\text{ml}} \tag{27}$$

taking U as the same values of those mentioned above.

7. Cold production techniques for the tartaric stabilization of wines

To carry out the tartaric stabilization, the wine is cooled to the temperature previously set according to the system used continuous or discontinuous. The temperature of the wine must be lowered to −5°C in discontinuous systems and from 0 to −2°C in continuous systems, to cause the crystallization and precipitation of potassium bitartrate and calcium tartrate. The required cold is generally supplied by a scraped surface exchanger, with glycol water or with direct expansion of the refrigerant.

An exchanger with scraped surface is constituted by a cylinder of 0.75–1 m of length and 0.15–0.20 m of diameter, in whose interior a series of pallets is located around an axial axis with a rotation movement between 300 and 600 rpm. Inside the cylinder circulates the wine to be treated. In this way, concentric to the previous one, is arranged a cylinder or cooling jacket through which the refrigerating fluid is counter flow with the wine. The mission of the pallets is to remove and circulate the ice formed and deposited on the wall of the exchanger, around 10–20% according to the treatment temperature. According to McCabe et al. [8] and Geankoplis [9], the energy transferred from the glycolic water or the refrigerating fluid to the wine in a range t is calculated according to the expression (Eq. (28)):

$$\frac{Q}{S} = 2\ Uk\ (Tv - T\alpha)\ \sqrt{\frac{t}{\pi\alpha}} \tag{28}$$

where

Q is the dissipated energy (kJ).

S is the exchange surface (m^2).

U is the global coefficient of heat transfer ($w/m^{2\circ}C$).

K is the wine thermal conductivity ($w/m^{2\circ}C$).

T_v is the wine initial temperature (°C).

T_α: is the initial temperature of glycol water or refrigeration liquid (°C).

t is the total contact time (h).

α: is the thermal diffusivity of wine ($w/m^{2\circ}C$).

$$\frac{UD_\alpha}{k} = 4.9\left(\frac{D_\alpha V\rho}{\mu}\right)^{0.57}\left(\frac{C_e\mu}{K}\right)^{0.47}\left(\frac{D_a n}{V}\right)^{0.17}\left(\frac{D_a}{L}\right)^{0.37}$$

U is the global coefficient of heat transfer (w/m$^{2\circ}$C).

K is the wine thermal conductivity (w/m$^{2\circ}$C).

D_a is the internal diameter of the exchanger (m).

V is the speed of wine circulating (m/h).

ρ: is the wine density (kg/m^3).

C_e is the wine specific heat (kJ/kg$^\circ$C).

m is the wine viscosity (cP).

n is the stirring speed of the blades (rph).

L is the length of the exchanger (m).

Due to the difficulty of calculation, for practical purposes, the dimensioning of a scraped surface exchanger is performed according to the simplified energy transfer equation (Eq. (29)) [10, 13, 34].

$$Q_c = U \times S \times (T_{\text{wine}} - T_{\text{glycolic water}})_{\text{ml}} \tag{29}$$

Q is the dissipated energy (kJ).

U is the global coefficient of heat transfer (w/m$^{2\circ}$C).

S is the exchange surface (m^2).

$(\Delta T)_{\text{ml}}$ is the logarithmic mean temperature difference between glycol water/refrigerant and wine (Eq. (30)).

$$(\Delta \text{T})_{\text{ml}} = \frac{(t_{em} - t_{sa}) - (t_{sm} - t_{ea})}{ln\frac{(t_{em} - t_{sa})}{(t_{sm} - t_{ea})}} \tag{30}$$

As values of U, are taken those empirically calculated by different authors. According to López [39], U = 580–870 w/m$^{2\circ}$C. For McCabe et al. [40], U = 700–900 w/m$^{2\circ}$C. Boulton et al. [10, 13] establish an average value of U = 600–2000 w/m$^{2\circ}$C.

Author details

Ángel Benito Sáez, Eva Navascues Lopez-Cordon, Fernando Calderón Fernández and Santiago Benito Sáez*

*Address all correspondence to: santiago.benito@upm.es

Department of Chemistry and Food Technology, Polytechnic University of Madrid, Madrid, Spain

References

[1] Suárez JA, Iñigo B, editors. Microbiología enológica. Fundamentos de vinificación. 1st ed. Madrid: Mundiprensa; 1992. p. 157

[2] Ribereau Gayón P, Dubordieu D, Donèche B, Lonvaud A, editors. Traité d'Oenologie. Buenos Aires: Hemisferio Sur; 1997. p. 111

[3] Flanzy C, editor. Enología Fundamentos científicos y tecnológicos. Madrid: AMV Ediciones; 2000. p. 116

[4] Bernard M. Une nouvelle technique: La maceration préfermentaire à la neige carbonique. Revue dés Oenologues et des Techniques Vitivinicoles et Oenologiques. 1999;**92**:26–30

[5] Delteil D. Presentation d'une technique de débourbage des jus blancs et rosés méditerranéens. Revue Française d'œnologie. 1998;**173**:34–36

[6] Varela F, Calderón F, González MC, Colomo B, Suárez JA. Effect of clarification on the fatty acid composition of grape must and the fermentation kinetics. European Food Research and Technology. 1999;**209**:439–444

[7] Baillere J.B., et al. Mâtrise des témperatueres en oenologie. 1993. Available from: http://www.matevi-france.com/oenologie/114-maitrise-des-temperatures.html [Accessed: March 29, 2017]

[8] McCabe W, Smith J, Harriot P, editors. Unit Operations of Chemical Engineering. 5th ed. New Delhi: McGraw Hill; 1993. p. 44

[9] Geankoplis CJ, editor. Transport Processes and Unit Operations. 3rd ed. New Jersey: Prentice Hall Press; 2003. p. 22

[10] Boulton R, Singleton VL, Bisson L, Kundee R. Principles and Practices of Winemaking. New York: Chapman and Hall; 1996. p. 492

[11] Avilés A. El frío y la enología. Vitivinicultura. 1990;**1(1)**:30–44

[12] Escudier JL, Saint-Pierre B, Battle JL, Moutoner M. Procedé et dispositive de stabilisation tartrique des vins. Brevet [Internet]. 1993 [Accessed: March 29, 2017]

[13] Bertin S. Équipements de mâtrise thermique. Journal International des Sciences de la Vigne et du Vin. 1998;**31**:155–157

[14] Boulton R. Winemaking. In: King D, editor. ASHRAE Handbook. Chapter 38. New York: American Society of Heating Refrigeration and Air-Conditioning Engineering; 1982. pp. 7–9

[15] Brugirard P, Dubois C, Doutsias G. Aspects pratiques des traitements thermiques du vins. Chaintré: Bourgogne Publications; 1991. p. 113

[16] López A, Secanell P. A simple mathematical empirical model for estimating the rate of heat generation during fermentation in white-wine making. International Journal of Refrigeration. 1992;**15(5)**:276–280

[17] Beltrán G, Novo M, Torija MJ, Poblet M, Rozés J, Guillarmón JM, Mas A. Fermentaciones a bajas temperaturas. Tecnología del vino. 2001;**2**:73–76

[18] Navascués E, Calderón F, Colomo B, Suárez JA. Producción de volátiles en función de la temperatura. In: Proceedings of XVIII Jornadas de Viticultura y Enología de Tierra de Barros; 4-6 June 1997; Badajoz, congress in Spain

[19] Heard GM, Fleet HG. The effects of temperature and pH on the growth of the yeast species during the fermentation grape juice. Journal of Applied Bacteriology. 1998;**65**:23–28

[20] Suárez JA, editor. Levaduras vínicas. Funcionalidad y uso en bodega. Madrid: Mundiprensa; 1997. p. 56

[21] Rozés N, Larue F, Ribereau-Gayon P. Effect of a variation of grape must temperature on the fermentative ability and the neutral lipid content. Biotechnology Letters. 1998;**10**:821–824

[22] Bouffards A. Determination de la chaleur degagee dans la fermentation alcolique. Programme Agriculture Viticulture. 1895;**24**:345–347

[23] Willians LA. Heat release in alcoholic fermentation. A critical reappraisal. American Journal of Enology and Viticulture. 1982;**33(3)**:149–153

[24] Willians LA, Boulton R. Modelling and prediction of evaporative ethanol loss during wine fermentations. American Journal of Enology and Viticulture. 1983;**34(4)**:234–242

[25] Boulton R. A kinetic model for the control of wine fermentation. Biotechnology and Bioengineering. 1978;**9**:167–172

[26] El-Haloui NE, Picke D, Corrieu G. Mesures physiques permettant le suivi biologique de la fermentation alcoolique en oenologie. Sciences des Aliments. 1988;**7**:241–265

[27] Barre P, Chabas J, Corrieu G, Davenel A, El-Haloui N, Grenier P, Navarro JM, Picque D, Sablayrolles JM, Sevila F, Vannobel C. Procédé de prévision et de contrôle de la fermentation alcoolique. Office Européen des Brevets: EP 0 271 380 B1. 1988. p. 31

[28] Gurret JM, Merlet I, editors. Le vin. Maîtrise des temperatures de vinification et de stockage. Seine: Pyc Editions; 1991. p. 86

[29] El-Halouli NE, Cleran Y, Sablayroles JM, Grenier P, Barre P, Corrieu G. Suivi et controle de la fermentation alcoholique en oenoligie. Revue française oenologie. 1987;**115**:12–17

[30] Maujean A, editor. Traitement par le froid artificial des vins en relation avec leur stabilisation vis-à-vis des troubles cristalins tartriques. Paris: Lavoisier Tec&Doc; 1994. p. 28

[31] Moutonet M, Saint-Pierre B, Batlle JL, Escudier JL. Le stabilisateur tartrique: principe et description du proceed. Revue française oenologie. 1997;**162**:15–17

[32] Blouin J, Dronieau T. Stabilité tartrique nouvelle méthode d'appreciation. Journal International des Sciences de la Vigne et du Vin. 1998;**33**:125–129

[33] Madrid A. Modernas técnicas para el tratamiento por frío del vino. Alimentación, equipos y tecnología. 1991;**10(1)**:305–308

[34] Sanchez MT, editor. Ingeniería del frío. Teoría y práctica. Madrid: AMV Ediciones y Mundi prensa; 2000. p. 74

[35] Spiegel R, Howell JR, editors. Thermal Radiation Heat Transfer. 2nd ed. New York: McGraw Hill; 1981. p. 101

[36] Brugirard P, Dubois C, Doutsias G, editors. Aspects pratiques des traitements thermiques du vins. Chaintré: Bourgogne Publications; 1991. p. 13

[37] Lamua M, editor. Aplicación del frío a los alimentos. Madrid: AMV Ediciones y Mundi prensa; 2000. p. 97

[38] Koelet PC, editor. Frío industrial: Fundamentos, diseño y aplicaciones. Madrid: Madrid Vicente; 1997. p. 52

[39] López A, editor. Las instalaciones frigoríficas en las bodegas. Manual de diseño. Madrid: Madrid Vicente; 1992. p. 48

[40] McCabe W, Smith J, Harriot P, editors. Unit Operations of Chemical Engineering. 5th ed. New Delhi: McGraw Hill; 1993. p. 112

Chapter 5

Energy-Efficient Air-Conditioning Systems for Nonhuman Applications

Muhammad Sultan and Takahiko Miyazaki

Additional information is available at the end of the chapter

http://dx.doi.org/10.5772/intechopen.68865

Abstract

In addition to humans' thermal comfort, air-conditioning (AC) could be required for various nonhuman applications, for example, animals' AC, greenhouse AC, food storage and transportation, industrial processes, and so on. In this regard, optimum conditions of air temperature and humidity are explored and compared on psychrometric charts. Thermodynamic limitations of existing AC systems are discussed from the subject point of view. Consequently, four kinds of low-cost energy-efficient AC systems, namely: (i) direct evaporative cooling (DEC), (ii) indirect evaporative cooling (IEC), (iii) Maisotsenko cycle (M-Cycle) evaporative cooling (MEC), and (iv) desiccant AC (DAC), are investigated for climatic conditions of two cities, that is, Multan (Pakistan) and Fukuoka (Japan). In addition, systems' fundamentals and principles are explained by means of schematic diagrams and basic heat/mass transfer relationships. According to the results, performance of all systems is influenced by ambient air conditions; therefore, a particular AC system cannot provide optimum AC for all nonhuman applications. However, one or other AC system can successfully provide desired conditions of temperature and relative humidity. It has been concluded that evaporative cooling systems provide low-cost AC for dry climates, whereas DAC system is found energy efficient and viable for humid climates.

Keywords: air-conditioning, nonhuman applications, evaporative cooling, desiccant

1. Introduction

The word air-conditioning (AC) literally means conditioning of subjected air according to required conditions of air temperature (T_a) and relative humidity (RH) [1]. The AC phenomena usually involve five modes of conditioning, that is, (i) heating, (ii) cooling, (iii) humidification, (iv) dehumidification, and (v) ventilation. More than one AC mode could be required depending upon the nature of AC application as well as ambient conditions [2]. For example,

cooling and humidification is required in summer season of Multan (Pakistan), whereas heating and humidification is required in dry winters of Fukuoka (Japan) [3]. Certainly, there could be numerous AC applications which may require specific conditions of T_a and RH, for example, animals' AC [4], greenhouse AC [2, 5], agricultural products' storage and preservation [6, 7], and so on. The requirements of T_a and RH vary dynamically with respect to time and may even vary from species to species [4]. On the other hand, the AC term is mostly associated with humans' thermal comfort as far as conventional literature and primary objectives are concerned [8, 9]. Therefore, lots of AC technologies have been established for humans' thermal comfort and are under practice in order to obtain typical conditions of T_a and RH, particularly for summer and winter seasons [1, 10]. Out of them, most popular and highly efficient systems are based on electric-driven compressors. Although compressor-based AC systems achieve desired T_a and RH conditions efficiently, these are thermodynamically inefficient and consume huge amount of primary energy [1, 10]. Moreover, these systems are based on environmentally harmful technologies and consume hydro-fluorocarbons (HFCs)/chlorofluoro-carbons (CFCs)/hydrochlorofluoro-carbons (HCFCs). Consequently, the conventional vapor compression–based AC (VAC) systems possess certain global warming potential (GWP) and ozone layer depletion potential (ODP). Thermodynamic limitations as well as merits/demerits of typical VAC system are highlighted in Section 3.

In the twenty-first century, lots of energy-efficient and low-cost AC systems have been studied, designed, developed and are under practice for various AC applications, for example, data center [11–13], museums [14–16], hospitals [17], automobiles [18, 19], wet markets [20], marine ships [21], greenhouses [22], agricultural products storage [7], animals' thermal comfort [6], industrial processes [23], electronic cooling [24], turbine inlet air cooling [25], and so on. Most of these systems are either thermally driven or based on evaporative cooling conception. These systems are not involved in the use of any kind of refrigerants, thus enabling zero GWP and ODP. As heat is the input energy source for thermally driven AC systems, these systems can be employed for efficient utilization of low-grade waste heat, solar thermal energy, and biogas or biomass, and so on. On the other hand, evaporative cooling-based AC systems are always handy (wherever applicable), because they only require water with small energy to run the fan. However, evaporative cooling or thermally driven AC systems are highly influenced by ambient air conditions; therefore, systems optimization will be required for each and every AC application.

From the above perspective, this chapter discusses sensible and latent load of AC required for various nonhuman AC applications. Ideal temperature and humidity zones are represented and compared on psychrometric charts. Consequently, various low-cost energy-efficient AC systems are proposed and discussed for the subjected applications. In addition, thermodynamic limitation of VAC system and scope of proposed systems is also highlighted.

2. Nonhuman air-conditioning (AC)

Apart from humans' thermal comfort, ideal temperature and humidity could be required in many situations as discussed in the introduction section. The intensity of the required AC is

typically based on the nature of application which could be static and dynamic. This section presents some of the key nonhuman AC application. The upcoming subheading will explain each application in detail.

2.1. Animals' thermal comfort

In general, designing of animals' housing according to the required temperature and humidity is usually complicated due to the environmental factors which affect the well-being and production of animals [26]. Similarly, designing of animals' AC system is directly affected by the economic factor; therefore, animals' AC is not very popular especially in developing countries, for example, Asia and Africa regions. However, lots of low-cost techniques are adopted in these regions in order to achieve the desired conditions that may not be sufficient in many cases. It is worth mentioning that the air-flow/ventilation rate is an important parameter for animals' AC similar to temperature and humidity. Therefore, designing of sensible and latent load of AC is provided after finalizing the optimum air-flow rates. Air-flow rate is a dynamic parameter in case of animals' AC, and it varies from season to season as well as from species to species. American society of heating, refrigeration, and air-conditioning engineers (ASHRAE) provides basic guidelines for animals' AC which can be found from references [26–29]. For example, according to ASHRAE, ventilation rate of 17–22 L/s is required for cows (weight 500 kg each) in winter season, whereas it is 67–90 L/s and 110–220 L/s for spring and summer seasons, respectively. Similarly, growing pigs (weight 34–68 kg) require 3–35 L/s flow, whereas finishing pigs (weight 68–100 kg) require 5–60 L/s. **Figure 1(a)** shows typical constraints while selecting the optimum ventilation rate for livestock buildings [30, 26]. It can be observed that there are many factors which need to be addressed for selecting optimum ventilation rate. In addition, supplied air temperature and humidity from the AC unit is directly associated with the air-flow rates [3]. Consequently, the ideal temperature and humidity required for various animals is shown in **Figure 1(b)** [4, 26]. It can be noticed that the animals require higher relative humidity in general as compared to human beings [3]. On the other hand, animals are relatively less sensitive to temperature but require distinctive conditions for each breed. Moreover, potential of livestock industry can also be determined from **Figure 1(b)** simply by plotting the ambient air conditions of different cities and/or regions.

2.2. Greenhouse AC

Agricultural plants are living things; they grow, move, eat, and reproduce. They are basic entities for food production and associated industries. Plants are sensitive to temperature and humidity similar to human beings and, therefore, require proper AC.

However, plants' AC phenomena are quite complicated due the photosynthesis and evapotranspiration processes by which they require CO_2 and/or O_2 from the air. Therefore, plants' AC is quite different in day times (active photosynthesis and evapotranspiration) and night times (active evapotranspiration only) [2]. According to a study [31, 32], plants grow well when its vapor pressure deficit (VPD) is ranging from 0.45 kPa to 1.25 kPa, and ideal yield could be obtained for VPD = 0.80–0.90 kPa. In this regard, influence of greenhouse conditions

on plants' VPD has been determined as shown in **Figure 2(a)**. Moreover, the figure provides a comparison of ideal VPDs for different growth stages of tomatoes [33]. It can be noted that plants are very sensitive to air conditions and require dynamic humidity and temperature at different growth stages. Similarly, using the concept of VPD, the ideal AC zones can be formulated for various greenhouse products as shown in **Figure 2(b)**. It can be seen that each agricultural product requires typical thermal conditions, which may or may not be achievable for many AC systems.

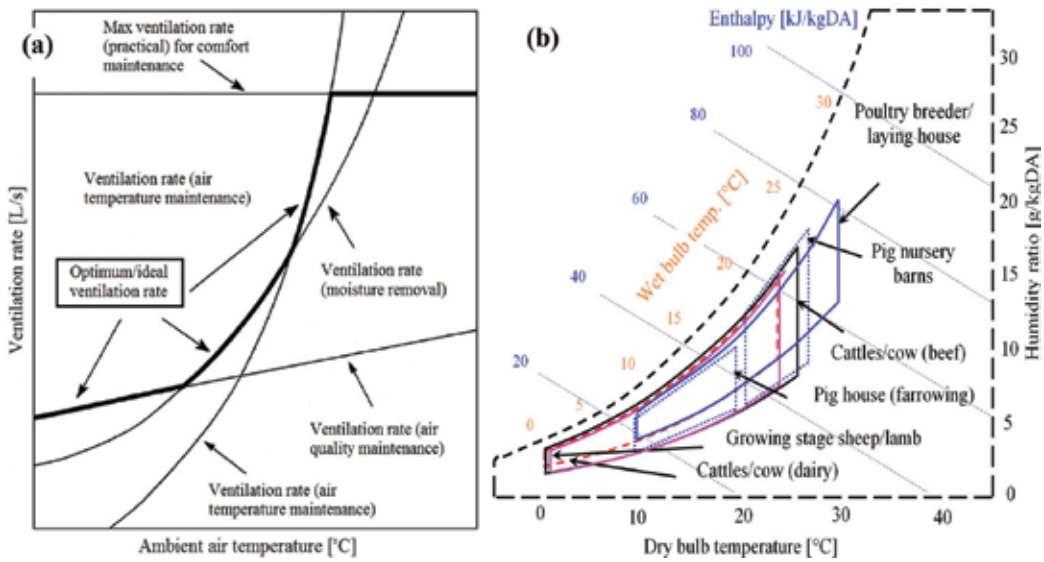

Figure 1. Animals' air-conditioning (AC): (a) optimum ventilation rate for livestock building [26, 30]; and (b) optimum air temperature and humidity levels.

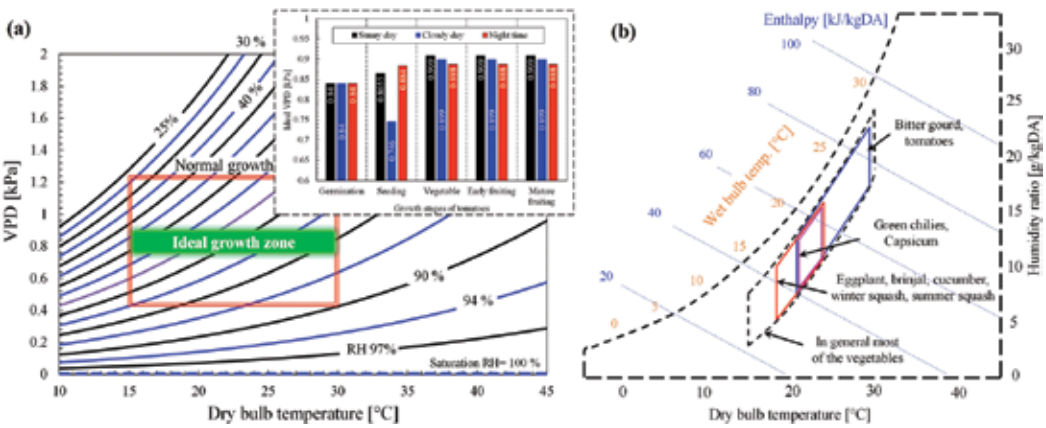

Figure 2. Greenhouse AC: (a) influences of greenhouse conditions on plants' vapor pressure deficit (VPD); and (b) optimum air temperature and humidity levels.

2.3. Food storage and transportation

Post-harvest storage and handling of agricultural products is one of the burning issues of the twenty-first century where we have lots of food but still many people are suffering from food shortage and malnutrition. It is mainly due to food wasting, improper management, and high cost of food storage and transportation. Food storage is usually expensive and complicated due to the involvement of numerous physiochemical and biological processes, for example, respiration, transpiration, fermentation, and so on [7]. Moreover, storage conditions and nature of storage are completely different for different types of food, which may be categorized as follows:

- Grain, cereal, beans, and pulses storage
- Vegetable storage (fresh and frozen)
- Fresh fruit storage
- Dry fruit storage
- Meat and seafood storage
- Milk, cheese, and dairy food storage
- Cooked and processed food storage

As far as conventional storage practices used for above-mentioned food types are concerned, most popular storage techniques are: (i) drying, (ii) mechanical isolation, (iii) refrigeration, (iv) chemical treatment, (v) vacuum, (vi) ionizing radiation, (vii) silo and storage structures, and so on. On the other hand, it is important to mention here that the AC systems could be extremely required in many cases of food storage and transportation, for example, storage of fresh dates. In addition, AC storage method could be considered on top priority for the food products involved in transpiration, respiration, and/or fermentation (i.e., supply or removal of O_2 and CO_2) [34]. However, AC is not popular for longtime storage of food products due to the expensive technology of VAC systems and lack of distinctive control of T_a and RH. Therefore, low-cost and technically viable AC technology is the dire need for the food industry. From the discussion point of view, ideal temperature and humidity requirements for the storage of fruits and vegetables are compared on psychrometric chart as shown in **Figure 3** [4]. The fundamental knowledge used in **Figure 3** is obtained from the guidelines provided by the reference [34]. The shelf life of vegetables and fruits can be increased considerably by storing them at desired conditions of T_a and RH (**Figure 3**). The AC systems can generate these conditions effectively and can also control level of O_2 and CO_2 by means of fresh/return air flow and, therefore, can be considered for food storage and transportation. Similarly, the AC use could be crucial for the storage and transportation of dry fruits which may require particular moisture contents. In this regard, water vapor mass transfer between air and food (role of water activity) can be controlled by means of relative humidity, RH.

2.4. Industrial processes AC

Lots of industrial processes require particular AC in order to increase the industrial productivity, and it is usually dissimilar to humans' thermal comfort [1]. Intensity of required

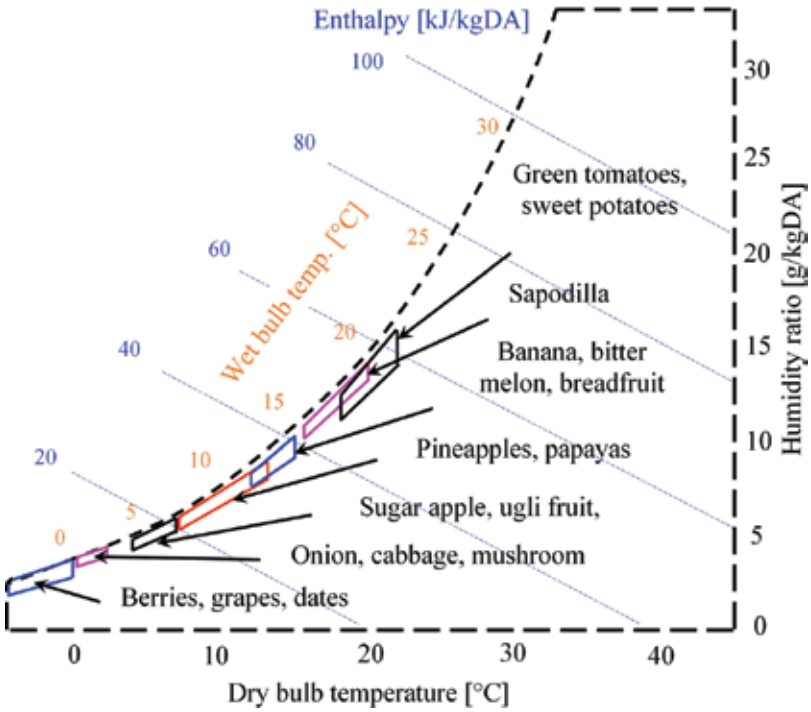

Figure 3. Optimum air temperature and humidity level for the storage of fruits and vegetables.

temperature and humidity control is based on nature of industry and its manufactured products [3]. The industrial processes can be categorized in many ways depending upon the industry type, objectives, and/or productivity [26–29]. Some of the typical industrial processes that require AC include agricultural implements and machinery industry, leather and paper industry, fur and gum industry, water/wastewater treatment industry, medicine/pharmaceutical industry, electronic products industry, paints and plywood industry, tea and tobacco industry, insect/pest/fungus control process, fuel purification–based petrochemical processing, metallurgy-based processes, food and beverages process, clinical processes, heat treatment processes, surface coating processes, manufacturing of additives, and so on. It is worth mentioning that the employees' requirements must be considered in the designing of the industrial processes AC. In this regard, ASHRAE provides fundamental guidelines for the AC of various industrial processes [26]. Nature of industrial construction, building usage, operational conditions, and insurance are the key parameters needed to be considered for proper designing. Similarly, AC loads (sensible/latent) need to be calculated carefully from the viewpoint of heat generation (internal/external), transmission/solar load, fresh air-flow rate including O_2 and CO_2 requirements. The details can be found from reference [26]. For the comparison and general viewpoint, optimum air temperature and humidity required for few industrial processes is presented on psychrometric chart as shown in **Figure 4** [26]. It can be noticed that each industrial process requires different scheme of T_a and RH, which cannot be achieved by a particular AC system. Therefore, this is a dire need of the twenty-first century to transform and

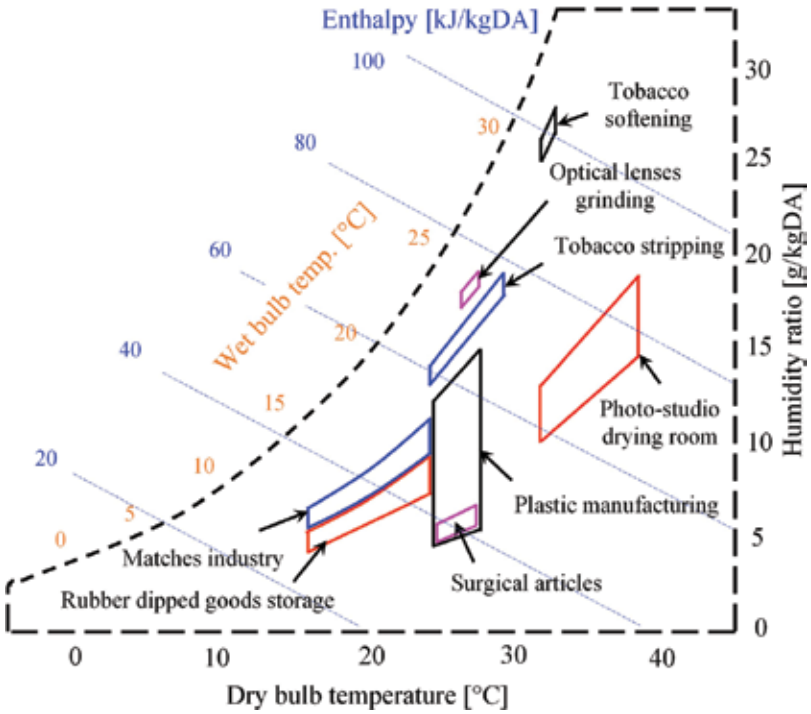

Figure 4. Optimum air temperature and humidity level for industrial processes AC.

optimize the existing AC technologies, including hybrid systems for the establishment of low-cost energy-efficient AC systems for industrial processes.

2.5. Miscellaneous applications

Similar to Sections 2.1–2.4, there could be many more nonhuman AC applications that require distinctive control of humidity and temperature. Some of them can be listed as follows:

- Data center AC [11, 13, 35]
- Turbine inlet air cooling [25, 36, 37]
- Museum AC [15, 16, 38, 39]
- Ships and marine AC [40, 41]
- Storage of machinery, pharmacy, artifact, and electronic devices [42]

Lots of research have been conducted worldwide in order to establish low-cost energy-efficient AC system for above-mentioned AC applications. Therefore, many systems have been resulted suitable depending upon the nature of AC application, availability of low-cost energy type, economics, efficiency, and sustainability. In this regard, upcoming sections will present some suitable low-cost AC options for these applications.

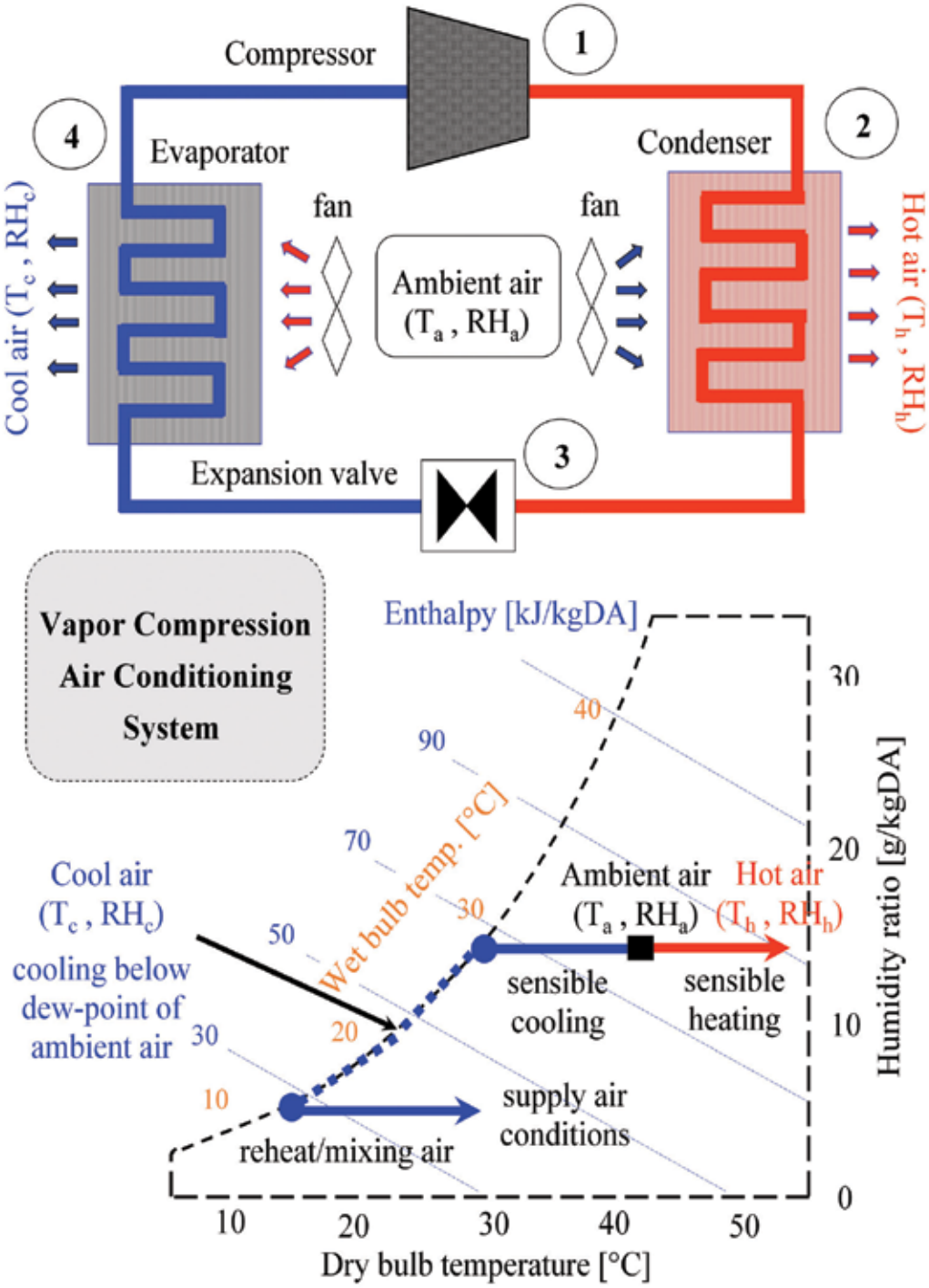

Figure 5. Working principle of conventional vapor compression air-conditioning (VAC) systems.

3. Conventional AC system

Before we discuss the low-cost energy-efficient AC systems, it is important to highlight the scope, significance, and thermodynamic limitations of existing AC technology, that is, vapor compression–based AC systems (VAC). Vapor compression refrigeration cycle is one of the basic and key thermodynamic cycles [43–45]. Therefore, it has been well known in the literature and, consequently, millions of refrigeration and heating, ventilation, and air-conditioning (HVAC) units are working worldwide on this conception due to its consistency and higher coefficient of performance (COP) [1]. Basic VAC cycle and its psychrometric representation for heating and cooling processes are expressed in **Figure 5**. It can be observed that the VAC cycle can provide cooled air (via evaporator) by cooling below dew-point of the ambient air. However, RH is controlled indirectly by means of dry-bulb temperature (DBT), which is one of the key thermodynamic limitations of VAC cycle. Similarly, it can provide sensible heating (via condenser) while providing reduced RH for the identical humidity ratio. Overall, it can be concluded that VAC cannot control the temperature and RH distinctly. In addition, it uses environmentally harmful refrigerants which are responsible for global warming and ozone layer depletion. Moreover, it consumes huge primary energy, thus indirectly responsible for environmental pollution too.

4. Energy-efficient AC systems

Numerous energy-efficient AC are working worldwide which are mainly based on evaporative cooling, adsorption, absorption, membrane, ejector, renewable energy, solar photovoltaic, solar thermal, low-grade waste heat, and hybrid technologies. From the perspective of nonhuman applications, this chapter focuses on low-cost AC systems particularly based on evaporative cooling and thermally driven technologies. The upcoming three headings discuss evaporating cooling options, followed next by the heating of thermally driven AC. Evaporative cooling is one of the ancient techniques (~2500 B.C.) for providing AC. It is popular worldwide (wherever applicable) due to its low-cost and simple designing. In principle, evaporative cooling produces the cooling effect by means of water vapor evaporation. In literature and worldwide market, numerous arrangements and designing of evaporative cooling systems are available. However, upcoming three headings are important from the subject of thermodynamic conception, that is, isenthalpic cooling [46, 47], sensible cooling, and dew-point (or below wet-bulb) cooling [10, 48, 49]. In order to highlight the significance of temporal and spatial variations on AC performance, 24 h–based ambient air conditions of two cities, that is, Multan (Pakistan) and Fukuoka (Japan), are investigated for nonhuman AC applications. **Figure 6** shows ambient air conditions of both cities, archetypally for summer season [3].

4.1. Direct evaporative cooling (DEC)

Direct evaporative cooling [46, 49] (DEC) is the fundamental sense of typical evaporative cooling conception in which water vapors continuously evaporate into air until condition of air saturation arises. Therefore, cooling effect is produced by means of heat of water

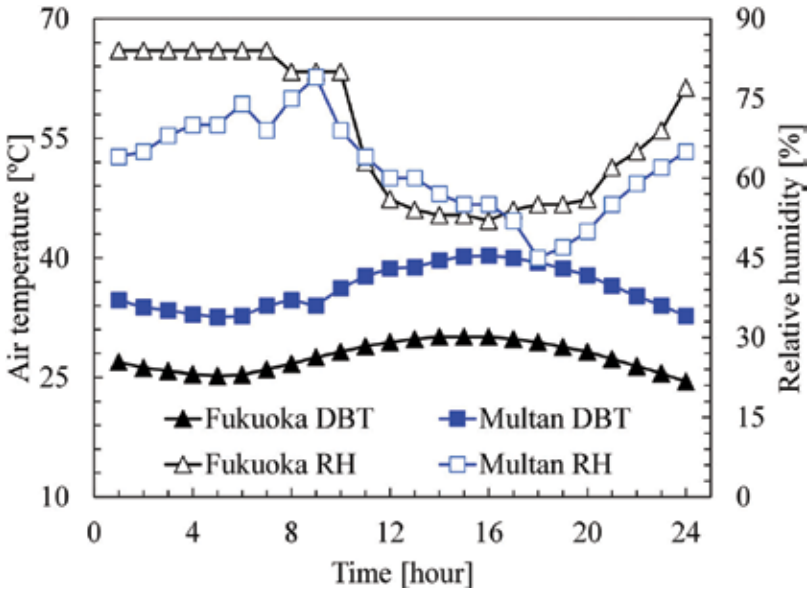

Figure 6. Ambient air conditions of Multan and Fukuoka archetypally for summer season. Each point represents hourly value (average) for 24 h in a day.

vaporization as shown in **Figure 7(a)**. The process can be realized from the fundamental equation of air enthalpy given by Eq. (1) [29].

$$h_a = 1.006\ T_a + w\ (2501 + 1.86T_a) \tag{1}$$

where h_a represents enthalpy of moist air [kJ/kg], T_a represents dry-bulb temperature [°C] and w represents humidity ratio [kg_w/kg_{DA}]. It is worth mentioning that the term 1.006 $T_a$expresses specific enthalpy of dry air, whereas the term w (2501 + 1.86T_a)embodies specific enthalpy of saturated water vapors. In DEC system, enthalpy of the inlet and outlet air streams remains constant, thus cooling limit of DEC system is ambient air wet-bulb temperature. Hence, isenthalpic cooling potential of DEC will be function of $(T_{in})_{db} - (T_{in})_{wb}$. For insight of DEC, inlet and outlet air conditions are described by Eqs. (2)–(5).

$$(T_{out})_{db} \geq (T_{in})_{wb} \tag{2}$$

$$RH_{out} > RH_{in} \tag{3}$$

$$w_{out} > w_{in} \tag{4}$$

$$h_{out} = h_{in} \tag{5}$$

where h and w represent enthalpy of moist air [kJ/kg] and humidity ratio [g/kgDA], respectively. Subscripts *in*, *out*, *db*, and *wb* represent inlet, outlet, dry-bulb, and wet-bulb, respectively. Similarly, wet-bulb effectiveness ε_{wb} [–] of the DEC systems can be written as:

$$(\varepsilon_{wb})_{DEC} = \frac{(T_{in})_{db} - (T_{out})_{db}}{(T_{in})_{db} - (T_{in})_{wb}} \tag{6}$$

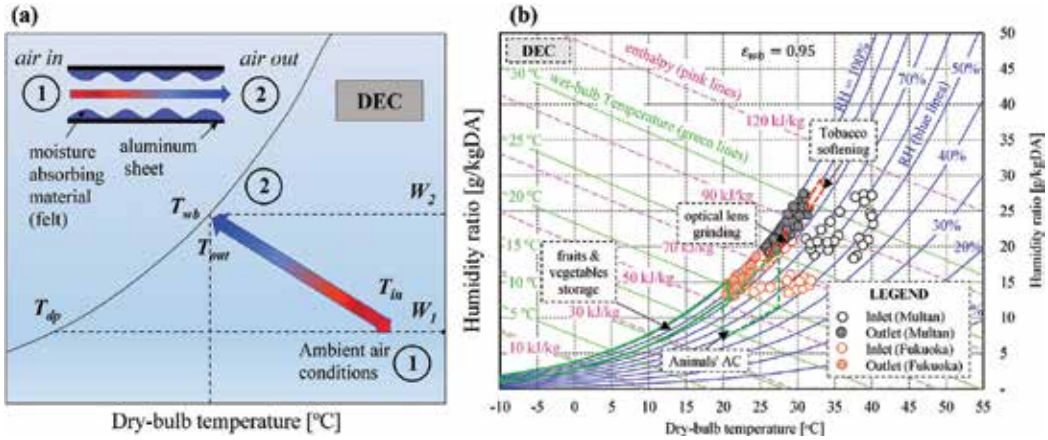

Figure 7. Direct evaporative cooling (DEC) system: (a) schematic representing the fundamentals and thermodynamic principle; and (b) system performance for nonhuman AC applications for Multan and Fukuoka, where each legend point represents hourly value (average) of a day.

Performance of DEC system is analyzed for Multan and Fukuoka cities, archetypally for summer season. Results are expressed on psychrometric chart for ε_{wb}= 0.95, in order to highlight its applicability for nonhuman AC applications as shown in **Figure 7(b)**. It can be observed for both cities that the DEC system cannot provide required conditions for "tobacco softening" and for "storage of fruits & vegetables." On the other hand, DEC can support/assist conventional AC unit for "optical lens grinding" and "animals' AC" for Multan and Fukuoka climates, respectively. Similarly, all the nonhuman AC applications can be examined for DEC system applicability using **Figure 7(b)**.

4.2. Indirect evaporative cooling (IEC)

Increase in product air humidity is the key limitation of typical DEC system; therefore, indirect evaporative cooling (IEC) system can be employed for constant absolute humidity [49]. As no moisture is added in the air by IEC, it enables hygiene air quality. Fundamentals and thermodynamic principle of IEC system is expressed by the schematic diagram shown in **Figure 8(a)**. Referring to **Figure 8(a)**, the IEC cooling is achieved by combination of two thermodynamic processes: (i) isenthalpic cooling by water vapor evaporation into the air, that is, DEC process (wet-channel) and (ii) sensible heat transfer from process (i) (dry-channel). As the cooling effect is based on water vapor evaporation, the cooling limit of IEC is also wet-bulb temperature. Thus, the cooling potential of IEC will be function of $(T_{in})_{db} - (T_{in})_{wb}$, similar to DEC. In addition of DEC efficiency parameters, the net efficiency of IEC device is influenced by air-flow ratio and heat transfer between dry and wet channels. For insight of IEC, inlet and outlet air conditions along with wet-bulb effectiveness are expressed by Eqs. (7)–(11).

$$(T_{out})_{db} \geq (T_{in})_{wb} \tag{7}$$

$$RH_{out} > RH_{in} \tag{8}$$

$$w_{out} = w_{in} \tag{9}$$

$$h_{out} < h_{in} \tag{10}$$

$$(\varepsilon_{wb})_{IEC} = \frac{(T_{in})_{db} - (T_{out})_{db}}{(T_{in})_{db} - (T_{in})_{wb}} \tag{11}$$

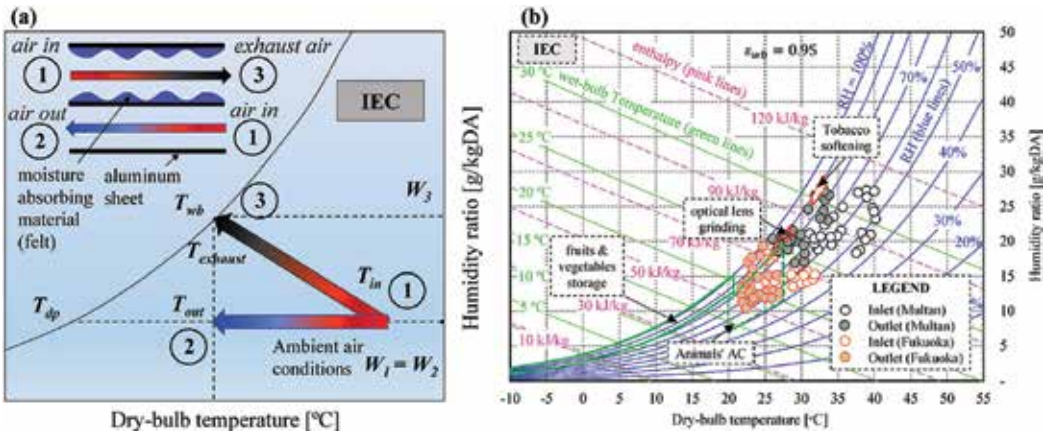

Figure 8. Indirect evaporative cooling (IEC) system: (a) schematic representing the fundamentals and thermodynamic principle; and (b) system performance for nonhuman AC applications for Multan and Fukuoka, where each legend point represents hourly value (average) of a day.

It can be observed from Eqs. (2)–(11) that the numerical value of outlet temperature by DEC and IEC units will be identical for same effectiveness; however, humidity makes the difference in cooling performance. In this regard, IEC system performance is investigated for summer season of Multan and Fukuoka cities for nonhuman AC applications as shown in **Figure 8(b)** for ε_{wb} = 0.95. According to the results, "tobacco softening" and "storage of fruits & vegetables" cannot be entertained by IEC system for both cities. On the other hand, unlike DEC, the IEC can provide optimum conditions for "animals' AC" for Fukuoka city. In addition, IEC can support/assist conventional AC system for the industrial AC process of "optical lens grinding" for Multan. Similarly, rest of the nonhuman AC applications can be examined by **Figure 8(b)**.

4.3. M-Cycle evaporative cooling (MEC)

The Maisotsenko cycle (M-Cycle) evaporative cooling (MEC) is an advance thermodynamic conception of IEC by which the product air can be cooled to the ambient air dew-point temperature [10]. The fundamental scheme of MEC operation is presented by **Figure 9(a)**, whereas details can be found from reference [10]. The MEC apparatus (dry and wet channels in **Figure 9(a)**) exploits the psychrometric renewable energy (available from the latent heat of water vaporization) in such a way that product air can be cooled to the ambient air dew-point.

http://dx.doi.org/10.5772/intechopen.68865

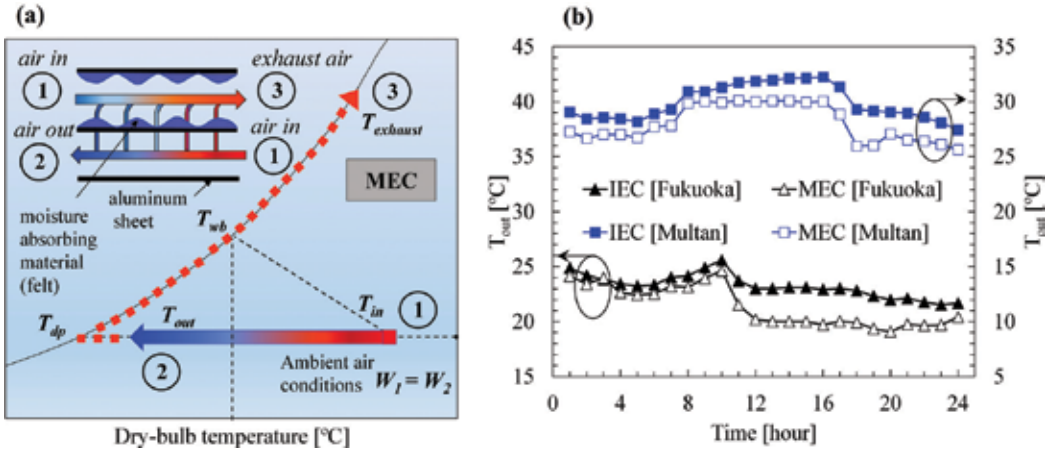

Figure 9. Maisotsenko cycle evaporative cooling (MEC) system: (a) schematic representing the fundamentals and thermodynamic principle; and (b) comparison of outlet air temperatures with DEC/IEC system for Multan and Fukuoka, where each point represents hourly value (average) of a day.

According to experimental results available in the literature, MEC systems have resulted the wet-bulb effectiveness substantially more than unity, which means that MEC can sensibly cool the product air below the ambient air wet-bulb temperature. For insights into MEC, inlet and outlet air conditions are presented by Eqs. (12)–(15).

$$(T_{in})_{dp} \leq (T_{out})_{db} \leq (T_{in})_{wb} \tag{12}$$

$$RH_{out} > RH_{in} \tag{13}$$

$$w_{out} = w_{in} \tag{14}$$

$$h_{out} < h_{in} \tag{15}$$

Unlike DEC and IEC systems, the thermodynamic limit of MEC cooling is dew-point temperature; therefore, cooling potential of MEC is function of $(T_{in})_{db} - (T_{in})_{dp}$. Accordingly, dew-bulb effectiveness of MEC ε_{dp} [–] can be expressed as follows:

$$(\varepsilon_{dp})_{MEC} = \frac{(T_{in})_{db} - (T_{out})_{db}}{(T_{in})_{db} - (T_{in})_{dp}} \tag{16}$$

For general overview, outlet air temperature of MEC unit for Fukuoka and Multan climates is calculated for ε_{dp} = 0.95, and the results are compared with IEC as shown in **Figure 9(b)**. It can be seen that the MEC can provide much better conditions as compared to conventional IEC throughout the day for both cities. Moreover, the performance of MEC can be further improved as compared to IEC at drier ambient air conditions. For brief understanding, the applicability of standalone MEC can be considered limited when $w \geq 11.2$ g/kgDA [10]; however, it may not be limited if utilized intelligently, for example, pre-dehumidification of ambient air (by desiccant dehumidifier) before it passes through MEC channels. As the results

presented in **Figure 9(b)** are based on constant ε_{dp}, they may not be exactly similar to real experiments. In this regard, lots of studies have reported experimental results along with numerical models for MEC which can be found from references [50–52]. In addition, a recent study [6] provides basic correlation for performance evaluation of MEC, which can be represented by Eq. (17). The correction is valid for the range of T_{in} = 20–45°C and w_{in} = 10–25 g/kgDA.

$$(T_{out})_{db} = A_1 + B_1(T_{in})_{db} + C_1(w_{in}) \tag{17}$$

where w_{in}, T_{in}, and T_{out} represent inlet humidity ratio [g/kgDA], inlet, and outlet air temperatures [°C], respectively. The values of constant A_1, B_1, and C_1 are 6.70, 0.26, and 0.53, respectively.

4.4. Desiccant AC (DAC)

It can be noticed from Sections 4.1–4.3 that cooling potential of evaporative cooling techniques is function of $(T_{in})_{db} - (T_{in})_{wb}$ or $(T_{in})_{db} - (T_{in})_{dp}$; therefore, it can be only applied in dry regions/climates. In contrary, desiccant AC (DAC) could be an energy-efficient and viable solution for humid climates [1]. The DAC possesses ability to deal sensible and latent load of AC distinctly and can be operated on low-grade waste heat, biogas, and/or solar energy. The ability of desiccant material to adsorb water vapors from ambient air makes DAC system a suitable choice for AC in high humidity regions [3]. A typical DAC system based on solid desiccant rotor is shown in **Figure 10(a)**. First, ambient air (1) is passed through the desiccant dehumidifier where it is dehumidified due to water vapor pressure difference between air and desiccant (process 1–2). This process will be isenthalpic in case of ideal situation, that is, neglecting sorption heat. Thus, the temperature of dehumidified air (2) is increased due to heat of water vapor condensation. Second, the dehumidified air (2) is sensibly cooled initially by heat exchanger (process 2–3) followed by low-cost cooling processes (process 3–4), for example, IEC. On the other hand, desiccant will be saturated with water vapor adsorption after some time. Therefore, regeneration/hot air (6) is passed through the desiccant (process 6–7) which removes the adsorbed water vapors for cyclic usage of desiccant. Referring to **Figure 10(a)**, inlet and outlet air conditions of DAC can be simply expressed by Eqs. (18)–(25), while detailed DAC models can be found from references [4, 53].

$$(T_2)_{wb} = (T_1)_{wb} \tag{18}$$

$$(T_3)_{db} = (T_2)_{db} - \varepsilon_{HX}\left((T_2)_{db} - (T_1)_{db}\right) \tag{19}$$

$$(T_4)_{db} = (T_3)_{db} - \varepsilon_{IEC}\left((T_3)_{db} - (T_1)_{wb}\right) \tag{20}$$

$$(T_5)_{db} = (T_1)_{db} + \varepsilon_{HX}\left((T_2)_{db} - (T_1)_{db}\right) \tag{21}$$

$$(T_6)_{db} = f(w_1, RH_2) \tag{22}$$

$$RH_6 \leq RH_2 \tag{23}$$

$$w_4 = w_3 = w_2 \tag{24}$$

$$w_6 = w_5 = w_1 \tag{25}$$

where subscript numbers are associated with **Figure 10(a)**. Effectiveness of heat exchanger (HX) and cooling source (IEC), that is, ε_{HX} and ε_{IEC}, is considered 0.95 for analysis. For the analysis of DAC system, ambient air conditions of both cities (**Figure 6**) are considered on average basis, that is, T = 36.2°C, RH = 62% for Multan and T = 27.6°C, RH = 69% for Fukuoka. Consequently, effect of regeneration temperature (T_6) on supply air condition (4) is investigated as shown in **Figure 10(b)**. It can be seen that supply air relative humidity is reduced linearly with the increase in regeneration temperature for both cities. Similarly, supply air enthalpy is also reduced at higher regeneration temperatures by which the conditioning is improved. While the supply air temperature at all regeneration temperatures is found 30 ± 0.1°C and 23.5 ± 0.10°C for Multan and Fukuoka, respectively. It can be observed that DAC system can provide variety of supply air conditions by manipulating regeneration temperature; therefore, it can be considered a viable AC system for various nonhuman applications expressed in Section 2.

Finally, it can be summarized that evaporative cooling systems (Sections 4.1–4.3) could provide low-cost AC for dry regions, whereas DAC system can be used efficiently for humid climates. Additionally hybrid systems based on evaporative cooling and/or DAC can also be established for efficient and sustainable AC performance. Hence, it can be concluded that one or other AC system (presented in Section 4) can provide optimum AC for presented nonhuman applications.

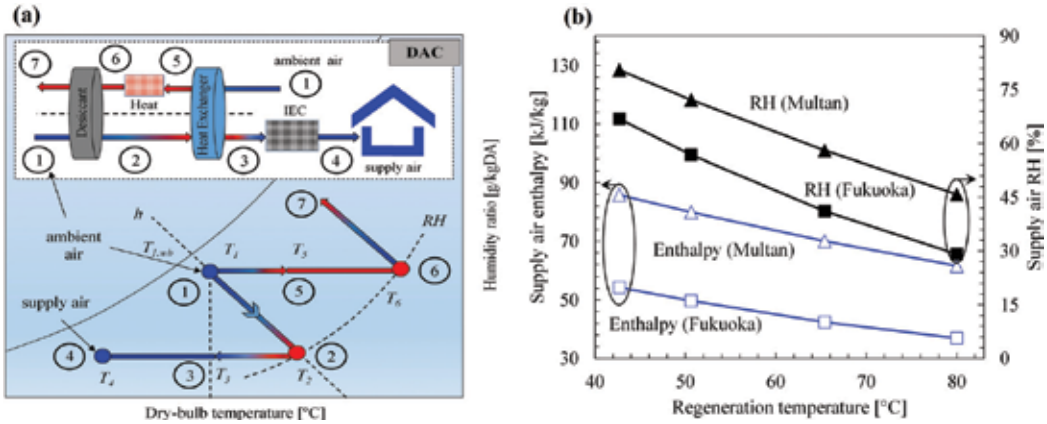

Figure 10. Desiccant air-conditioning (DAC) system: (a) schematic representing the fundamentals and thermodynamic principle; and (b) effect of regeneration temperature on supply air enthalpy and relative humidity.

5. Conclusions

The chapter discusses the fundamentals of various nonhuman air-conditioning (AC) applications from the viewpoint of low-cost and energy-efficient AC. In this regard, optimum conditions are explored and compared on psychrometric charts for numerous nonhuman AC applications. Most of them require dissimilar conditions as compared to conventional humans' thermal

comfort. Conventional vapor compression based AC systems are found thermodynamically inefficient and expensive; therefore, it has been realized that low-cost energy-efficient AC is direly needed. Thus, study proposes four kinds of low-cost energy-efficient AC systems which are based on evaporative cooling and thermally driven conceptions. Fundamentals and principle of each system is explained by means of basic heat/mass transfer relationships. Moreover, system performance is evaluated for climatic conditions of two cities, that is, Multan and Fukuoka. According to the results, performance of all systems is highly influenced by ambient air conditions, and, therefore, a particular AC system cannot provide optimum AC for all applications. However, one or other AC system can successfully provide desired conditions of temperature and relative humidity. In general, following conclusions have been made for this study.

- Evaporative cooling systems provide low-cost AC, which can be utilized for various non-human applications. However, the cooling potential is the function of $(T_{in})_{db} - (T_{in})_{wb}$ or $(T_{in})_{db} - (T_{in})_{dp}$ and, therefore, can be only employed for dry climatic conditions. Due to simple designing and operation, these systems should be considered on top priority for AC wherever applicable.
- Instead, desiccant AC systems are found to be an energy-efficient and viable solution for humid climatic conditions and can be operated on low-grade waste heat, biomass, and/or solar thermal energy. As DAC performance is directly related to regeneration temperature, they can provide various supply air conditions, which are required by many non-human AC applications.
- Additionally, hybrid systems based on evaporative cooling and/or desiccant AC can also be established for efficient and sustainable AC.

Nomenclature

AC	Air-conditioning
ASHRAE	American society of heating, refrigeration, and AC engineers
CFCs	Chlorofluoro-carbons
COP	Coefficient of performance [–]
DAC	Desiccant air-conditioning
DBT	Dry-bulb temperature [°C]
DEC	Direct evaporative cooling
GWP	Global warming potential
h	Enthalpy [kJ/kg]
HCFCs	Hydrochlorofluoro-carbons
HFCs	Hydro-fluorocarbons

HVAC	Heating, ventilation, and air-conditioning
IEC	Indirect evaporative cooling
L/s	Litter per second
M-Cycle	Maisotsenko cycle
ODP	Ozone layer depletion potential
RH	Relative humidity [–] or [%]
T	Temperature [K] or [°C]
VAC	Vapor compression–based air-conditioning
VPD	Vapor pressure deficit [kPa]
w	Humidity ratio [g_w/kg_{DA}]
ε	Effectiveness [–]
Subscripts	
a	Air
db	Dry-bulb
dp	Dew-point
in	Inlet/input
out	Outlet/output
wb	Wet-bulb

Author details

Muhammad Sultan[1]* and Takahiko Miyazaki[2]

*Address all correspondence to: muhammadsultan@bzu.edu.pk

1 Department of Agricultural Engineering, Bahauddin Zakariya University, Multan, Pakistan

2 Faculty of Engineering Sciences, Kyushu University, Kasuga-shi, Fukuoka, Japan

References

[1] Sultan M, El-Sharkawy II, Miyazaki T, Saha BB, Koyama S. An overview of solid desiccant dehumidification and air conditioning systems. Renewable and Sustainable Energy Reviews. 2015;**46**:16–29. DOI: 10.1016/j.rser.2015.02.038

[2] Sultan M, Miyazaki T, Saha BB, Koyama S. Steady-state investigation of water vapor adsorption for thermally driven adsorption based greenhouse air-conditioning system. Renewable Energy. 2016;**86**:785–795. DOI: 10.1016/j.renene.2015.09.015

[3] Sultan M. Study on sorption characteristics of water adsorbents for agricultural air-conditioning systems. Dr. Eng. Thesis. Kyushu University. 2015.

[4] Sultan M, Miyazaki T, Koyama S, Khan ZM. Performance evaluation of hydrophilic organic polymer sorbents for desiccant air-conditioning applications. Adsorption Science and Technology. 2017;**35**(1):1–16.

[5] Sultan M, El-Sharkawy II, Miyazaki T, Saha BB, Koyama S. Experimental study on carbon-based adsorbents for greenhouse dehumidification. Evergreen – Joint Journal of Novel Carbon Resource Sciences & Green Asia Strategy. 2014;**1**:5–11

[6] Sultan M, Miyazaki T, et al. Thermodynamic assessment of solar chimney based air-conditioning system for agricultural and livestock applications. Proc. of 4th Int. Conference on Energy, Environment and Sustainable Development (EESD-2016), Jamshoro, Pakistan. Paper#52, 2016:1–9, ISBN# 978-969-7710-00-3.

[7] Mahmood MH, Sultan M, Miyazaki T, Koyama S. Desiccant air-conditioning system for storage of fruits and vegetables: Pakistan preview. Evergreen – Joint Journal of Novel Carbon Resource Sciences & Green Asia Strategy. 2016;**3**:12–17

[8] Sarbu I. A review on substitution strategy of non-ecological refrigerants from vapour compression-based refrigeration, air-conditioning and heat pump systems. International Journal of Refrigeration. 2014;**46**:123–141. DOI: 10.1016/j.ijrefrig.2014.04.023

[9] Wang CC. System performance of R-1234yf refrigerant in air-conditioning and heat pump system—An overview of current status. Applied Thermal Engineering. 2014;**73**: 1412–1420. DOI: 10.1016/j.applthermaleng.2014.08.012

[10] Mahmood MH, Sultan M, Miyazaki T, Koyama S, Maisotsenko VS. Overview of the Maisotsenko cycle—A way towards dew point evaporative cooling. Renewable and Sustainable Energy Reviews. 2016;**66**:537–555. DOI: 10.1016/j.rser.2016.08.022

[11] Zhang H, Shao S, Xu H, Zou H, Tian C. Free cooling of data centers: A review. Renewable and Sustainable Energy Reviews. 2014;**35**:171–182. DOI: 10.1016/j.rser.2014.04.017

[12] Kim JY, Chang HJ, Jung YH, Cho KM, Augenbroe G. Energy conservation effects of a multi-stage outdoor air enabled cooling system in a data center. Energy and Buildings. 2017;**138**:257–270. DOI: 10.1016/j.enbuild.2016.12.057

[13] Weerts BA, Gallaher D, Weaver R, Van Geet O. Green Data Center Cooling: Achieving 90% Reduction: Airside Economization and Unique Indirect Evaporative Cooling. In: 2012 IEEE Green Technologies Conference; Tulsa, Oklahoma: IEEE; 2012. pp. 1–6. DOI: 10.1109/GREEN.2012.6200950

[14] Zorpas AA, Skouroupatis A. Indoor air quality evaluation of two museums in a subtropical climate conditions. Sustainable Cities and Society. 2016;**20**:52–60. DOI: 10.1016/j.scs.2015.10.002

[15] Ascione F, Bellia L, Capozzoli A. A coupled numerical approach on museum air conditioning: Energy and fluid-dynamic analysis. Applied Energy. 2013;**103**:416–427. DOI: 10.1016/j.apenergy.2012.10.007

[16] Ascione F, Bellia L, Capozzoli A, Minichiello F. Energy saving strategies in air-conditioning for museums. Applied Thermal Engineering. 2009;**29**:676–686. DOI: 10.1016/j.applthermaleng.2008.03.040

[17] Jung CC, Wu PC, Tseng CH, Su HJ. Indoor air quality varies with ventilation types and working areas in hospitals. Building and Environment. 2015;**85**:190–195. DOI: 10.1016/j.buildenv.2014.11.026

[18] Verde M, Harby K, Corberán JM. Optimization of thermal design and geometrical parameters of a flat tube-fin adsorbent bed for automobile air-conditioning. Applied Thermal Engineering. 2017;**111**:489–502. DOI: 10.1016/j.applthermaleng.2016.09.099

[19] Abdullah MO, Tan IAW, Lim LS. Automobile adsorption air-conditioning system using oil palm biomass-based activated carbon: A review. Renewable and Sustainable Energy Reviews. 2011;**15**:2061–2072. DOI: 10.1016/j.rser.2011.01.012

[20] Lee SH, Lee WL. Site verification and modeling of desiccant-based system as an alternative to conventional air-conditioning systems for wet markets. Energy. 2013;**55**:1076–1083. DOI: 10.1016/j.energy.2013.04.029

[21] Guojie Z, Chaoyu Z, Guanghai Y, Wu C. Development of a new marine rotary desiccant airconditioning System and its energy consumption analysis. Energy Procedia. 2012;**16** (Part B):1095–1101. DOI: 10.1016/j.egypro.2012.01.175

[22] Sultan M, Miyazaki T, Koyama S, Saha BB. Utilization of desiccant air-conditioning system for improvement in greenhouse productivity: A neglected area of research in Pakistan. International Journal of Environment. 2014;**4**:1–10

[23] Sultan M, Miyazaki T, Saha BB, Koyama S. Optimization of adsorption isotherm taxonomy for open-cycle desiccant air-conditioning applications. In: 24th IIR International Congress of Refrigeration. ICR-2015. Yokohama, Japan: IIR-ICR-2015; 2015. pp. 1–8

[24] Maisotsenko V, Treyger I. Way to energy abundance can be found through the Maisotsenko cycle. International Journal of Energy for a Clean Environment. 2011;**12**:319–326. DOI: 10.1615/InterJEnerCleanEnv.2012005830

[25] Saghafifar M, Gadalla M. Innovative inlet air cooling technology for gas turbine power plants using integrated solid desiccant and Maisotsenko cooler. Energy. 2015;**87**:663–677. DOI: 10.1016/j.energy.2015.05.035

[26] ASHRAE. Handbook—HVAC Applications. 2007

[27] ASHRAE. Handbook—Refrigeration. 2006

[28] ASHRAE. Handbook—HVAC Systems and Equipment. 2008

[29] ASHRAE. Handbook—Fundamentals. 2009

[30] Christianson LL, Fehr RL. Ventilation—Energy and Economics. Ventilation of Agricultural Structures. American Society of Agricultural Engineers. 1983. pp. 335–349. St. Joseph, Michigan.

[31] López-Morales V, López-Ortega O, Ramos-Fernández J, Muñoz LB. JAPIEST: An integral intelligent system for the diagnosis and control of tomatoes diseases and pests in hydroponic greenhouses. Expert Systems with Applications. 2008;**35**:1506–1512. DOI: 10.1016/j.eswa.2007.08.098

[32] Prenger JJ, Ling PP. Greenhouse Condensation Control Understanding and Using Vapor Pressure Deficit (VPD). 1680 Madison Ave., Wooster OH 44691: The Ohio State University Extension's FactSheet: Food, Agricultural and Biological Engineering (AEX–804); 2001

[33] Shamshiri R, Ismail WIW. Performance evaluation of ventilation and pad-and-fan systems for greenhouse production of tomato in lowland Malaysia. World Research Journal of Agricultural & Biosystems Engineering. 2012;**1**:1–5

[34] Kitinoja L, Kader AA. Small-scale postharvest handling practices: A manual for horticultural crops. 4th ed. Davis: University of California; 2002

[35] Weerts BA. NSIDC green data center project: Coolerado and modeling an application of the Maisotsenko cycle. M.S. Thesis, 2012. Department of Civil, Environmental & Architectural Engineering, University of Colorado Boulder, Colorado, United States.

[36] Barigozzi G, Perdichizzi A, Gritti C, Guaiatelli I. Techno-economic analysis of gas turbine inlet air cooling for combined cycle power plant for different climatic conditions. Applied Thermal Engineering. 2015;**82**:57–67. DOI: 10.1016/j.applthermaleng.2015.02.049

[37] Comodi G, Renzi M, Caresana F, Pelagalli L. Enhancing micro gas turbine performance in hot climates through inlet air cooling vapour compression technique. Applied Energy. 2015;**147**:40–48. DOI: 10.1016/j.apenergy.2015.02.076

[38] Zhang XJ, Yu CY, Li S, Zheng YM, Xiao F. A museum storeroom air-conditioning system employing the temperature and humidity independent control device in the cooling coil. Applied Thermal Engineering. 2011;**31**:3653–3657. DOI: 10.1016/j.applthermaleng.2010.12.031

[39] Luo X, Gu Z, Wang Z, Tian W, Li K. An independent and simultaneous operational mode of air conditioning systems for visitors and relics in archaeology museum. Applied Thermal Engineering. 2016;**100**:911–924. DOI: 10.1016/j.applthermaleng.2016.02.052

[40] Hou S, Li H, Zhang H. An open air–vapor compression refrigeration system for air-conditioning and desalination on ship. Desalination. 2008;**222**:646–655. DOI: 10.1016/j.desal.2007.01.190

[41] Taylor DA. Chapter 9 - Refrigeration, air conditioning and ventilation. Introduction to Marine Engineering (Second Edition). Elsevier Ltd, Butterworth-Heinemann; 1990. pp. 163–178. https://doi.org/10.1016/B978-0-408-05706-6.50013-4

[42] Miyazaki T, Oda T, Ito M, Kawasaki N, Nikai I. The possibility of the energy cost savings by the electricity driven desiccant system with a high performance evaporative cooler. In: International Symposium on Innovative Materials for Processes in Energy Systems; 2010

[43] Arora CP. Refrigeration and Air Conditioning. Tata McGraw-Hill Education Pvt. Ltd. 2000. 2 Pennsylvania Plaza New York City. ISBN 10: 9351340163 / ISBN 13: 9789351340164.

[44] Jones WP. 9 - The Fundamentals of Vapour Compression Refrigeration. Air Conditioning Engineering. 5th ed. Oxford: Butterworth-Heinemann; 2001. pp. 241–278

[45] Spauschus HO, Doderer GC, Olsen RS, Sellers RA. Material Stabilities in Vapor Compression Refrigeration Systems. Pergamon: Progress in Refrigeration Science and Technology; 1965. pp. 685–691

[46] Guan L, Bennett M, Bell J. Evaluating the potential use of direct evaporative cooling in Australia. Energy and Buildings. 2015;**108**:185–194. DOI: 10.1016/j.enbuild.2015.09.020

[47] Kovačević I, Sourbron M. The numerical model for direct evaporative cooler. Applied Thermal Engineering. 2017;**113**:8–19. DOI: 10.1016/j.applthermaleng.2016.11.025

[48] Pandelidis D, Anisimov S. Numerical analysis of the heat and mass transfer processes in selected M-Cycle heat exchangers for the dew point evaporative cooling. Energy Conversion and Management. 2015;**90**:62–83. DOI: 10.1016/j.enconman.2014.11.008

[49] Duan Z, Zhan C, Zhang X, Mustafa M, Zhao X, Alimohammadisagvand B, et al. Indirect evaporative cooling: Past, present and future potentials. Renewable and Sustainable Energy Reviews. 2012;**16**:6823–6850. DOI: 10.1016/j.rser.2012.07.007

[50] Miyazaki T, Akisawa A, Nikai I. The cooling performance of a building integrated evaporative cooling system driven by solar energy. Energy and Buildings. 2011;**43**:2211–2218. DOI: 10.1016/j.enbuild.2011.05.004

[51] Anisimov S, Pandelidis D, Jedlikowski A, Polushkin V. Performance investigation of a M (Maisotsenko)-cycle cross-flow heat exchanger used for indirect evaporative cooling. Energy. 2014;**76**:593–606. DOI: 10.1016/j.energy.2014.08.055

[52] Pandelidis D, Anisimov S, Worek WM. Performance study of the Maisotsenko cycle heat exchangers in different air-conditioning applications. International Journal of Heat and Mass Transfer. 2015;**81**:207–221. DOI: 10.1016/j.ijheatmasstransfer.2014.10.033

[53] Antonellis SD, Joppolo CM. Simplified Models for the Evaluation of Desiccant Wheels Performance. In: Enteria N, Awbi H, Yoshino H, editors. Desiccant heating, ventilating and air-conditioning system. Singapore: Springer; 2017. pp. 63–85

Chapter 6

Refrigeration System: Capacity Modulation Methods

Orhan Ekren

Additional information is available at the end of the chapter

http://dx.doi.org/10.5772/intechopen.70433

Abstract

Energy conservation and reduction of the global warming effect become one of the most important subjects in the world. Since refrigeration system energy consumption is steadily increasing in overall energy consumption, this system is under research. Refrigeration systems are full of energy conservation that is having minimum energy consumption while satisfying the user's needs. Refrigeration system applications where the load may vary over a wide range, due to lighting, product loading, ambient weather variations, or other factors during operation, can be optimized by capacity modulation. There are many ways to achieve capacity modulation. This paper presents literature review of various capacity modulation methods which reduce the energy consumption of the refrigeration system and decrease CO_2 emission indirectly. In this paper, on/off control, digital scroll compressor, cylinder unloading, hot gas bypass, slide valve, multiple compressor, and variable speed capacity control methods are presented. In addition, electrical control techniques for the refrigeration capacity modulation applications are summarized.

Keywords: refrigeration capacity modulation, refrigeration system energy saving, reduce CO_2

1. Introduction

To meet the energy demand is the most critical problem in many countries because of steadily increasing energy consumption. If technologies and economic structures in the main world regions had remained at their 1990 level, in 2006 the world would have consumed 4.4 Gtoe more energy. The amount of electricity required to generate one unit of value added (electricity intensity) is increasing in most regions, especially in less industrialized regions in which the service sector is expanding rapidly, and in countries with air-conditioning (AC) requirements [1].

By 2050, it is expected that the world's energy supply will double today's demand [2]. Although some regions are moderate at this expected energy need since using more energy-efficient

technologies, higher amount of primary energy will be needed in 2020. Energy from renewable sources will have an important impact on markets during the time period, but will not dominate any market. The use of nonconventional energy decreases in Asia, Latin America, and Africa because of a lack of effective government engagement [2]. Global CO_2 emissions from energy use were 34% higher in 2006 than in 1990. Trends in CO_2 emissions vary significantly between countries. Developing countries with high economic growth have doubled their CO_2 emissions, while Europe has nearly stabilized its emissions, partly because of climate change policies (**Figure 1**).

The inefficient use of electricity in refrigeration and air-conditioning systems is regarded as an indirect contributor to the emission of greenhouse gases to the atmosphere. These emissions can be decreased by more energy conversion, efficient refrigeration systems. In addition to this, it is known that the overall energy consumption of a refrigeration, air-conditioning, or heat pump system during its service life is a considerable cost factor and frequently is a multiple of the initial investment. Generally, refrigeration systems are designed for fixed capacity to achieve cooling capacity based on the maximum demand at the highest ambient temperature. The consequence is that the refrigeration system delivers high cooling capacity, is selected to overcome the worst condition, and needs to be cycled on and off when normal conditions occur. However, refrigeration systems are operated at partial loads in most of their life cycle. For example, chillers typically run 99% of the time at part-load (off-design) conditions [3]. Therefore, to evaluate the refrigeration systems' partial load efficiency is mandatory. The European Commission has published seasonal efficiency standard EN 14,825 taking into account part load conditions. Furthermore, Air-Conditioning, Heating and Refrigeration Institute (AHRI) has published AHRI standard 551–591/2011 which explains water chiller and heat pump performance rating. In this standard, a part-load chapter contains calculation methods and performance rating of partial load heating and cooling loads [3]. Capacity modulation which matches the system capacity to the load improves overall system efficiency at partial loads. In this chapter, the previous published researches on refrigeration system capacity control methods will be reviewed.

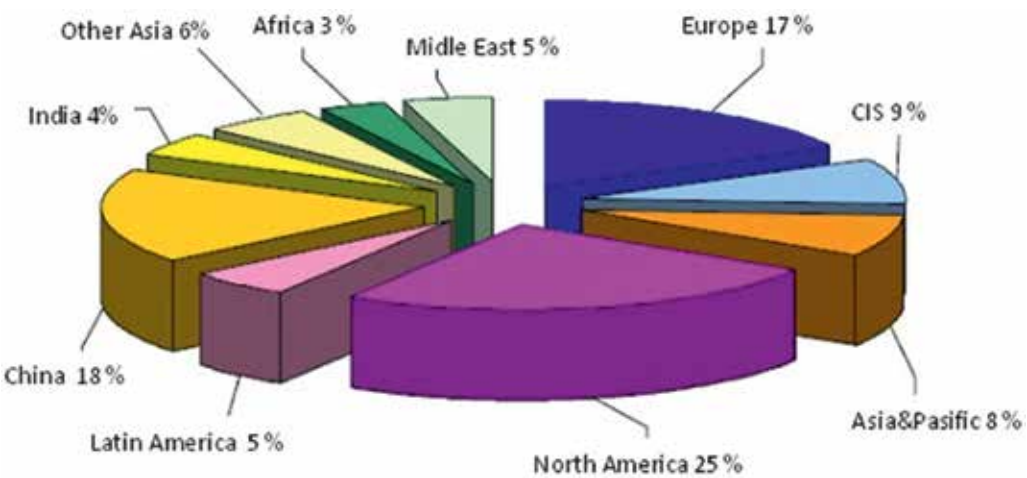

Figure 1. Distribution of world CO_2 emissions from energy use [2].

http://dx.doi.org/10.5772/intechopen.70433

2. Capacity control methods

Refrigeration system applications where the load may vary over a wide range, due to lighting, product loading, ambient weather variations, or other factors during operation, can be optimized by capacity control. Capacity control can be employed either within or outside the compressor, but their basic function of varying the refrigerant flow rate in the cycle remains the same. Depending on the system, the requirements may change; whereby, the following criteria should be assessed carefully: control performance, energy consumption, costs of selected solution, operation reliability, application range of the compressor, minimum compressor running time, and loading of the power supply. The most common methods are on/off control, digital scroll compressor, cylinder unloading, hot gas bypass, slide valve, multiple compressor, and variable speed [4–7]. The review of capacity modulation methods and electrical control techniques is illustrated in **Table 1** as a summary. And, various types of capacity control methods based on compressor are shown in **Figure 2**.

No	Year	Author	Objective	Compressor	Control
Digital scroll capacity control					
1	2005	Hu and Yang [10]	Application of digital scroll compressor to multi-evaporator system	Scroll	PID
2	2005	Kan et al. [12]	Application of digital scroll for cold storage	Scroll	Conventional
3	2005	Zhou and Zhang [13]	Energy saving of digital scroll compressor	Scroll	Conventional
4	2006	Ye and Chen [14]	Digital scroll compressor in multi-evaporator system	Scroll	Conventional
5	2006	Jiang et.al. [11]	Digital scroll compressor in multi-evaporator system	Scroll	Conventional
6	2006	Qui and Qiu [15]	Accuracy temperature application of digital scroll	Scroll	Conventional
7	2006	Shi [16]	Compared digital scroll with inverter-driven compressor	Scroll	Conventional
8	2006	Ma and Sun [17]	Compared digital scroll with inverter-driven compressor	Scroll	Conventional
9	2007	Huang et al. [18]	Compared with digital scroll and conventional scroll	Scroll	Proportional on/off cycle
Cylinder unloading capacity control					
10	1974	Cawley and Pfarrer [19]	Two-speed and cylinder unloading comparison	Reciprocating	Conventional
11	1988	Wong and James [20]	Cylinder unloading and variable speed comparison	Reciprocating	Conventional
12	1989	Wong and Legg [21]	Economic evaluation	Reciprocating	Conventional
13	1996	Yaqub and Zubair [22]	Cylinder unloading and suction throttling comparison	Reciprocating	Conventional

No	Year	Author	Objective	Compressor	Control
14	2001	Yaqub and Zubair [23]	Cylinder unloading and other methods comparison	Reciprocating	Conventional
Hot gas bypass capacity control					
15	1995	Yaqub et al. [27]	Hot gas bypass thermodynamic analysis	Reciprocating	Conventional
16	2000	Yaqub et al. [28]	Liquid and gas injection to compressor suction side	Reciprocating	Conventional
17	2001	Tso et al. [29]	Hot gas bypass and suction modulation comparison with mathematical model	Reciprocating	Conventional
18	2005	Cho et al. [30]	Compared hot gas bypass and on/off capacity control	Rotary	Conventional
Slide valve capacity control					
19	2002	Reindl [32]	Slide valve capacity control fact	Screw	Conventional
Multiple compressor capacity control					
29	2003	Winandy and Cristian [33]	Two-parallel compressor control	Scroll	Conventional
Variable speed capacity control					
21	1979	Muir and Griffith [36]	Variable speed and on/off control for domestic A/C		Conventional
22	1981	Tassou et al. [37]	Energy conservation on capacity control		Conventional
23	1982	Tassou et al. [38]	Effect of capacity modulation on the performance		Conventional
24	1982	Lida et al. [43]	Experimental analysis of variable speed	Rotary	Conventional
25	1982	Itami et al. [44]	Compressor lubrication problem and mechanical effect of variable speed capacity control	Reciprocating rotary	Conventional
26	1983	Tassou et al. [4]	Comparison of performance capacity-controlled system		Conventional
27	1984	Janssen and Kruse [5]	Continuous and discontinuous capacity control		Conventional
28	1984	Tassou et al. [39]	Economic comparison of fixed- and two-speed heat pump		Conventional
29	1985	Senshu et al. [45]	Small-capacity heat pump application with different compressors	Scroll reciprocating	Conventional
30	1988	Shimma et al. [41]	Energy saving of inverters		Conventional
31	1988	McGovern [47]	Variable speed performance of two-cylinder compressor	Reciprocating (open type)	Conventional
32	1988	Ischii et al. [48]	Dynamic behavior of variable speed compressor	Scroll rotary	Conventional

No	Year	Author	Objective	Compressor	Control
33	1988	Rice [57]	Energy saving of variable speed compressors		Conventional
34	1989	Zubair and Bahel [6]	Compressor capacity modulation schema		Conventional
35	1990	Ischii et al. [49]	Mechanical efficiency of variable speed compressor	Scroll	Conventional
36	1991	Tassou [40]	Dynamic performance of variable speed heat pump		Conventional
37	1992	Rice [58]	Performance analysis of reciprocating compressor	Reciprocating	Conventional
38	1992	Bose [61]	Variable frequency driver review	–	–
39	1994	Tassou and Qureshi [50]	Operating parameters for inverter-based variable speed rotary vane compressor	Rotary	Conventional
40	1996	Qureshi and Tassou [35]	Review of capacity control methods		Conventional
41	1997	Rasmussen [42]	Comparison of household single-phase fixed-speed and variable speed brushless DC motor drive	Reciprocating	Conventional
42	1998	Tassou and Qureshi [51]	Variable speed performance for different compressors	Reciprocating rotary	Conventional
43	2000	Ryska et al. [63]	Automotive application of variable speed	Automobile compressor	Conventional
44	2001	Park et al. [64]	Variable speed for multi-evaporator	Rotary	Conventional
45	2002	Saiz et al. [66]	Variable speed auto-compressor simulation	Automobile compressor	Conventional
46	2002	Park et al. [67]	Thermodynamic model for variable speed refrigeration system	Scroll	Conventional
47	2003	Cho et al. [54]	Inverter-driven compressor liquid injection	Scroll	Conventional
48	2003	Choi and Kim [65]	Variable speed for multi-evaporator	Scroll	Conventional
49	2004	Aprea et al. [55]	Effect of R22 R407C, R507, and R417A refrigerants for variable speed compressor	Reciprocating semi-hermetic	Conventional
50	2004	Aprea and Renno [68]	Modeling and experimental comparison of variable speed refrigeration system	Reciprocating	Conventional
51	2004	Shao et al. [69]	Variable speed compressor modeling and system simulation	Rotary	Conventional

No	Year	Author	Objective	Compressor	Control
52	2005	Kim and Kim [70]	Experimental study for artificial fault diagnosis variable speed refrigeration system	Reciprocating	Conventional
53	2006	Nasutin et al. [59]	Energy saving of variable speed and PID control		On/off P-PI-PD-PID
54	2007	Cho et al. [71]	CO_2 refrigerant for variable speed refrigeration system	Scroll	Conventional
55	2008	Cuevas and Lebrun [60]	Drawback of variable speed compressors	Scroll	Conventional
Electrical control applications					
56	1996	Cheung and Kamal [73]	Fuzzy and conventional control comparison for refrigeration system	Reciprocating	Fuzzy/PID
57	2003	Rahmati et al. [77]	Fuzzy and PID control comparison for HVAC systems		Fuzzy/PID
58	2004	Li et al. [80]	Fuzzy and PID control for automobile air-condition system	Automobile	Fuzzy/PID
59	2004	Aprea et al. [74]	Fuzzy control and on/off control comparison for refrigeration system	Reciprocating	On/ off-PID-fuzzy
60	2006	Aprea et al. [75]	Fuzzy-controlled and thermostat controlled-refrigeration system with EEV and TXV	Reciprocating	Fuzzy-on/off
61	2006	Aprea et al. [76]	Fuzzy control for chiller and heat pump variable speed driving methods	Scroll	Fuzzy/on/off
62	2006	Wang et al. [78]	PID, fuzzy, and fuzzy-PID control for HVAC system		Fuzzy/PID
63	2006	Navale [79]	Performance of fuzzy and PID control		Fuzzy/PID
64	2010	Ekren and Kucuka [72]	Performance of fuzzy control on compressor and electronic expansion valve	Scroll	Fuzzy

Table 1. Researches on capacity control methods and control applications.

2.1. On/off capacity control

The on/off capacity control is the simplest method adjusting the predetermined temperature (set point) using a thermostat. After the temperature reaches the set point, thermostat stops the compressor and circulating refrigerant in the cycle. Since the secondary fluid continues to circulate, the temperature of the water or air gradually raises. When the thermostat detects,

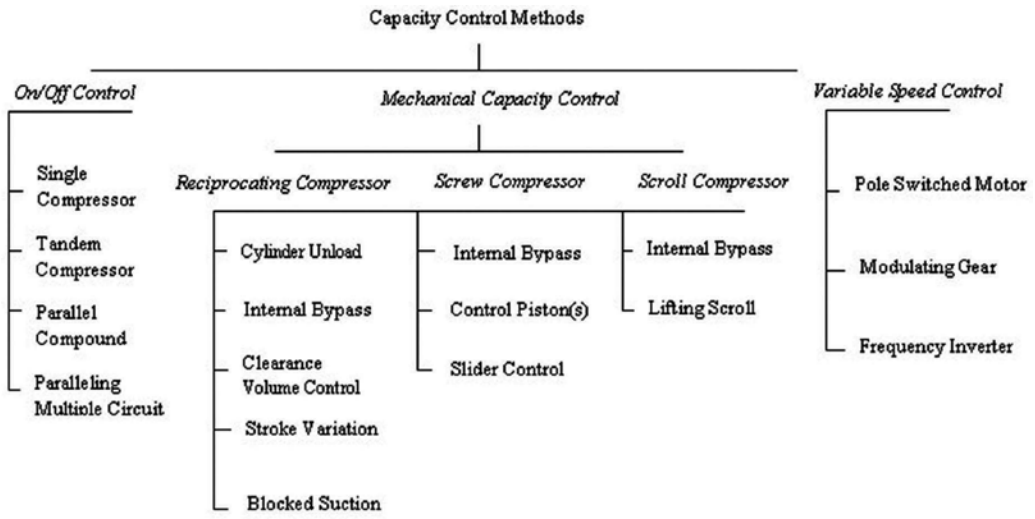

Figure 2. Capacity control methods [7].

this rise turns the compressor on. If the light-load conditions occur, this results on short cycling. Short cycling of the system reduces life of the compressor. In addition to that, the temperature of the secondary fluid fluctuates and uncomfortable conditions occur.

2.2. Digital scroll capacity control

In this method, scrolls force to separate and compression of refrigerant stops. This modulates refrigerant flow without changing or stopping the compressor motor. The separation of the scrolls is realized by using an external solenoid valve; also, there is a bypass connection line between the discharge chamber and the intake gas. The upper scrolls can separate from the bottom scroll by 1 mm vertically. A piston is fixed to the top of the upper scroll and lifts up the upper scroll when it moves up. There is a modulation chamber at the top of the piston that is connected to the discharge pressure through a bleed hole. An external solenoid valve connects the modulation chamber with the suction side pressure. If the solenoid valve is closed, the scrolls operate as a classical scroll compressor. If the solenoid is opened, the discharge chamber and intake gas pressure connect each other and decrease the discharge pressure. This leads to less pressure holding the piston down, thereby causing the piston to shift upward, which in turn lifts the upper scroll. This action separates the scrolls and results in no mass flow through the scrolls. De-energized external solenoid valve again loads the compressor fully, and the compression is resumed (**Figure 3**) [8].

During the loaded state, the compressor operates like a standard scroll and delivers full capacity and mass flow. However, during the unloaded state, there is no capacity and no mass flow through the compressor. The scrolls are separated in a periodic cycle (20 seconds) to obtain a time-averaged compressor capacity based on the ratio of loading and unloading times. This allows the digital scroll to achieve infinite capacity modulation between 10 and 100%.

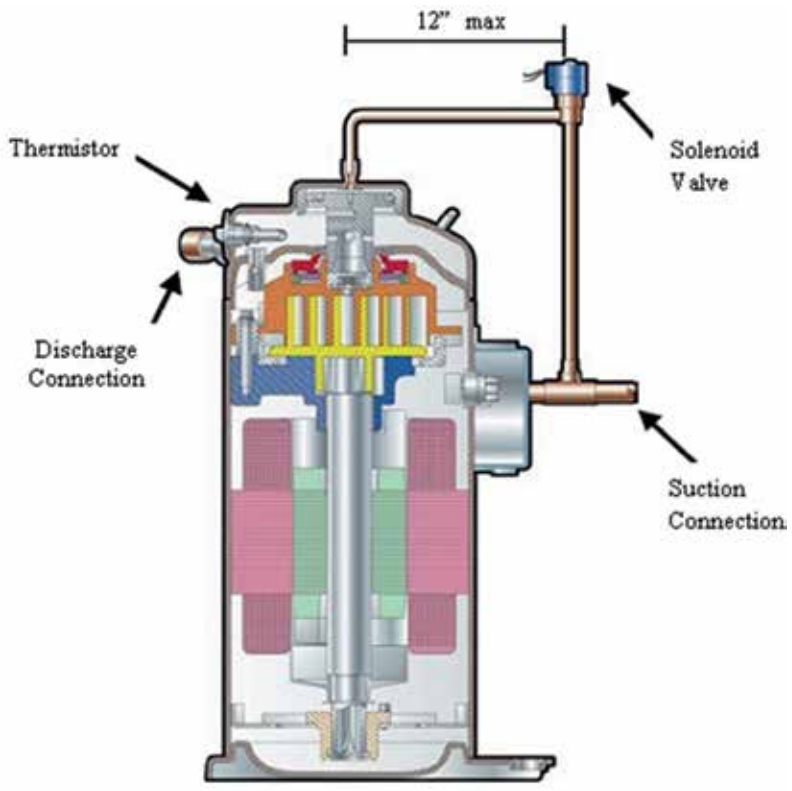

Figure 3. Digital scroll piping.

For example, 20-second cycle and the solenoid are de-energized for 16 seconds and then energized for 4 seconds; the resulting capacity will be 80% [8, 9]. This method provides very wide capacity range with continuous modulation, high efficiency, and very tight temperature control. But higher initial cost is the disadvantage of these methods compared to hot gas bypass method. Also, variable speed and digital scroll capacity controls are compared, and they give very close capacity modulation results [9].

The application of digital scroll compressor in multi-type air-conditioning system was introduced by Hu and Yang [10]. The authors reported the results from the development and performance testing of a cost-effective, energy-efficient, multi-type air-conditioner. In this system, about 75% reduction in power consumption was observed, while a partial load of 17% is occurred. The capacity modulation range of the system is in the range of 17–100%; on the other hand, an AC variable frequency control system has a range between 48 and 104%. In this method, system cost is 20% cheaper than an AC inverter. There are many studies on digital scroll; here, I will give summary of them such as Jiang et al. [11] discussed the control of digital compressor applied in multi-type air-conditioning system. Kan et al. [12] analyzed the application of digital scroll compressor in cold storage container. Zhou and Zhang [13] and Ye and Chen [14] studied the energy saving of digital scroll compressor. Qiu and Qiu [15]

discussed the application of digital scroll compressor in high-accuracy constant temperature and humidity air-conditioning. Analysis and comparison between digital scroll and inverter technology were studied by Shi [16] and Ma and Sun [17].

Huang et al. [18] conducted an experimental study on operation characteristics with variable air volume under refrigerating and heating condition of ducted air-conditioning (AC) unit with digital scroll compressor and conventional scroll compressor. The effects of air volume on the refrigerating (heating) capacity, input power, EER (COP), outlet temperature, discharge pressure, discharge temperature, and suction pressure were studied. As a result, the authors reached that the unit with digital scroll compressor was well adapted to the variable air volume system and good for the economical and reliable operation of the ducted AC unit.

2.3. Cylinder unloading capacity control

Capacity control also can be occurred through reciprocating compressor's cylinder unloading. The cylinder unloading capacity control method (suction valve unloading method) works by lifting the suction valves of some cylinders to the open position. A thermostat (or pressure transducer) energizes a solenoid (or solenoids if there are multiple cylinders in the compressor) that forces the suction valve to stay open. The gas cannot be compressed within the open cylinders, which results a drop in refrigeration capacity. In order to prevent overheating of the compressor, a thermostatic expansion valve should be installed to provide cooling to the compressor suction gas. This capacity reduction is then followed by hot gas bypass. Their construction is relatively low in cost, but they usually require a multicylinder compressor. The achievable capacity graduations depend on the constructional design. With 4, 6, and 8 cylinder compressors, it is usual to operate two cylinders per load stage, which permits graduations of (25)–50–(75)–100% or 33–66–100% [7].

Cawley and Pfarrer [19] have realized a comparative study regarding the part-load efficiency of two-speed compressors using compressor unloading capacity modulation. They found that 49% higher energy efficiency ratio (EER) could be reached using a two-speed compressor instead of a cylinder unloaded compressor. Lower frictional losses at half speed of the two-speed compressor reduce power input. Wong and James [20] resulted that variable compressor speed control is more efficient compared to cylinder unloading control. By using variable speed operation, volumetric efficiency and isentropic efficiency as well as coefficient of performance (COP) are increased at lower compressor speed. On the other hand, cylinder unloading control reduces isentropic efficiency and COP. Wong and Legg [21] also studied the economic benefits of a variable speed compressor in another work. It was shown that variable speed control leads to reduced energy consumption, but for intermittent operation, it may not be economically viable due to the high capital cost of the inverter.

The later study related with cylinder unloading method is investigated by Yaqub and Zubair [22]. They studied cylinder unloading and suction gas throttling schemes to reduce the capacity of refrigeration and air-conditioning systems at reduced load. In the first scheme, an unloaded valve was used to unload one or more cylinders at part-load conditions. The mass flow rate of refrigerant reduces by unloading of cylinders; therefore, the system

capacity reduces. A throttling valve is needed before the compressor to reduce the mass flow rate through the compressor. It was found that the cylinder-unloading method was the best and had the highest COP and minimum irreversible losses at any system capacity.

In another study, Yaqub and Zubair [23] investigated three different capacity control schemes. He compared cylinder unloading scheme with hot gas bypass and compressor suction throttling. These schemes are investigated for HFC-134a by considering finite size of the components that are used in the refrigeration systems. A comparative study was performed among these schemes in terms of the system coefficient of performance (COP), the operating temperatures, and percentage of refrigerant mass fraction as a function of the percentage of full-load system capacity. The models consider the finite-temperature difference in the heat exchangers, thus allowing the variations in the condenser and evaporator temperatures with respect to capacity and external fluid inlet temperatures.

2.4. Hot gas bypass capacity control

Hot gas bypass is a method that modulates refrigerant flow by bypassing some of the high pressure refrigerant gas (hot gas) discharged from the compressor back to the suction line without going through the evaporator, and the gas does any cooling. The capacity of reciprocating and centrifugal compressors can also be controlled by this method. Some applications use two or more methods for smoother switching and better control such as unloading in conjunction with hot gas bypass. Extra valves and piping are required for this capacity control, and capacity can be quickly adjusted by opening or closing a valve, but the number of capacity steps is finite. It may not prove precise and smooth temperature control [8, 24]. Suction pressures below the compressor designed limit are prevented because low suction densities result in poor compressor cooling. Therefore, hot gas bypasses into the systems' low pressure side.

Hot gas can be injected into different locations: the first one is the evaporator inlet after the distributor nozzle but before the distributor tubes, and the second one is the suction line [25, 26].

Bypass into evaporator inlet: on single evaporator and close connected systems, it is generally possible to introduce the hot gas into the evaporator inlet immediately after the expansion valve. Bypassing at the evaporator inlet results an artificial cooling load. Since the thermostatic expansion valve meters required refrigerant feed to maintain preset superheating value, the refrigerant returns to the compressor at normal operating temperatures and prevents motor heating problem. High flow velocity helps the oil returning in the evaporator [25].

Bypass into suction line: in this method, multiple evaporators are connected to a compressor, or if the condensing unit is remote from the evaporator, it may be necessary to bypass hot gas into the refrigerant suction line. Suction pressures can be controlled with this method. To meter liquid refrigerant into the suction line is required in order to keep the temperature of the refrigerant gas entering to the compressor within allowable limits. If this method is used by passed hot gas and liquid refrigerant must be mixed at correct amount in order to provide mixed gas into the compressor at desired temperature. For this purpose a mixing chamber is recommended. A suction line accumulator can serve as a mixing chamber and also protects the compressor from liquid flood back [25].

The first study related with this method is investigated by Yaqub et al. [27], and in this study, an automatic hot gas bypass technique is applied to reduce the capacity of refrigeration and air-conditioning systems at part-load conditions. Hot gas bypass valve sends high pressure refrigerant into the suction port. They discussed three hot-gas bypass schemes for HFC-134a and analyzed on the basis of the first and second laws of thermodynamics. Second-law-based thermodynamic analysis indicated that the total irreversible losses of the bypass valve increase substantially, as the capacity decreases. In another study, Yaqub et al. [28] investigated capacity control of a vapor-compression refrigeration system by injecting hot gas and liquid refrigerant into the suction side of the compressor. It was demonstrated that the compressor discharge temperatures increase significantly, when the hot gas from the compressor discharge is extracted and injected (without any liquid injection) directly into the suction side of the compressor.

Besides, Tso et al. [29] compared hot gas bypass control and suction modulation in refrigerated shipping containers by using mathematical model. They studied to analyze compressor power draw, coefficient of performance, and the sensible heat factor of evaporator against the container load. They resulted that suction modulation method is more energy efficient than hot gas bypass.

The performance of the showcase refrigeration system with three evaporators was measured during on/off cycling and hot gas bypass defrost by Cho et al. [30]. Based on the test results, the effects of off-period in the on/off cycling and electronic expansion valve (EEV) opening in the hot gas bypass defrosting cycle on the performance of showcase system were analyzed.

2.5. Slide valve capacity control

The slider control allows an adaptation of the compressor displacement to the power requirement by shifting the start of the compression process through an axial slide of the control slider. At the same time, the outlet window is adapted to the newly developing displacement in this series. Rotary-screw compressors use slide valves to adjust the necessary refrigeration capacity at partial loads by permitting the equipment to reduce the total volume of refrigerant compressed within the housing. The slide valve modulates compressor capacity between 25% to 100% range by 25% steps. The suction gas flow is measured in order to get the cooling capacity, and the volume ratio of the compressor is defined by the position of the suction contour and the size of the discharge port [31]. According to Reindl [32] one of the most common capacity control methods is capacity control slide valve for screw compressor. As the volume of refrigerant vapor to undergo compression is reduced, the compressor's capacity is reduced, and the effective volume ratio of the compressor also decreases.

2.6. Multiple compressor capacity control

Refrigeration system capacity can be modulated by using multiple refrigeration circuits or by using multiple compressors in single-circuit systems. Under partial load conditions, the compressors may be cycled in and out of service as required as well as providing a level of redundancy in the event one of the compressors should fail. Oil equalization is needed for these kinds of compressors. One of the least expensive forms of modulation, reliability,

can be seen as advantages of the multiple compressor capacity control. On the other hand, multiple compressor capacity provides finite number of capacity steps and limited efficiency gains. For example, in a 40 hp system requiring 25 hp of output at a given time, the system must operate at 30 hp output. Also, precise and smooth temperature and humidity control may not obtainable, because of the capacity modulation step [7, 8].

Winandy and Cridtian [33] realized a study regarding multiple compressors in which the condensing units have tandem scroll compressors. The main drawback on this configuration is oil returning to the compressor which is a serious trouble especially at part load.

According to ASHRAE [34], the gas velocities and piping geometry are the most important matter in multiple compressor control method because of ensuring adequate oil return. When working at part load, some modifications may be needed to ensure proper oil return. In addition, it is recommended that to separate the refrigerant circuits while parallel operating of compressors, however, this configuration is not always possible and does not give the same operational advantage at part load.

2.7. Variable speed capacity control

Variable speed control can be realized in different ways to regulate the speed of the compressor motor such as electronic variable frequency drives. Variable frequency drives (VFD) are also known as adjustable-frequency drives (AFD), variable speed drives (VSD), AC drives, micro-drives, or inverter drives. Compressor rotational speed can be varied to match the system's changing requirement for refrigeration capacity of a variable speed drive. Variable speed capacity control studies contain mechanical, electrical fact about compressor and other equipments. Primary studies on variable speed refrigeration systems were related with the theoretical analysis of the concept of variable speed capacity control and the investigation of the problems associated with the mechanical design of the system [35].

The following studies are related with main benefits and facts of the variable speed capacity control methods. Muir and Griffith [36] investigated different aspects of capacity modulation methods for refrigeration and domestic air-conditioning systems using the seasonal energy efficiency ratio (SEER). This method compares the seasonal efficiency of systems, taking into consideration the effects of on/off cycling and steady-state efficiency at several outdoor temperatures. The analysis showed that application of capacity modulation and significant energy savings can be possible due to decrease in on/off cycling losses and improvements in steady-state efficiency at partial loads.

Tassou et al. [4, 37–40] investigated the most fact of the variable speed capacity control methods, and they focused on the capacity modulation of domestic size of heat pumps. Energy conservation via capacity control and performance comparison with conventional systems, effects of capacity modulation, mathematical modeling of variable speed systems, part load, and dynamic performance analysis of heat pumps are the important issues investigated. The investigations showed that variable speed control could achieve a 15% improvement in energy conversion efficiency, compared to a conventional system. It was also found that superheat control with a thermostatic expansion valve was unsatisfactory during part-load

operation, and it was suggested that the problem could be effectively overcome by employing a microprocessor-controlled motorized expansion valve.

The study of Shimma et al. [41] is related with the evaluation of energy savings by using inverters in air-conditioners. According to the authors, the maximum energy savings and better system performance could be achieved by employing better control methods. Furthermore, improving the performance of individual components in the air-conditioning system could provide better system performance. The capacity-controlled system resulted in a reduction of the room temperature fluctuations to 50% of those for the conventional on-/off-controlled system. The authors pointed out various problems such as improvements in the refrigerant throttling mechanism, adoption of more effective noise suppression techniques (which is important to reduce radio wave interference noise and harmonic noise generated by the inverter), enhancement of the reliability and performance of inverter, and improvements in the overall system design to reduce noise at high-frequency operation and to overcome vibration problems at low-frequency operation.

According to Rasmussen [42], household refrigerators are usually thermostat (on/off)-controlled, constant speed, and mostly they have a single-phase induction motor as compressor drive. The author represents results of a prototype refrigerator using variable speed, three-phase, brushless DC motor drive. Test results of the motor and drive efficiency are presented; also, motor construction are described.

Also, different types of compressors are investigated in variable speed capacity control system by different authors. Papers dealing with rotary compressor were studied by Lida et al. [43]. On a heat pump equipped with a 4 hp (3 kW) hermetic rotary compressor, experimental studies are realized. They found that the practical limits for compressor speed variation were between 25 and 75 Hz. The results indicated improvements in EER with the inverter-driven compressor compared to a fixed-speed system. Cost and SEER analyses showed a 20% increase in the total cost for the inverter-controlled system and between 20 and 26% energy savings over the constant single capacity system. Other advantages identified for variable speed control over fixed-speed systems included accurate temperature control, system soft-start capabilities, and low-noise operation at reduced loads.

In the same year, Itami et al. [44] studied the performance and reliability factor of reciprocating and rotary compressors (frequency controlled). For the different type of compressor, modifications were suggested. For example, with the reciprocating compressor, a two-stage oil pump was used over the low-frequency range to ensure proper lubrication. For the rotary compressor, a liquid injection system was used to protect from overheating. Also, a disc mechanism was adopted to prevent increased amounts of discharge oil at the higher operating-frequency range. While the operating frequency was increased, the rotary compressor showed improvements in the volumetric and motor efficiencies; on the other hand, the reciprocating compressor shows improvement in mechanical and compression efficiencies, while the operating frequency was decreased. About 20–40% improvement in the SEER was reported with the variable speed air-conditioner compared to the conventional on/off-controlled system. In another related study, Senshu et al. [45] investigated on a small-capacity heat pump using a scroll compressor. This system showed a 30% improvement in annual performance

efficiency compared with the conventional reciprocating compressor. It is important that the EER of the inverter-driven heat pump at nominal load conditions was found less than a fixed-speed system, due to the inverter losses. In an ASHRAE research, project (RP-409) analyzed a large chiller operating with a variable speed controlled centrifugal compressor [46]. The results showed that variable speed control provides a 1.5% reduction in the compressor power consumption at maximum load and about 40% reduction at minimum load.

McGovern [47] investigated the performance of a two-cylinder and open-type reciprocating compressor with the speed range between 300 and 900 rpm. Different performance parameters, such as mass flow rate, shaft power, and compressor discharge gas temperature, showed a linear increase for the tested speed range; on the other hand, the volumetric efficiency was found to remain almost constant at 66% of the given speed range. The variation of mechanical efficiency with speed was 92–94% at the speed increased from 300 to 900 rpm, respectively.

Other authors studied with compressor were Ischii et al. [48, 49]. The authors compared mechanical efficiency and dynamic performance of scroll compressors with rolling piston rotary compressors. They found that the scroll compressors exhibited better vibration than the rolling piston rotary compressor; on the other hand, they exhibited lower mechanical efficiency. They reported that the mechanical efficiency of scroll compressors could be improved via design optimization.

Another study dealing with compressors was investigated by Tassou and Qureshi [50]. This study contains application of inverter-based variable speed drives for positive displacement rotary vane-type refrigeration compressors. The effects of the inverter on a number of operating parameters such as harmonic currents and voltages, power consumption and power factor, starting current, and overall system efficiency were investigated. Results showed that inverter may cause a reduction in the power factor and in the overall efficiency of the driver. According to results, variable speed operation of a rotary vane compressor can provide better temperature control and quick response to disturbances and changes in load.

Tassou and Qureshi [51] studied on positive displacement refrigeration compressors' variable speed capacity modulation. Compressors tested include an open-type reciprocating, a semi-hermetic reciprocating, and an open-type rotary vane. The results indicate that all three compressors were designed for maximum efficiency at nominal speed and all three compressors when operated at variable speed offer energy savings compared to their fixed-speed counterparts. Also, at constant head pressure, only the open-type compressor exhibited an improvement in the COP at reduced speeds. With variable head pressure control, all three compressors showed an increase in the COP with a reduction in speed. The analysis showed the open-type reciprocating compressor to be the most efficient system offering 12% savings when operating in a temperate climate and 24% savings when operating in a warm climate.

Rarely, gas and liquid refrigerant injection to the compressor is done. Gas injection is applied to increase compressor capacity and to save energy. Since more refrigerant passes through the condenser than through the evaporator compressor, capacity may increase some. Also, liquid refrigerant is injected to the compressor to decrease high discharge refrigerant temperatures which chemically degrade oil and refrigerant and cause

mechanical failure. High cost and additional component requirement are disadvantages of the gas and liquid injection system; also, liquid injection may cause slugging problem in the compressor [52, 53]. Cho et al. [54] applied the refrigerant injection to the variable speed compressor and measured performance of a liquid refrigerant injected inverter-driven scroll compressor with respect to variation of compressor frequency, injection pressure, and injection location. Furthermore, the influence of liquid injection on the performance was presented as a function of operating parameters and injection location. Results were compared with the non-injection case. For high frequency at a given injection ratio, the injection at 180°, for an injection angle at an injection port, yielded slightly better performance of the compressor as compared to that at 90°. It was found that liquid injection under high frequency was very effective, but injection under low frequency resulted some negative effects in the point-of-view compressor power, capacity, and adiabatic efficiency because of higher leakage through the scrolls.

Aprea et al. [55] presented a research dealing with compressors too. In this study, an experimental analysis has been realized, and they compared energetic performance of variable speed compressor and on/off control controlled with a classical thermostat. They used a semi-hermetic reciprocating compressor working with the refrigerants R22, R507, and R407C. The compressor was designed for a nominal frequency of 50 Hz, but they tested it in the range 30–50 Hz. The results showed that, using the R407C, an average of an electric energy consumption about 12% smaller when an inverter was employed to control the compressor refrigeration capacity instead of the thermostatic control is possible. So the R407C confirms its superiority in comparison with the R417A and R507; only the R22 shows a better performance.

Except this, energy-saving potential of the capacity control methods is studied by some researches. A feasibility and design study of a variable capacity refrigeration system was carried out by the *Energy Efficiency Demonstration Scheme* on behalf of the Department of Energy [56]. A commercially available variable speed compressor was monitored in a supermarket refrigerator. In this study at first, a conventional system was installed and then converted to variable speed for comparison. The results showed 56% power saving with high temperature (dairy applications) and a 30% saving with low temperature (frozen food applications). The energy savings achieved were attributed mainly to variable speed control and fully floating head pressure.

Rice [57, 58] studied on a heat pump, and he reported 27% energy savings for a modulating heat pump system. In that study reduced cycling losses, heat-exchanger unloading, reduced frosting/defrosting losses, and reduced backup heating were taken into account. He found that higher motor-slip losses and distorted inverter waveform decreased the conventional three-phase induction motor efficiency up to 20%, and he suggested that these losses could be reduced by a permanent magnet and electronically commutated motor-inverter combination.

Nasutin et al. [59] studied on the potential of energy saving of a variable speed compressor. The main aim of the system is to provide thermal comfort for application in air-conditioning system and to enhance load-matching capability of the system. In this study a constant speed

system was retrofitted using an inverter and a proportional-integral-derivative (PID) controller used. As a result, energy saving for the system was estimated about 25.3% at a temperature of 22°C via PID controllers.

Recently, Cuevas and Lebrun [60] introduced an experimental study dealing with drawbacks of variable speed compressors which are concerning the inverter efficiency, the effect of the inverter on the induction motor, and the effect of variable speed on the compressor isentropic and volumetric efficiencies. It was observed that the inverter efficiency varies between 95 and 98% for compressor electrical power varying between 1.5 and 6.5 kW and that compressor efficiencies are not enormously influenced by compressor supply frequency. When the compressor speed is 75 Hz, a slight degradation occurs because of the electromechanical losses. These losses increase with compressor speed. A maximal isentropic efficiency of 0.65 for a pressure ratio of the order of 2.2 was obtained. The experimental results obtained at 50 Hz were used to identify six parameters of a semi-empirical model which was then used to simulate the different tests developed at different compressor speeds. The simulated results were in very good agreement with those measured. The results showed that motor losses induced by the inverter are negligible.

Studies related with VFD are important for variable speed capacity control method. A comprehensive technology review of the application of power electronics was given by Bose [61]. According to author currently available VFD systems can be classified into three basic inverter types: the six-step voltage inverter (VSI), the six-step current inverter (CSI), and the pulse-width-modulated voltage source inverter (PWM). A report published by the Energy Efficiency Office [62] compares typical efficiencies of six VFD types of different ratings. The PWM inverter shows a slightly better efficiency over VSI and CSI.

In addition, automotive refrigeration system, multi-evaporator, system modeling, fault diagnosis, and CO_2 refrigerant were applied to variable speed compressor. These subjects are explained below, respectively.

Ryska et al. [63] presented that a new evaluation method allows the overall cooling performance improvement for truck or bus at different engine speeds and driving styles. This method was demonstrated in two refrigeration units.

Park et al. [64] investigated multi-type inverter air-conditioner with a variable speed rotary compressor and an electronic expansion valve. Performance of the system was analyzed with different operating frequencies of the compressor, different cooling loads and cooling load fraction between rooms. The optimum opening amount of the electric expansion valve (EEV) was also calculated.

Choi and Kim [65] measured performance of an inverter-driven multi-air-conditioner with two indoor units using electronic expansion valves (EEV). For the performance varying indoor loads, EEV opening and scroll compressor speed have been investigated. According to the experimental results, the author suggested around 4°C superheats for both indoor units by using EEV also as the compressor speed needs to be adjusted to provide optimum cooling capacity for the indoor units.

Saiz et al. [66] have developed a steady-state computer simulation model for refrigeration circuits of automobile air-conditioning systems. The simulation model includes a variable capacity compressor and a thermostatic expansion valve in addition to the evaporator and micro-channel parallel flow condenser. The refrigeration circuit was equipped with a variable capacity compressor run by an electric motor controlled by a frequency converter.

Park et al. [67] developed a thermodynamic model for a refrigerant injected variable speed scroll compressor with using continuity energy conservation and real gas equation. In this model, energy balance at the low-pressure compressor, suction gas heating, motor efficiency, and volumetric efficiency were considered. Also, gas leaking was considered as a function of compressor frequency. Results showed deviations from the measured values about 10% at the 90% of the experimental data. According to the model, mass flow rate, suction gas heating, cooling capacity, and power consumption of the compressor were estimated and analyzed as a function of frequency. Furthermore, the effects of the injection on the performance of the compressor were discussed as a function of frequency, injection geometry, and injection conditions. Another modeling study was investigated by Aprea and Renno [68]. The main aim of this study is a thermodynamic model simulating the working of a vapor compression refrigeration system. The model could evaluate the system performance, while the compressor capacity is regulated with an inverter inserted into the compressor electric motor. The author compared the outputs of the model with the experimental results. The comparison of model and experimental results is realized by varying the supply of current frequency of the compressor in the range 30–50 Hz using the R407C. The model and experimental result comparison is completely acceptable in terms of condensation temperature, compression ratio, condensation power, and coefficient of performance. Also, an exergetic analysis represented to explain the performance of the plant components at variable speed operation.

In addition to this study, Shao et al. [69] analyzed modeling of variable speed compressor for air-conditioner and heat pump. For the real operation performance of inverter-driven compressor, a map-based method was used. Since the second-order function of condensation and evaporation temperature, the model was built at the basic frequency and map conditions. The model is validated by the actual operating conditions. The author compared the data provided by the compressor manufacturers, the average relative errors are less than 2, 3, and 4% for refrigerant mass flow rate, compressor power input, and coefficient of performance (COP), respectively, and the author found out that this model of variable speed compressor is suitable for the simulation of inverter air-conditioner and heat pump systems.

Kim and Kim [70] studied on an experimental study to define the effect of four artificial faults on the performance for a variable speed refrigeration system. For the evaluation of the performance, a conventional vapor compression test system was modified to test several artificial faults by observing the variation of cooling capacity. The four major faults were compressor fault, condenser fault, evaporator fault, and refrigerant leakage. Two different rule-based modules for constant and variable speed operations were organized for an easy diagnosis of the faults. As a result, COP degradation due to the fault in a variable speed system was severer than that in a constant speed system.

Cho et al. [71] measured the cooling performance of a variable speed CO_2 cycle and analyzed by varying the refrigerant charge amount, compressor frequency, EEV opening, and length of an internal heat exchanger (IHX). As a result the cooling COP decreased with the increase of compressor frequency at all normalized charges. The optimum EEV opening increased with compressor frequency. The optimal compressor discharge pressure of the modified CO_2 cycle with the IHX was reduced by 0.5 MPa. The IHX increased the cooling capacity and COP of the CO_2 cycle by 6.2–11.9% and 7.1–9.1%, respectively, at the tested compressor frequencies from 40 to 60 Hz.

In addition to these studies, the Ekren and Kucuka study [72] has been carried out by a fuzzy logic-controlled chiller system with variable speed compressor. In this study, not only variable capacity modulation has been studied, but also fuzzy logic control effect on chiller system has been investigated. Scroll compressor, designed to study as fixed-speed compressor, was operated as variable speed with a PWM inverter. Also, electronic expansion valve, fuzzy controlled, was used. In this system 33.4% COP increase was obtained according to on-/off-controlled system. This increase has been obtained because of the less temperature difference between condensing and evaporation temperature.

3. Electrical control research for capacity-modulated refrigeration systems

Any system, whose outputs are controlled by some inputs of the system, is called a control system. Electrical control techniques of the capacity-modulated refrigeration systems are very important, because of the quick response of the load changes. On/off control, proportional-integral-derivative (PID), stochastic control, adaptive control, nonlinear methods, and robust control are known as conventional control systems. On/off and PID controls are the most commonly used methods in the heating ventilating and air-conditioning system control. Recent developments in artificial intelligence-based control systems have brought into focus a possibility of replacing control system with fuzzy logic control (FLC) equivalent. Therefore, fuzzy logic control is needed in the investigation on capacity-controlled refrigeration system. A standard PID controller is based on mathematical modeling of the system being controlled, whereas a fuzzy logic controls relies on physical rules rather than mathematical equations. In addition, fuzzy logic control provides a formal methodology for representing, manipulating, and implementing a human's heuristic knowledge about how to control a system.

Comparison of fuzzy logic and conventional controllers for a refrigeration system was investigated by Cheung and Kamal [73]. Fuzzy control application is realized on various compressor types following two authors. Aprea et al. [74] investigated fuzzy logic-based control algorithm which could select the most suitable compressor speed according to function of the cold store room air temperature. They found that this algorithm provides 13% energy saving when the R407C refrigerant was used at fuzzy logic-controlled variable speed reciprocating compressor. Furthermore, regarding the inverter cost, the payback period was more acceptable than for the examined cold storage plant.

Aprea and Mastrullo [75] investigated a vapor compression system which is able to operate as a water chiller and as a heat pump. The main aim of this study is to evaluate energy-saving

potential of a scroll compressor at varying speed instead of classical thermostatic (on/off) control. The compressor speed was continuously controlled via fuzzy logic algorithm. For different working conditions, a significant energy saving on average equal to about 20% was obtained adopting a scroll compressor speed control algorithm, based on the fuzzy logic, in comparison with the classical thermostatic control.

In a different study by Aprea et al. [76], energy consumption of an electronic valve and a thermostatic expansion valve were compared in a cold store. The main aim of the study was to verify the best type of expansion valve for the energy point of view. The results showed that with a fuzzy algorithm, the thermostatic expansion valve allows an energy saving of about 8% in comparison with the electronic valve.

Heating, ventilating, and air-conditioning (HVAC) control application is also studied in control researches, broadly. Rahmati et al. [77] presented a new approach to control heating, ventilating, and air-conditioning (HVAC) system. The proposed method was a hybrid of fuzzy logic and PID controller. Fuzzy logic control showed better control performance than PID controller. According to Wang et al. [78], the controlled object in HVAC system has large inertia, pure lag, and nonlinear characteristic. Combined with the fuzzy control and general PID control, the temperature and humidity of the room were controlled in HVAC system of a TV building. The temperature of the studio was controlled through PID control, fuzzy control, and fuzzy-PID control. It was found that hybrid fuzzy-PID control has better adaptability and stability, less overshoot, faster response, and higher precision than PID control and fuzzy control. Navale [79] conducted experiments on two real HVAC systems to compare the performance of fuzz logic control and PID control. Results of this study showed that fuzzy control system required 0–185% more rise time, had 9–68% less overshoot, and required 11–45% less settling time as compared to the conventional PID-controlled system.

In a different study from the others, Li et al. [80] investigated a PID and a fuzzy logic control study for automobile air-conditioning system. In the study, improvement of the refrigerant flow control method by using an electronic expansion valve (EEV) was described. Also, the flow rate characteristic of the EEV for automobile air-conditioning was presented. A microcontroller was used to receive input signal and generate output signal to control the opening amount of the EEV. They employed a fuzzy self-tuning proportional-integral-derivative (PID) control method. Experimental results showed that the new control method can feed adequate refrigerant flow into the evaporator in various operations. Also, evaporator discharge air temperature dropped by approximately 3°C as compared with the conventional PID control system.

4. Conclusion

In this paper, the literature review of capacity control methods is completed. The application of capacity control methods to refrigeration systems offers the potential for substantial energy saving or energy efficiency. Also, it is known that the overall energy consumption of a refrigeration, air-conditioning, or heat pump during its service life is a considerable cost factor and frequently is a multiple of the initial investment. Consequently, with a view to indirect

environmental impact (CO_2 emission due to power generation), optimum capacity control should be aimed for, that is, closely matched to demand. According to previous researches, variable speed capacity control is the most common and efficient methods in the capacity control studies. In addition to this, both of variable speed and digital scroll modulation present close modulation result. Also, it is seen that artificial intelligence control techniques show superiority toward conventional control methods on refrigeration system.

Author details

Orhan Ekren

Address all correspondence to: orhanekren@gmail.com

Solar Energy Institute, Ege University, İzmir, Turkey

References

[1] Deciding the Future: Energy Policy Scenarios to 2050 Executive Summary. World Energy Council (WEC); London, UK. 2007

[2] Energy Efficiency Policies around the World: Review and Evaluation Executive Summary. World Energy Council (WEC); London, UK. 2008

[3] Performance Rating of Water Chilling Packages Using the Vapor Compression Cycle. Air Conditioning and Refrigeration Institute (ARI) Standart, Arlington, VA, USA 550/590; 2003

[4] Tassou SA, Marquand CJ, Wilson DR. Comparison of the performance of capacity-controlled and conventional-controlled heat-pumps. Applied Energy. 1983;14:241-256

[5] Janssen H, Kruse H. Continuous and discontinuous capacity control for high-speed refrigeration compressors. Purdue Compressor Technology Conference. USA: Purdue University; 1984

[6] Zubair SM, Bahel V. Compressor capacity modulation schemes. Heating, Piping and Air-Conditioning. 1989, January;1:135-143

[7] Competance in Capacity Control. Report A-600-1, Bitzer International; Sindelfingen, Germany. 2006

[8] Digital capacity control for refrigeration scroll compressor. Emerson Climate Technology, Application Engineering Bulletin. AE21-1319R1 November 2003;21:1-5

[9] Hundy GF. Capacity control solution with scroll compressor. Institute of Refrigeration. 2002;98:101-111

[10] Hu SC, Yang RH. Development and testing of a multi-type air conditioner without using A.C. inverters. Energy Conversion and Management. 2005;46:373-383

[11] Jiang YT, Lai XJ, Yang CZ. Application and discussion of the digital scroll technology in VRV air-conditioning system. Refrigeration. 2006;25:49-53

[12] Kan AK, Han HD, Chen W. The application of cold storage container with digital scroll compressor. Compression Technology. 2005;6:30-33

[13] Zhou GZ, Zhang BH. The characteristic of air conditioning system with digital scroll. Energy Research Utilization. 2005;3:41-43

[14] Cuevas C., Lebrun J., Testing and modelling of a variable speed scroll compressor, Applied Thermal Engineering. 2009; 29:469-478

[15] Qiu YQ, Qiu ZG. Research and development and the experiment confirmation of high accuracy constant temperature and humidity air conditioning. Refrigeration Air-Condition. 2006;6:82-83

[16] Shi L. Analysis and comparison between digital scroll and invert technology. Refrigeration Technology. 2006;2:25-31

[17] Ma L, Sun H. Comparison of characteristics between digital scroll and frequency conversion scroll air conditioning system. Refrigeration Air Condition Electrical Power Mach. 2006;27:52-55

[18] Huang H, Li Q, Yuan D, Qin Z, Zhang Z. An experimental study on variable air volume operation of ducted air-conditioning with digital scroll compressor and conventional scroll compressor. Applied Thermal Engineering. 2007;28:761-766

[19] Cawley RE, Pfarrer DM. Part-load efficiency advantages of two-speed refrigerant compressors. Proceeding of International Refrigeration Conference. Purdue University; 1974. 42-46

[20] Wong AK, James RW. Capacity control of a refrigeration system using a variable-speed compressor. Building Service Engineering Research Technology. 1988;9:63-68

[21] Wong AK, Legg RC. Variable compressor speed control: Economic evaluation. Building Service Engineering Research Technology. 1989;10:21-27

[22] Yaqub M, Zubair SY. Thermodynamic analysis of capacity-control schemes for refrigeration and air-conditioning systems. Energy. 1996;21:463-472

[23] Yaqub M, Zubair SM. Capacity control for refrigeration and air-conditioning systems: A comparative study. Journal of Energy Resources Technology. 2001;123:92-99

[24] Solberg P. Hot gas by-pass report. Trane Engineers Newsletter. 2003;32:1-8

[25] Hot gas by-pass control system. Application Engineering Bulletin Copeland, AE-1160, Sidney, OH, USA, 1 October 1965.

[26] Application Guidelines: Enhanced Vapour Injection Refrigeration Scroll Compressors. C6.2.11/0504-0904/E, Emerson Climate Technology; Europe. 2004

[27] Yaqub M, Zubair SM, Khan SH. Second-law-based thermodynamic analysis of hot-gas, by-pass, capacity-control schemes for refrigeration and air-conditioning systems. Energy. 1995;20:483-493

[28] Yaqub M, Zubair SM, Khan JR. Performance evaluation of hot-gas by-pass capacity control schemes for refrigeration and air-conditioning systems. Energy. 2000;25:543-561

[29] Tso CS, Wong YV, Jolly PG, Ng SM. Comp hot gas by pass and suction modulation method partial load. International Journal of Refrigeration. 2001;24:544-553

[30] Cho H, Kim Y, Jang I. Performance multi evap during on-off and hot gas by-pass. Energy. 2005;30:1915-1930

[31] Capacity Control of Screw Compressors: Speed or Slider Control-a Comparative Study. SV-0402-GB, Bitzer International; 2006

[32] Reindl D. Screw compressors: Selection considerations for efficient operation-I. IRC The Cold Front Newsletter. Sindelfingen, Germany. 2002;2:2-5

[33] Winandy EL, Cristian CB. Analysis of the oil return in a pair of scroll compressors working in parallel at part load. Applied Thermal Engineering. 2003;23:623-636

[34] ASHRAE Handbook, Refrigeration Handbook, American Society of Heating. Atlanta, USA: Refrigerating and Air-conditioning Engineers; 1998

[35] Qureshi TQ, Tassou SA. Review paper variable-speed capacity control in refrigeration systems. Applied Thermal Engineering. 1996;16:103-113

[36] Muir EB, Griffith RW. Capacity modulation for air-conditioner and refrigeration system. Air-conditioning, Heating and Refrigeration News. 1979

[37] Tassou SA, Green RK, Wilson DR. Energy conservation through the use of capacity control in heat pumps. Journal of Energy Institute. 1981;54:30-34

[38] Tassou SA, Marquand CJ, Wilson DR. The Effect of Capacity Modulation on the Performance of Vapour Compression Heat Pump System. UK: International Syrup. on the Industrial Application of Heat Pumps; 1982

[39] Tassou SA, Marquand CJ, Wang YT, Wilson DR. An economic comparison of a fixed speed, a two speed, and a variable speed vapour compression heat pump. Applied Energy. 1984;16:59-66

[40] Tassou SA. Experimental investigation of the dynamic performance of variable-speed heat-pumps. Journal of the Energy Institute. 1991;64:95-98

[41] Shimma Y, Tateuchi T, Sugiura H. Inverter control systems in a residential heat-pump air-conditioner. ASHRAE Transactions. 1988;85:1541-1550

[42] Rasmussen CB. Variable Speed Brushless DC Motor Drive for Household Refrigerator Compressor. 8th International Conference on Electrical Machines and Drives, The Institution o Engineering and Technology, EMD Conference (Pub 444). Denmark; 1997

[43] Lida K, Yamamoto T, Kuroda T, Hibi H. Development of an energy-saving-oriented variable-capacity system heat-pump. ASHRAE Transactions. 1982;88:441-449

[44] Itami T, Okoma K, Misawa K. An experimental study of frequency-controlled compressors. Proc. Purdue Comp. Tech. Conf. Proceeding of international compressor engineering conference, Purdue University, Purdue, USA; 1982. 297-304

[45] Senshu T, Arai A, Oguni K, Harada F. Annual energy saving effect of capacity-modulated air-conditioner equipped with inverter-driven scroll compressor. ASHRAE Transactions. 1985;91:1569-1584

[46] Analysis of energy use and control characteristics of a large variable-speed drive chiller system. ASHRAE Journal. 1985;63:33-34

[47] McGovern JA. Performance characteristics of a reciprocating refrigerant compressor over a range of speeds. Proc. Purdue Comp. Tech. Conj. Proceeding of international compressor engineering conference, Purdue University, Purdue, USA; 1988. 146-153

[48] Ischii N, Yamamura M, Morokoski H, Fukushima M, Yamamoto S, Sakai M. On the superior dynamic behaviour of a variable rotating speed scroll compressor. Proc. Purdue Comp. Tech, Conf. Proceeding of international compressor engineering conference, Purdue University, Purdue, USA. 1988. 75-82

[49] Ischii N, Yamamura M, Muramatsy S, Yamamoto S, Sakai M. Mechanical efficiency of a variable speed scroll compressor. Proc. Comp. Tech. Conf. Purdue, USA. 1990. 192-199

[50] Tassou SA, Qureshi TQ. Performance of a variable speed inverter/motor drive. Computing & Control Engineering Journal, Aug. 1994;5(4):193-199

[51] Tassou SA, Qureshi TQ. Comparative performance evaluation of positive displacement compressors in variable-speed refrigeration applications. International Journal of Refrigeration. 1998;21:29-41

[52] Dutta A, Yanagisawa T, Fukuta M. An investigation of the performance of a scroll compressor under liquid refrigerant injection. International Journal of Refrigeration. 2001;24:577-587

[53] Winandy EL, Lebrun J. Scroll compressors using gas and liquid injection: Experimental analysis and modeling. International Journal of Refrigeration. 2002;25:1143-1156

[54] Cho H, Chung JT, Kim Y. Influence of liquid refrigerant injection on the performance of an inverter-driven scroll compressor speed in function of the water temperature. International Journal of Refrigeration. 2003;26:87-94

[55] Aprea C, Mastrullo R, Renno C, Vanoli GP. An evaluation of R22 substitutes performances regulating continuously the compressor refrigeration capacity. Applied Thermal Engineering. 2004;24:127-139

[56] Feasibility and Design Study of Continuously Variable Capacity Refrigeration. Energy Efficiency Best Practice Programme. UK: General Report 3, Dept of Energy; 1991

[57] Rice CK. Efficiency characteristics of speed-modulated drives at predicted torque conditions for air-to-air-heat pumps. ASHRAE Transactions. 1988;94:892-921

[58] Rice CK. Benchmark performance analysis of an ECM-modulated air-to-air heat-pump with a reciprocating compressor. ASHRAE Transactions. 1992;98:430-450

[59] Nasutin H, Mat Nawi Wan H. Potential electricity savings by variable speed control of compressor for air conditioning systems. Clean Technologies and Environmental Policy. 2006;8:105-111

[60] Cuevas C, Lebrun J. Testing and modeling of a variable speed scroll compressor. Applied Thermal Engineering (article in press)

[61] Bose KB. Power electronics: A technology review. Proceedings of the IEEE. 1992;80: 1303-1334

[62] Retrofitting A.C. Variable-Speed. UK: Energy Efficiency Office Practice Guide 14, Dept. of Energy; 1991

[63] Ryska A, Kral F, Ota J. Method of determination of the effective capacity of refrigeration and A/C units of variable speeds. International Journal of Refrigeration. 2000;23:402-405

[64] Park YC, Kim YC, Min M. Performance analysis on a multi-type inverter air conditioner. Energy Conversion and Management. 2001;42:1607-1621

[65] Choi M, Kim YC. Capacity modulation of an inverter-driven multi-air conditioner using electronic expansion valves. Energy. 2003;28:141-155

[66] Saiz JM, Jabardo W, Mamani G, Ianella MR. Modeling and experimental evaluation of an automotive air conditioning system with a variable capacity compressor. International Journal of Refrigeration. 2002;25:1157-1172

[67] Park YC, Kim YC, Cho H. Thermodynamic analysis on the performance of a variable speed scroll compressor with refrigerant injection. International Journal of Refrigeration. 2002;25:1072-1082

[68] Aprea C, Renno C. An experimental analysis of a thermodynamic model of a vapour compression refrigeration plant on varying the compressor speed. International Journal of Energy Research. 2004;28:537-549

[69] Shao S, Shi W, Li X, Chen H. Performance representation of variable-speed compressor for inverter air conditioners based on experimental data. International Journal of Refrigeration. 2004;27:805-815

[70] Kim M, Kim MS. Performance investigation of a variable speed vapor compression system for fault detection and diagnosis. International Journal of Refrigeration. 2005;28:481-488

[71] Cho H, Ryu C, Kim Y. Cooling performance variable speed with CO_2. International Journal of Refrigeration. 2007;30:664-671

[72] Ekren O, Kucuka S. Energy saving potential of chiller system with fuzzy logic control. International Journal of Energy Research. 2010;34:pp.879-906

[73] Cheung JYM, Kamal AS. Fuzzy logic control of refrigerant flow. UKACC International Conference (Conf. Publ. No. 427). 1996;1:125-130

[74] Aprea C, Mastrullo R, Renno C. Fuzzy control of the compressor speed in a refrigeration plant. International Journal of Refrigeration. 2004;27:639-648

[75] Aprea C, Mastrullo R. Performance of thermostatic and electronic valves controlling the compressor capacity. International Journal of Energy Research. 2006;30:1313-1322

[76] Aprea C, Mastrullo R, Renno C. Experimental analysis of the scroll compressor performances varying its speed. Applied Thermal Engineering. 2006;26:983-992

[77] Rahmati A, Rashidi F, Rashidi M. A Hybrid fuzzy logic and PID controller for control of nonlinear HVAC systems. IEEE International Conference. 2003;3:2249-2254

[78] Wang J, An D, Lou C. Application of Fuzzy-PID Controller in heating ventilating and air-conditioning system. Proceedings of the IEEE International Conference on Mechatronics andAutomation. 2006. pp. 2217-2222

[79] Navale RL. Development of an adaptive fuzzy logic controller for HVAC. PhD Thesis. Iowa State Unv.; 2006

[80] Li X, Chen J, Chen Z, Liu W, Hu W, Liu X. A new method for controlling refrigerant flow in automobile air conditioning. Applied Thermal Engineering. 2004;24:1073-1085

Edited by Orhan Ekren

In the beginning, the sole purpose of utilization of the refrigeration was to conserve food (BC 1100). But today in our daily life, refrigeration is one of the necessary areas for the aim of not only food conservation but also comfort, industrial production, electronic equipments' performance, safe and proper operation of telecommunication stations and computer rooms, space studies, etc. The importance and wide application range of the refrigeration require new techniques and researches. In this respect, the scope and topics of the book are: Multistage refrigeration cycle analysis, Electrocaloric cooling method, Food chilling-freezing methods and equipments, CFD modeling of airflow in the display cabinet, Industrial application of refrigeration, Energy-efficient air-conditioning system comparison, Capacity modulation methods for energy-efficient refrigeration.

ISBN 978-953-51-4693-3

IntechOpen